

**Self-assembly and Structure Investigation of Recombinant  
S-layer Proteins Expressed in Yeast for Nanobiotechnological  
Applications**

**Dissertation**

**zur Erlangung des akademischen Grades  
Doctor rerum naturalium  
(Dr. rer. nat.)**

**eingereicht an der  
Fakultät Mathematik und Naturwissenschaften  
der Technischen Universität Dresden**

**von  
Nuriye Korkmaz  
aus Rize, Türkei**

**Gutachter: 1. Prof. Dr. Gerhard Rödel  
2. Prof. Dr. Michael Mertig**

**Eingereicht am: 08. 10. 2010  
Tag der Disputation: 22. 12. 2010**

**Die Dissertation wurde in der Zeit von September 2007 bis  
Oktober 2010 im Institut für Genetik angefertigt.**

**Part of this work was published or is submitted for publication:**

**Scientific papers**

**Korkmaz N**, Ostermann K, Rödel G (2010) Expression and assembly of recombinant surface layer proteins in *Saccharomyces cerevisiae*. *Curr Microbiol* DOI 10.1007/s00284-010-9715-1

**Korkmaz N**, Ostermann K, Rödel G (2010) Calcium dependent formation of tubular assemblies by recombinant S-layer proteins *in vivo* and *in vitro*. *Nanotechnology* (accepted)

**Book Chapters**

Varga M, **Korkmaz N** “S-layer Proteins as Self-Assembly Tool in Nano Bio Technology” *Bio and Nano Packaging Techniques for Electron Devices* (Gerlach G and Wolter K-J eds). Springer (2010, in press)

**Posters**

**Korkmaz N**, Mertig M, Rödel G, Self-assembly and Structure Investigation of S-layers Expressed in Yeast. Workshop “DFG Report and Defense Colloquium, Bio-Nano-Tech 2010”, 09.09.2010. Dresden, Germany

**Korkmaz N**, Ostermann K, Rödel G, Self-assembly and Structure Investigation of Recombinant S-layer Proteins Expressed in Yeast. 6th Nanoscience and Nanotechnology Conference. 15-18.06.2010. Izmir, Turkey

**Korkmaz N**, Ostermann K, Rödel G, Self-assembly and Structure Investigation of Recombinant S-layers Expressed in Yeast. Nano-Molecular Analysis for Emerging Technologies III & Surface Science of Biologically Important Interfaces 10 NPL. 05-06.11.2008. Teddington, UK.

Varga M, **Korkmaz N**, Ostermann K, Pompe W, Rödel G, Recombinant S-layer protein SslA of *Sporosarcina ureae* ATCC 13881 as a tool in nanobiotechnology. Max Bergmann Symposium 2008. 04-06.11.2008. Dresden, Germany.

# Contents

Abbreviations.....	6
Aim of the study.....	8
<b>I. INTRODUCTION.....</b>	<b>9</b>
<b>1.1. Morphological Structure and Occurrence of SL Proteins.....</b>	<b>9</b>
<b>1.2. Chemical Structure, Synthesis and Genetics.....</b>	<b>12</b>
<b>1.3. Functions.....</b>	<b>14</b>
<b>1.4. Self-assembly .....</b>	<b>15</b>
<b>1.5. Applications .....</b>	<b>16</b>
1.5.1. Biomimetic and Biotechnological Applications .....	16
1.5.1.1. <i>Isoporous Ultrafiltration Membranes</i> .....	17
1.5.1.2. <i>Immobilization Matrices</i> .....	18
1.5.1.3. <i>Vaccine Technology</i> .....	19
1.5.1.4. <i>Functional lipid membranes</i> .....	20
1.5.2. Nanotechnological Applications.....	22
1.5.2.1. <i>Coupling of Inorganic Molecules</i> .....	22
1.5.2.2. <i>Formation of Metal Clusters</i> .....	23
<b>1.6. Expression of SL Proteins in Eukaryotic Systems.....</b>	<b>24</b>
1.6.1. <i>Saccharomyces cerevisiae</i> as a Host Organism in Protein Expression.....	24
1.6.2. SL proteins Investigated in This Study .....	27
<b>II. MATERIALS AND METHODS .....</b>	<b>30</b>
<b>2.1. Materials.....</b>	<b>30</b>
2.1.1. Equipments .....	30
2.1.2. Kits and Similar products.....	31
2.1.3. Chemicals.....	31
2.1.4. Enzymes.....	33
2.1.5. Buffers and Solutions.....	33
2.1.5.1. <i>Commercial Buffers and Stock Solutions</i> .....	34
2.1.5.2. <i>Self-made Buffers and Solutions</i> .....	34
2.1.6. Media .....	36
2.1.7. Strains .....	37
2.1.8. Primers.....	37
2.1.9. Plasmids .....	39
<b>2.2. Methods.....</b>	<b>39</b>
2.2.1. DNA Techniques .....	39
2.2.1.1. <i>DNA Gel Electrophoresis</i> .....	39
2.2.1.2. <i>Isolation of Plasmid DNA from E. coli Cells</i> .....	40
2.2.1.3. <i>Polymerase Chain Reaction (PCR)</i> .....	40
2.2.1.4. <i>DNA Purification Techniques</i> .....	41

2.2.1.4.1. Purification of PCR Products .....	41
2.2.1.4.2. DNA Fragment Purification from Gel .....	41
2.2.1.5. Digestion of DNA with Restriction Endonucleases .....	41
2.2.1.6. Ligation .....	41
2.2.1.7. Transformation .....	42
2.2.1.7.1. Preparation of Electrocomponent Cells .....	42
2.2.1.7.2. Transformation of <i>E. Coli</i> Cells by Electroporation .....	42
2.2.1.7.3. Transformation of Yeast Cells .....	42
2.2.2. Protein Techniques.....	43
2.2.2.1. SDS-PAGE and Western Blot Analysis.....	43
2.2.2.2. Protein Concentration Assay and Cell Lysis .....	44
2.2.3. Growth and Fluorescence Measurements .....	44
2.2.4. <i>In vivo</i> Protein Structure Investigation .....	44
2.2.5. Live Cell Imaging .....	45
2.2.6. Sporulation.....	45
2.2.7. Colocalization Investigation Techniques.....	45
2.2.7.1. $\alpha$ -tubulin Staining .....	45
2.2.7.2. Phalloidin Staining of Fixed Cells.....	46
2.2.7.3. DAPI staining.....	46
2.2.8. <i>In situ</i> Protein Extraction .....	46
2.2.9. <i>In vitro</i> Recrystallization of SL Monomers .....	47
2.2.10. Metallization .....	47
2.2.11. Fluorescence Microscopy .....	47
2.2.12. Electron Microscopy .....	48
<b>III. RESULTS .....</b>	<b>49</b>
<b>3.1. Expression of Recombinant SL Proteins in Yeast .....</b>	<b>49</b>
<b>3.2. <i>In vivo</i> Thermal Stability of SL-eGFP Proteins .....</b>	<b>55</b>
<b>3.3. <i>In vivo</i> Self-assembly Kinetics of mSbsC-eGFP .....</b>	<b>60</b>
3.3.1. Formation of SL Assemblies during Mitosis.....	60
3.3.2. Formation of SL Assemblies during Meiosis .....	62
3.3.3. Formation of SL Assemblies during Sporulation .....	64
<b>3.4. Colocalization Studies.....</b>	<b>65</b>
3.4.1. Colocalization with Microtubules.....	66
3.4.2. Colocalization with Actin Network .....	68
3.4.3. Colocalization with Nucleus and Mitochondrial Network .....	69
<b>3.5. <i>In vitro</i> Recrystallization .....</b>	<b>70</b>
3.5.1. <i>In vitro</i> Recrystallization of mSbsC-eGFP .....	70
3.5.2. <i>In vitro</i> Recrystallization of S13240-eGFP.....	72
3.5.3. <i>In vitro</i> Recrystallization of SslA-eGFP .....	73
3.5.4. eGFP as Control.....	74
3.5.5. Characterization of <i>in vitro</i> Recrystallized SL-eGFP Structures.....	75
3.5.6. Recrystallization of mSbsC-eGFP on Surfaces .....	77
3.5.7. Influence of Calcium Concentration, pH and Dialysis Time on <i>in vitro</i> Recrystallization Process .....	78
3.5.7.1. Effect of Calcium Concentration .....	78



---

3.5.7.2. <i>Effect of pH and Dialysis Time</i> .....	81
<b>3.6. Metallization of mSbsC-eGFP Tubes</b> .....	<b>82</b>
3.6.1. Effect of Temperature on Metallization.....	83
3.6.2. Effect of Platinum Concentration on Metallization .....	83
<b>IV. DISCUSSION</b> .....	<b>87</b>
<b>4.1. Expression Analyses of Recombinant SL Proteins in Yeast</b> .....	<b>87</b>
<b>4.2. <i>In vivo</i> Thermal Stability of SL-eGFP Proteins</b> .....	<b>89</b>
<b>4.3. Formation of SL Assemblies during Mitosis and Meiosis</b> .....	<b>91</b>
<b>4.4. Colocalization Studies</b> .....	<b>93</b>
<b>4.5. <i>In vitro</i> Recrystallization</b> .....	<b>94</b>
<b>4.6. Influence of Calcium Concentration, pH and Dialysis Time on <i>in vitro</i> Recrystallization Process of mSbsC-eGFP Monomers</b> .....	<b>96</b>
<b>4.7. Metallization of mSbsC-eGFP Tubes with Platinum</b> .....	<b>97</b>
<b>V. SUMMARY</b> .....	<b>99</b>
<b>VI. REFERENCES</b> .....	<b>101</b>
Acknowledgements.....	108
Curriculum Vitae .....	109
Selbständigkeitserklärung.....	111

## Abbreviations

aa	Amino acid
AFM	Atomic force microscopy
AMP	Affinity micro particles
bp	Base pairs
BP	Band pass
BS	Beam splitter
C-terminal	Carboxy-terminal
DNA	Deoxyribonucleic acid
dNTP	Deoxynucleosidetriphosphate
eGFP	Enhanced green fluorescent protein
EBV	Epstein–Barr virus
Em	Emission
Ex	Excitation
GRAS	Generally recognized as safe
GFP	Green fluorescent protein
IgG	Immunoglobulin G
kDa	Kilodalton
N-terminal	Amino-terminal
OD	Optical density
PCR	Polymerase chain reaction
RNA	Ribonucleic acid
RT	Room temperature
SCWP	Secondary cell wall polymer
SDS	Sodium dodecyl sulfate
SDS-PAGE	SDS polyacrylamide gel electrophoresis
SEM	Scanning electron microscopy
S-layer	Surface layer
SLH-domain	S-layer homology domain
SslA	<i>Sporosarcina ureae</i> S-layer protein A

<i>sslA</i>	<i>Sporosarcina ureae</i> S-layer gene A
SbsC	<i>B. stearothermophilus</i> ATCC 12980 S-layer protein C
<i>sbsC</i>	<i>B. stearothermophilus</i> ATCC 12980 S-layer gene C
S13240	<i>B. stearothermophilus</i> DSM 13240 S-layer protein
<i>s13240</i>	<i>B. stearothermophilus</i> DSM 13240 S-layer gene
SUM	S-layer ultrafiltration membrane
TEM	Transmission electron microscopy
V	Volt
v/v	Volume per volume
w/v	Weight per volume

## Amino acids

A	Ala	alanine	M	Met	methionine
C	Cys	cysteine	N	Asn	asparagine
D	Asp	aspartate	P	Pro	proline
E	Glu	glutamate	Q	Gln	glutamine
F	Phe	phenylalanine	R	Arg	arginine
G	Gly	glycin	S	Ser	serine
H	His	histidine	T	Thr	threonine
I	Ile	isoleucine	V	Val	valine
K	Lys	lysine	W	Trp	tryptophan
L	Leu	leucine	Y	Tyr	tyrosine

## Aim of the Study

Numerous Gram-negative, Gram-positive bacteria and archaea possess S-layers (SLs) covering their outermost layers. SLs which consist of protein (or glycoprotein) subunits can self-assemble into highly regular planar structures [1]. Up to 20% of total protein content of the corresponding prokaryotic cells is composed of these two-dimensional arrays [2]. Morphological, structural and genetic investigations indicated that SLs are the simplest form of membranes [3]. SL subunits interact with each other and with the underlying cell surface by relatively weak non-covalent forces such as hydrogen-bonds, ionic bonds, salt-bridges or hydrophobic interactions. This makes them easy to isolate by applying chaotropic agents like urea and guanidine hydrochloride (GuHCl), chelating chemicals, or by changing the pH of the environment [10]. Upon dialysis in an ambient buffer monomers recrystallize into regular arrays in the form of flat sheets, open ended cylinders, or spheres on solid substrates, at air-water interfaces and on lipid films, making them appealing for nanobiotechnological applications [5]. The aim of this study was to investigate the structure, thermal stability, *in vivo* self-assembly, recrystallization and metallization of three different recombinant SL proteins (SslA-eGFP, mSbsC-eGFP and S13240-eGFP) expressed in yeast *Saccharomyces (S.) cerevisiae* BY4741 which could be further used in nanobiotechnological applications.

The first aim was to characterize the heterologous expression and structure of *in vivo* SL-eGFP fusion proteins with growth and fluorescence measurements coupled with Western blot analyses and fluorescence microscopy. Secondly, I was interested in thermal stabilities of *in vivo* expressed SL-eGFP fusion proteins which could be analyzed by fluorescence microscopy and immuno-detection techniques. Third aim was to investigate *in vivo* self-assembly mechanism of SL-eGFP constructs in *S. cerevisiae* cells during mitosis and meiosis. In parallel, possible association of *in vivo* SL-eGFP structures with the cellular components was of interest. The next issue was to determine if *in vivo* SL-eGFP assemblies could be obtained stably outside the cells (*in situ*). Following the *in situ* extraction analyses, it was aimed to investigate monomerization, subsequent recrystallization and metallization of SL-eGFP fusion proteins and the factors affecting the underlying recrystallization process.

## I. Introduction

S-layers (SLs) are composed of protein (or glycoprotein) subunits covering the outermost layer of many Gram-negative, Gram-positive bacteria and archaea forming planar self-assembly structures [1]. These two-dimensional arrays occupy up to 20% of total protein structure of the cell [2]. Morphological, structural and genetic studies showed that SLs are the simplest form of membranes evolved [3]. During all stages of cell cycle, they assemble into highly porous, regularly patterned structures onto the cell surface [4]. They can be recrystallized into monomolecular arrays in suspensions, on solid surfaces e.g. silicon, glass, carbon and synthetic polymers or on lipid films [5]. Regularly sized pores having similar morphologies make them appealing for biotechnological applications such as molecular filtration processes [6]. Presence of functional groups on protein lattices in well-defined positions and orientations reveal their immobilization potential for functional molecules [7]. Due to these characteristic features, SLs have become appealing for biotechnology, biomimetics and nanotechnology. In this section, structure, synthesis, function, applications of SL proteins, characteristics of specific SL proteins investigated in this study were presented with introduction to yeast *S. cerevisiae* as a model organism.

### 1.1. Morphological Structure and Occurrence of SL Proteins

SLs were reported to be found in many bacteria and archaea. Interaction of SL monomeric subunits with the underlying cellular envelope during the reassembly process can be grouped into three groups (Fig. 1) depending on the type of species owning SLs [9]. These subunits interact with each other and with the underlying cell surface by relatively weak forces such as hydrogen-bonding, salt-bridging, ionic bonding or hydrophobic interactions. These non-covalent weak interactions make SL proteins easy to isolate by hydrogen-bond breaking agents, chelating chemicals or by changing the pH of the environment [10]. SLs of various microorganisms have been identified by electron microscopy through freeze etching (Fig. 2a.). Scanning force microscopy and electron crystallography enabled scientists to identify the three-dimensional structure of SL arrays (Fig. 2b) [11]. These arrays are composed of identical protein or glycoprotein subunits self-assembling in hexagonal (p6), tetragonal (p4), trimeric (p3) or oblique (p1, p2) symmetrical structures (Fig. 3) [12]. The center to center distance between each subunit ranges from 2.5 nm to 35 nm and the thickness of the array varies in bacteria between 5 nm and 25 nm, and in archaea up to 70 nm [13]. SL protein

networks have highly porous surfaces (up to 70%) with pores of generally identical size (2-8 nm range) and morphology (Fig. 4) [14].

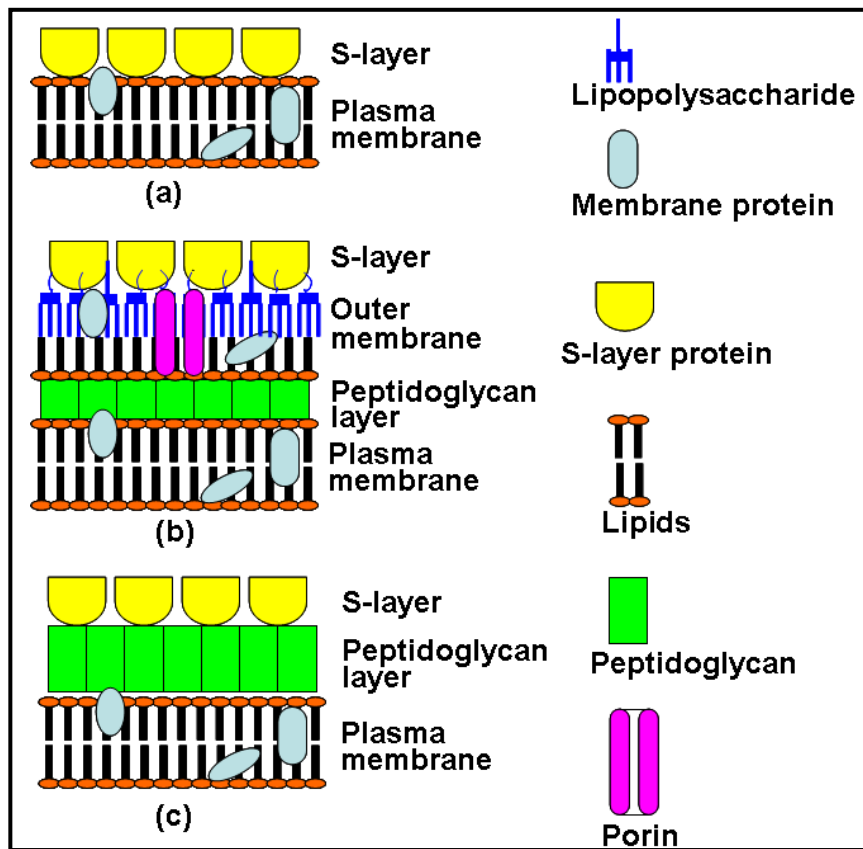


**Figure 1.** Cell envelope structures of three types of prokaryotes possessing SLs. (a) Archaea with SLs bound to the cell membrane. (b) Gram-negative bacteria with SLs associated directly with lipopolysaccharides of the outer membrane. (c) Gram-positive bacteria with SLs interacting with the cell wall composed of peptidoglycan (modified from [11]).

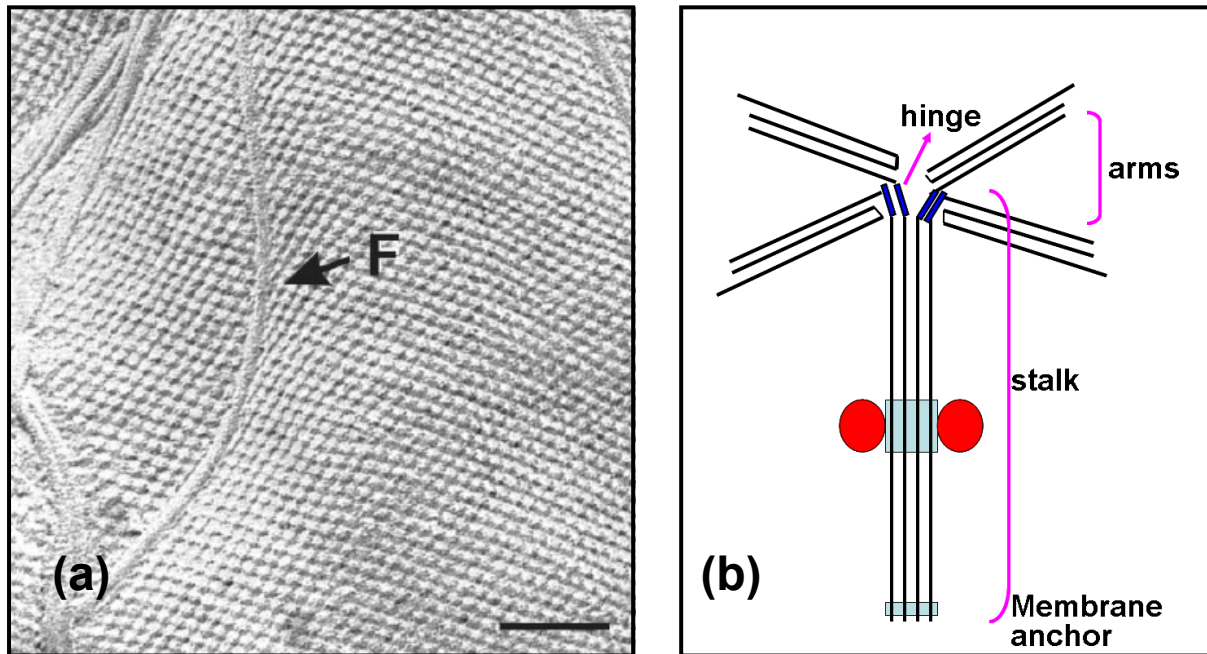


**Figure 2.** SL characterization by electron microscopy and modeling. a) Freeze-etched electron microscope image of *Thermoanaerobacter thermohydrosulfuricus* surface layer. F, flagellum; Scale bar = 100 nm [15] b) Structural scheme of one SL unit (Tetrabrachion) of *Staphylothermus marinus* (modified from [16])

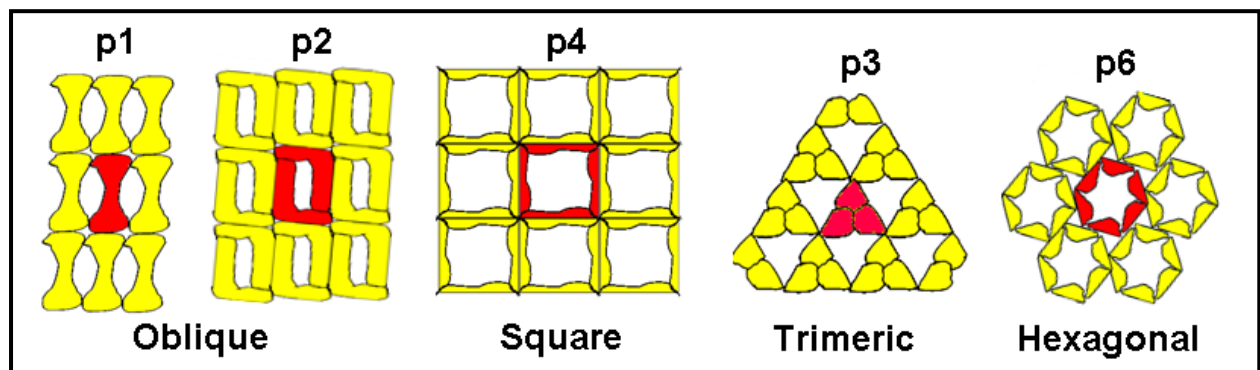


**Figure 3.** Different SL lattice symmetry types. The well ordered SL lattices show either oblique (p1, p2), square (p4), or hexagonal symmetry (p3, p6) consisting of one, two, three, four, or six identical subunits (modified from [3]).

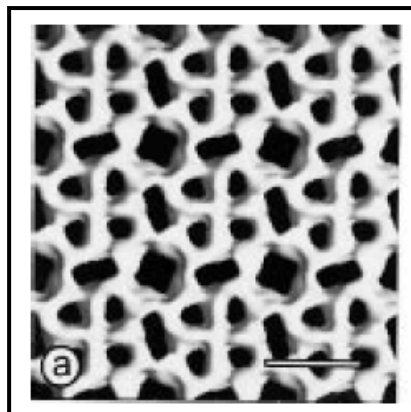


**Figure 4.** Three-dimensional model of highly porous *Bacillus stearothermophilus* (*B. stearothermophilus*) NRS 2004/3a/V2 SL (outer face). The thickness of SL is about 8 nm and its center-to-center spacing between subunits is 13.5 nm. The protein network exhibits one square-shaped, two elongated, and four small pores per morphological unit. Bar = 100 nm [11]

## 1.2. Chemical Structure, Synthesis and Genetics

Highly purified SLs from archaea and bacteria show a common overall chemical composition regardless of the origin of the microorganism. According to these findings, they are consisting of 40-60% of hydrophobic amino acids (aa). They are generally weakly acidic proteins (pI~4-6, except for *Methanothermus fervidus* (pI 8.4) and lactobacilli (pI>9.5)) composed of protein or glycoprotein subunits. They possess nearly 15% of glutamic and aspartic acid, about 10% lysine and 40-60% hydrophobic aa. Mostly all SL proteins are composed of 20%  $\alpha$ -helices and 40%  $\beta$ - sheets [11].

Under the scope of synthesis and secretion of SLs, the first complete pathway was identified by Noonan *et al.* [17]. They have published a specific pathway for SL secretion in *Aeromonas salmonicida* across the outer membrane which is also the general secretion system for other proteins like hemolysin and proteases.

Genetical studies revealed that the SLs originating from different phylogenetic branches did not show any sequence identities. It has been found that sequential homologies depend on evolutionary backgrounds. For some species, signal peptide encoding sequences are conserved. SbsA and SbsC surface layer proteins of two *B. stearothermophilus* wild-type strains (PV72/p6 and ATCC 12980) are highly identical for the 270 N-terminal aa, but weakly identical (<25%) for the remaining sequences. However for some other evolutionary related species, these findings are not applicable because the sequential identities can not be



related only to evolutionary relationships but other factors like growth conditions or environmental pressures. It has been shown that, when the N- and C-terminal truncated forms of SL encoding genes are expressed in various host organisms, they are still capable of self-assembling on the cell envelope [11, 18].

Glycosylation is a common post-translational modification observed in SLs from archaea, Gram-positive and Gram-negative bacteria (Fig. 5). Until now, at least 40 different glycan structures of glycosylated SLs have been characterized. In archaea, SL glycan chains are composed of short oligosaccharides whereas in bacteria, they are mostly linear or branched homo-/heterosaccharides composed of 20-50 repeating units. *O*-glycosidic linkages have been identified in both, archaeal and bacterial glycosylated SLs, while *N*-glycosidic linkages are specific to archaea [15]. Characterization of bacterial and archaeal glycosylated SL proteins is summarized in Table 1.

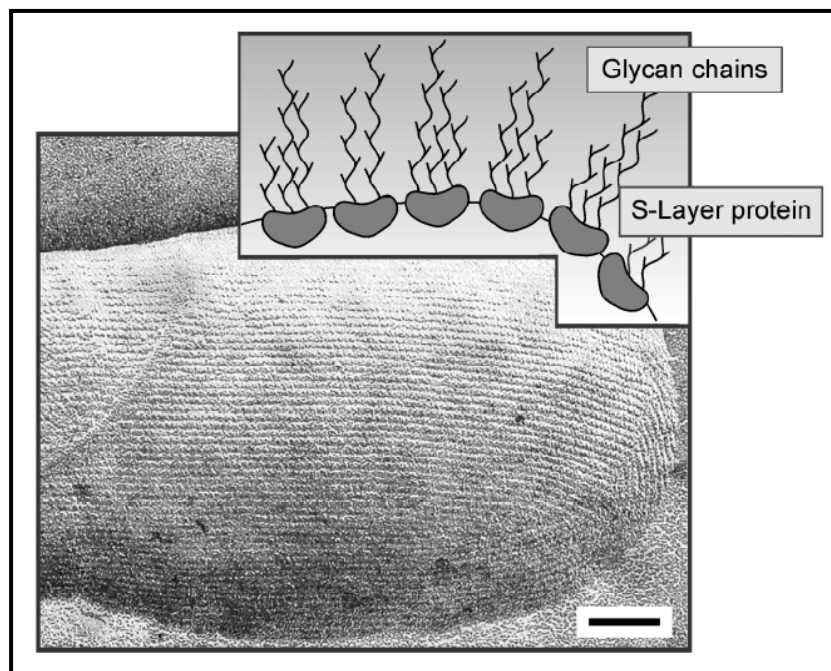


**Figure 5.** Schematic representation of 30-40 nm glycan chains projected from the cell surface of *Geobacillus stearothermophilus* NRS 2004/3a [19]

**Table 1.** Characteristics of bacterial and archaeal glycosylated SL proteins (modified from [15])

Aspect	Bacteria	Archaea
Glycan type	O-glycan	N-glycan, O-glycan
Region of linkages	$\beta$ -Glc to Tyr $\beta$ -Gal to Tyr/Ser $\beta$ -GalNAc to Tyr/Ser $\alpha$ -Glc to Ser	$\beta$ -Glc to Asn GalNAc to Asn Rha to Asn Gal to Thr
Glycan composition	Heteropolysaccharides of 20-50 repeating units	Short heteropolysaccharides up to 10 sugars
Repeating unit	2-6 sugars	Not discovered
Sugar components	$\beta$ -D-Glcp $\alpha$ -D-Galp, $\beta$ -D-Galp, $\beta$ -D-Galf $\alpha$ -D-Manp $\alpha$ -D-Rhap, $\alpha$ -L-Rhap $\alpha$ -D-GlcpNAc $\alpha$ -D-GalpNAc, $\beta$ -D-GalpNAc, etc.	$\alpha$ -D-Glcp, $\beta$ -D-Glcp Galp, Galf $\alpha$ -D-Manp D-GlcpNAc, etc.
Glycosylation sequences	YD, YPV, YNP, YSPA, etc.	NXS/T

### 1.3. Functions

In nature, SLs function as cell shape and rigidity determining tools (especially in Gram-negative archaea where SLs are directly bound to the cytoplasmic membrane) and protective coats against environmental stresses e.g. high temperature, low pH, high ionic strength, etc. [20]. It has been reported that SLs can also act as molecular sieves and ion traps. For example, SL from *B. coagulans* E38-66 was reported to act as a neutral charged molecular sieve allowing molecules up to 17 kDa to pass [21, 22]. In some Gram-negative bacteria, SLs can act as a barrier against bacterial parasites [23]. They can contribute to the virulence of some pathogens [9, 24] or can function as adhesion sites for cell-associated exoenzymes, e.g. exoamylase from *G. stearothermophilus* [25, 26] and as crystallization nuclei for

biomineralization. *Synechococcus sp.* strain GL24 uses its SL structure for the biomineralization of gypsum and calcite [27, 28]

#### **1.4. Self-assembly**

An SL of a moderate size, rod shaped prokaryote is composed of nearly  $5 \times 10^5$  subunits. Since the cell generation time is about 20-30 min, for this cell to cover the whole cell envelope with the SL, at least 500 copies of monomers have to be synthesized and located per second. Microscopic techniques enable scientist to understand the dynamics behind the SL assembly process both *in vivo* [29] and *in vitro* [14].

*In vivo* self-assembly observations conducted by labeling the SL with colloidal gold or fluorescent markers showed the way of extension during the cell growth. It was shown that in Gram-negative and Gram-positive bacteria SL growth depends on the growth of underlying cell envelope layer and the lattice growth can start at specific regions or random domains. Moreover, dislocations and disclinations were observed in freeze-etched intact bacteria preparations. It has been theoretically predicted that these areas of dislocations can function as the domains for new subunits to be translocated into the array or as initiation sites for cell division [11, 30]. Recently it was demonstrated that there exists a second layer underlying the SL taking role in promoting the 2D self-assembly process [31].

There are various ways of disintegrating the SL monomers from the cellular envelope. Since monomeric subunits interact with each other and with the underlying cell surface by relatively weak forces such as hydrogen-bonding, salt-bridging, ionic bonding or some hydrophobic interactions, these non-covalent weak interactions make them easy to be isolated by high concentrations of chaotropic agents such as urea and guanidine hydrochloride, by using metal chelating chemicals such as ethylenediaminetetraacetic acid (EDTA) and ethylenebis (oxyethylenenitrilo) tetraacetic acid (EGTA) or by changing the pH of the environment [10]. After the isolation of monomers, upon the removal of disintegrating agents from the environment by means of dialysis, subunits can be recrystallized into regular arrays on solid substrates e.g. silicon, noble metals, glass, carbon and synthetic polymers, at air-water interfaces and on lipid films [11, 5, 3]. These self-assembly products can be formed as flat sheets, open ended cylinders or spheres (Fig. 6). The rate and extent of self-assembly process depends on various factors such as: temperature, ionic strength, protein concentration [11].

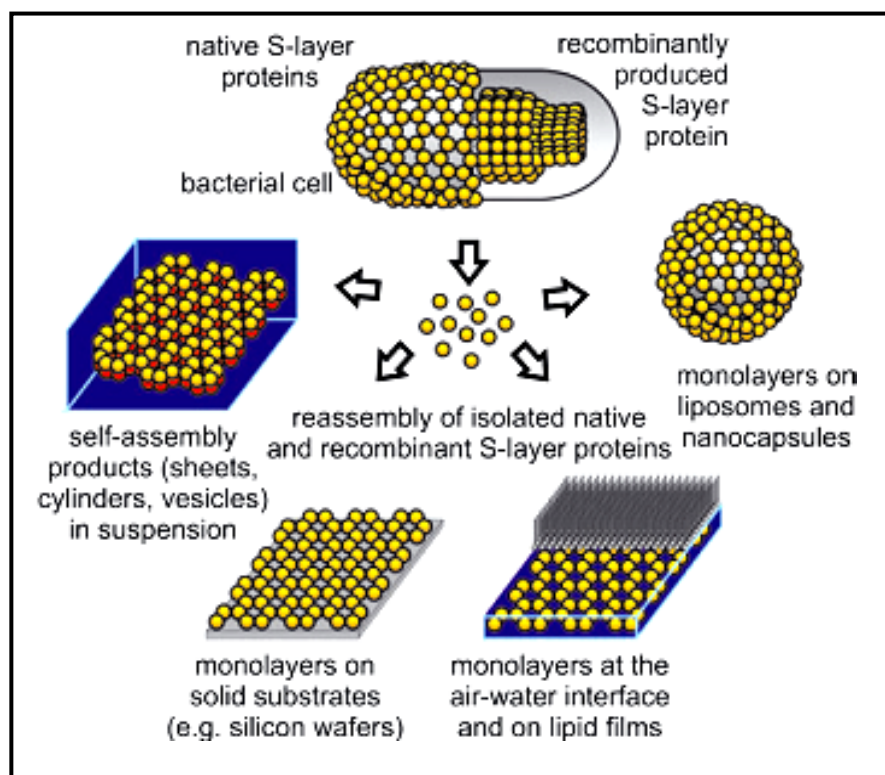


**Figure 6.** *In-vitro* reassembly of isolated SL subunits on various substrates [3]

## 1.5. Applications

Self-assembly abilities into monomolecular arrays in suspensions, on solid surfaces or lipid films enable SL proteins to be recrystallized on silicon, glass, carbon and synthetic polymers. SLs possess regularly sized pores having similar morphologies. Presence of functional groups on protein lattices in well-defined positions and orientations reveal their immobilization potential for functional molecules. Due to these characteristic features, SLs have become appealing for biotechnology, biomimetics and nanotechnology [5, 6, 7, 11, 8].

### 1.5.1. Biomimetic and Biotechnological Applications

Production of isoporous ultrafiltration membranes with good molecular sieving and antifouling characteristics, production of matrices for the immobilization of many molecules like enzymes, antibodies, biotin, avidin, etc. (used in amperometric or optical biosensors), production of vaccine and vaccine derivatives and supporting structures for the production of functional lipid membranes are the most remarkable biotechnological and biomimetic applications of SLs [11].

### ***1.5.1.1. Isoporous Ultrafiltration Membranes***

Due to the presence of highly porous structure of SLs having mostly identical size and morphology, SL lattices are applicable in production of ultrafiltration membranes (SUMs) with good molecular sieving and antifouling characteristics [8]. It has been reported on molecular sieving capacity of *B. stearothermophilus* SL lattices [6]. It was shown that the examined *Bacillus* strains are capable of transporting molecules up to the molecular weights of 30,000 Da. SUMs can be obtained by crosslinking the SL self-assembly products or cell envelope fragments containing SLs on nylon microfiltration membranes with glutaraldehyde (Fig. 7) [32].

One can obtain SUMs with neutral, negative or positive charges and with different hydrophobicities by manipulating the free carboxyl groups of aa located on the surface of SLs or inside the pores that can allow the scientists to study the passage of different molecules through the ultrafiltration membranes and to conduct flux analyses [48]. SUMs are also model systems for protein adsorption and membrane fouling studies [33]. Recently, the electrochemical properties of a SUM constructed with SbpA (SL protein of *Lysinibacillus sphaericus*) has been determined giving hints about the potential usage of such supports for the production of membrane protein based systems such as biosensors [34]. Sotiropoulou *et al.* [35] evaluated the gating properties of nanoporous membranes (pore size in the range of 2-7 nm) obtained by recrystallization of isolated SL monomers of *Deinococcus radiodurans* on silicon substrates. They showed the presence of ionic currents gating through the pores of synthetic membrane.

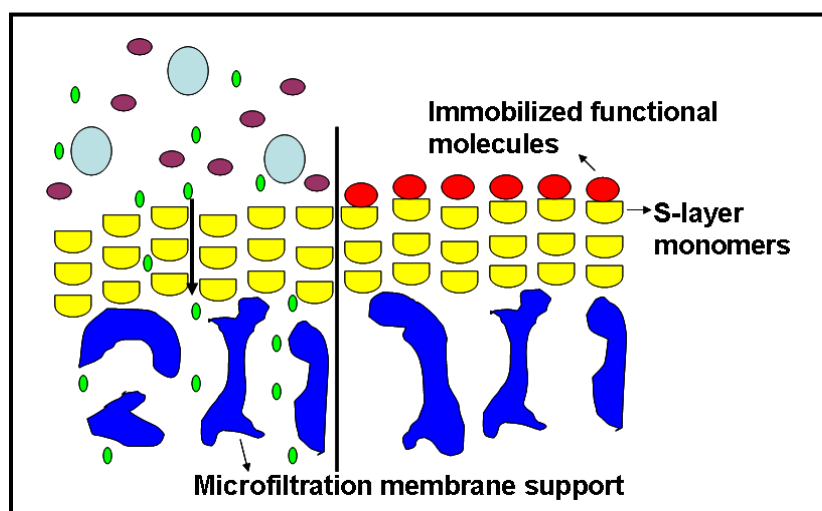


**Figure 7.** Schematic representation of SL ultrafiltration membranes (SUMs) (modified from [11])

#### 1.5.1.2. Immobilization Matrices

Due to the presence of regularly located free carboxyl groups on SL lattices, SLs have been appealing as matrices for the immobilization of functional groups in a well-defined fashion (Fig. 7).

It has been reported on an affinity matrix prepared from *Clostridium thermohydrosulfuricum* L111-69 SL lattice (hexagonal symmetry) by crosslinking the SL with glutaraldehyde to a membrane which was further used in affinity cross-flow filtration investigations [36]. In this study, free carboxyl groups of acidic aa were functionalized with carbodiimide in order to immobilize Protein A molecules onto the SL as a monolayer. Protein A is a ligand which can recognize and specifically bind to most of the mammalian antibodies [14]. Then, the obtained affinity micro-particles were investigated in terms of their IgG (immunoglobulin G) binding capacities. It has been found that even after eluting the bound IgG at very low pH values (1.5-2), after centrifugation at very high forces (40,000xg), after applying highly concentrated salt or chaotropic agents, organic solvents and different temperatures (-20° to 80°C), there was not any decrease in performance of the affinity matrix to IgG molecules after regeneration with glycine-NaOH. A schematic representation of affinity micro particles (AMPs) can be seen in Fig. 8.

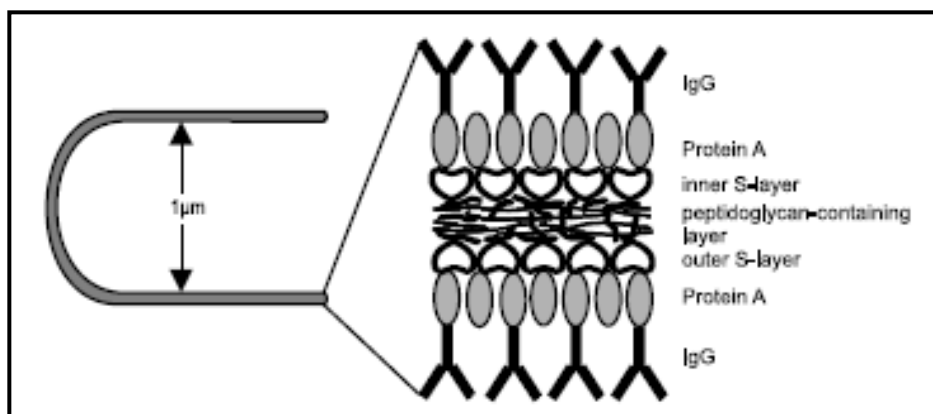


**Figure 8.** Scheme of affinity micro particles (AMPs) used for isolating IgG [14].

As densely packed monolayers, many enzymes have been immobilized on SL matrices for developing new biosensors. For example, invertase (270 kDa) has been linked to a hexagonally ordered SL lattice (2-3 enzyme molecules per each SL unit) with a retained enzymatic activity of 70%. Beta-glucosidase (66 kDa) was linked to an SL lattice via spacers (4-amino butyric acid or 6-amino caproic acid) and an activity of 160% was reached. A glucose sensor was developed by immobilizing an oxygen sensitive fluorescent dye on the SL which is linked to glucose oxidase enzyme molecules. A decrease in oxygen concentration due to the enzymatic reaction could be detected via the fluorescent dye, thus a measurable signal was produced [14].

Tschiggerl *et al.* [37] have constructed fusion proteins of SLs of *B. sphaericus* CCM 2177 (SbpA) and *Geobacillus stearothermophilus* PV72/p2 (SbsB) with F1 peptide (mimicking immunodominant epitope of Epstein–Barr virus (EBV)). The recombinant proteins were expressed in *Escherichia (E.) coli* and the SL chimeric proteins were able to self-assemble by localizing the F1 residue on the outer surface of the matrix making it possible to immobilize the corresponding antibodies to F1 proteins.

### 1.5.1.3. Vaccine Technology

SL (glyco)proteins have been used as carriers/adjuvants in vaccination and immunotherapy with both native and chemically or genetically modified forms. Since the conventional carriers such as tetanus or diptheria toxoids are obtained as monomers in solutions or as aggregated structures on aluminum salts, it is difficult to obtain a regular, well-defined reproducible immobilization of ligands on the carrier. At this point, SLs provide the advantage of self-assembly on solid supports as well as on liposomes or between air-water

interfaces having identical well-defined subunits possessing functional groups that can bind proteins or carbohydrate ligands at identical positions and orientations [14].

SLs were first studied as potential carrier/adjuvants for cancer vaccines by Smith *et al.* [38]. In conventional vaccines, an external adjuvant should be administered with the conjugate antigens to induce strong immune responses. Unfortunately there are just a few licensed adjuvants available for humans. Smith *et al.* [38] showed that the use of SLs as carriers is an excellent method to immunopotentiate the T-cell responses to small oligosaccharide haptens without the need of using any adjuvant. It has been concluded that SLs can be useful tools in mediating carrier/adjuvants for cancer immunotherapy by developing SL-carbohydrate based tumor antigens.

Moreover, SLs were used to study the immunotherapy of type I allergies by conjugating them with Betv1 which is known to be the major allergen of birch pollen [14]. Hollmann *et al.* [39] have isolated the SL proteins from lactobacilli and covered liposomes with them in order to conduct a stability analysis for a potential usage of coated liposomes as oral vaccine vesicles. Independent of the glycosylation of SL coat, liposomes covered with SLs showed an increased stability against pancreatic enzymes, salts, pH changes and thermal shocks. Additionally, effect of self-assembly of the fusion rSbpA-Betv1 protein on reduced allergenicity was studied showing no specific relationship or influence of self-assembly on allergic response [40].

#### **1.5.1.4. Functional Lipid Membranes**

Construction of functional biological membranes has been always in focus due to the fact that a large number of biological processes are membrane dependent. Investigations have been conducted generally with artificial planar lipid bilayers and liposomes until the need of obtaining the same system not fragile but robust and at the same time functional [11]. The idea was to mimic the archaeal cell envelope (Fig. 1) by using SLs. In this model, artificial lipid molecules are replacing the natural lipids of cell membrane and SLs from different microorganisms such as Bacillaceae are attached to one or both sides of the lipid membrane [4]. The application range of such layers (so-called “semifluid” membranes) (Fig. 9) has been broadened up to diagnostics, biosensor developments and physiology by the possibility of applying Langmuir-Blodgett (LB) techniques to such membranes [11, 41]. Voltage clamp



studies revealed that the SL support does not interfere with the function of the lipid membrane [42].

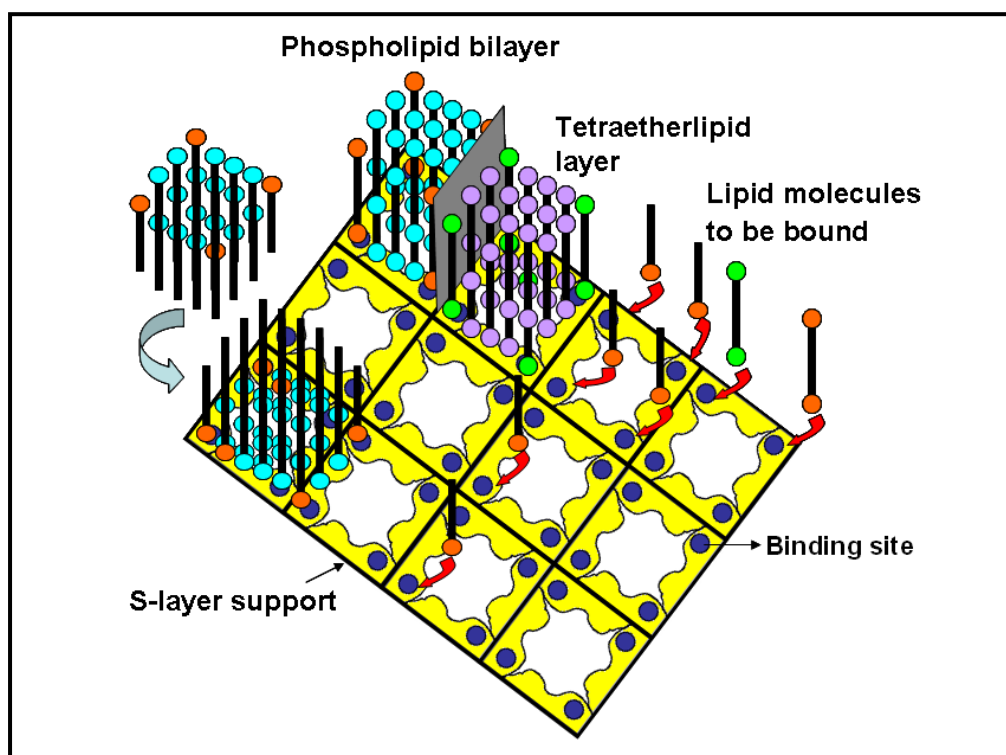


**Figure 8.** Scheme of a “semifluid” membrane consisting of an SL supporting a phospholipid bilayer or tetraetherlipid monolayer Langmuir film (modified from [11])

SL monomers have been also recrystallized on liposomes which are vesicles made of lipids (Fig. 10). Liposomes coated with SLs mimic the archeal cells. SLs covering the liposomes can be crosslinked and can become accessible for covalent attachment of molecules. This enables them to entrap molecules which make them an alternative tool in gene therapy, drug-targeting and drug delivery studies [7].

Ilk *et al.* [43] have expressed and isolated a functional chimeric SL-enhanced green fluorescent protein (SL-eGFP) and covered liposomes with this recombinant protein in order to observe the uptake of SL-eGFP coated liposomes by eukaryotic cells. Hollmann *et al.* [39] have isolated the SL proteins from lactobacilli and covered liposomes with them in order to conduct a stability analysis for a potential usage of coted liposomes in drug-delivery as an oral vaccine vesicle. Liposomes covered with SLs showed a remarkable stability against pancreatic enzymes, salts, pH changes and thermal shocks.

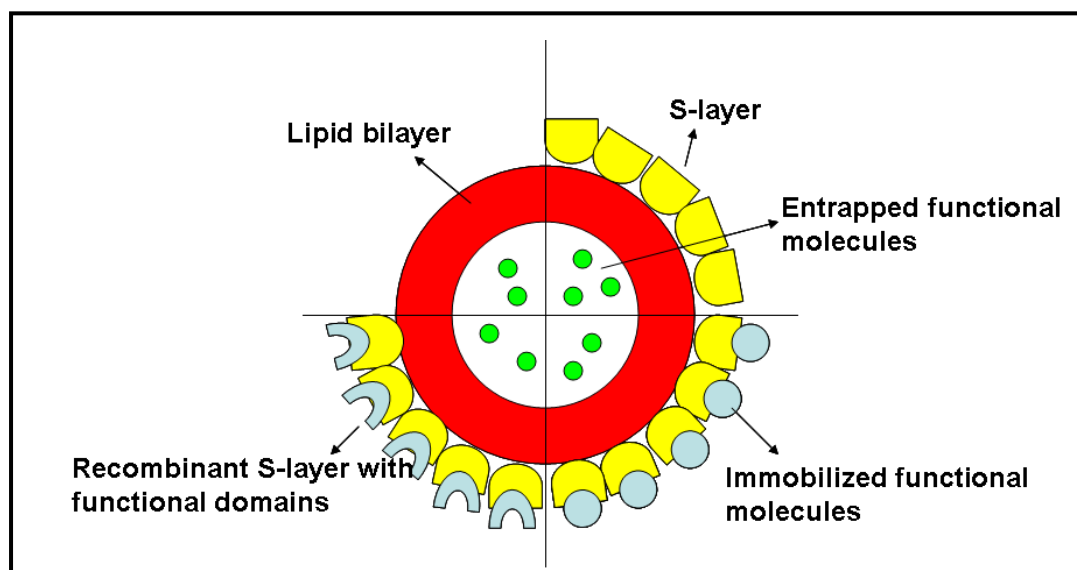


**Figure 10.** Schematic representation of a liposome coated with SL proteins, with molecules immobilized on SL proteins or with genetically engineered SL proteins with functional domains (modified from [11])

## 1.5.2. Nanotechnological Applications

As nanotechnological applications, native or tailored SL proteins can be recrystallized on various substrates such as silicon and gallium arsenide (microelectrical applications and integrated biosensors), glass (electro-optical and optical sensors) and noble metals (amperometric biosensor ultrathin electrodes) [5, 11]. Patterning of SLs recrystallized on solid surfaces is of importance to obtain ultrathin high-resolution resists [45]. SLs can also be used as templates for the production of regularly distributed nanoparticles (metallic i.e. cadmium, platinum, gold, iron, palladium, titanium, etc. or semiconducting) [46, 32].

### 1.5.2.1. Coupling of Inorganic Molecules

Due to the presence of regularly located free carboxyl groups on SL lattices, SLs have been appealing as matrices for the immobilization of functional groups in a well-defined fashion. A glucose sensor was developed by immobilizing an oxygen sensitive fluorescent dye on the SL in close vicinity to the glucose oxidase sensing layer. A decrease in oxygen concentration resulted in a measurable signal via the fluorescent dye [14]. Scheicher *et al.* [47] have developed optical oxygen sensors based on covalent immobilization of an oxygen sensitive Pt (II) porphyrin dye on SL matrices. This is another example that documents the potential of SL proteins as immobilization matrices for (bio-) sensor technology.

### 1.5.2.2. Formation of Metal Clusters

Inspired by the biomineralization potential of bacteria in nature (*e.g. Synechococcus sp.* strain GL24 for the biomineralization of gypsum and calcite [27]), the idea of depositing metallic particles in a well defined and controlled fashion has appeared. This would allow the formation of metal nanoparticle arrays with identical size and morphology on SL supported surfaces. The approach is first to self-assemble SL monomers on solid surfaces such as Si, then to deposit metal nanoparticles on the SL surface by chemical reduction of metal salts [49]. SLs have been used in nano-scale lithography as patterning templates for the formation of highly ordered and identical metal nanoparticle arrays that can be applied in downscaling of many components, *e.g.* logic and memory devices, in nanoelectronics.

One of the earliest studies reporting a method for nano-scale molecular lithography coupling SLs with metallic coatings was published by Douglas *et al.* [50]. SL of *S. acidocaldarius* with trimeric lattice symmetry (with a lattice constant of 22 nm) was recrystallized on a carbon substrate, coated with (Ta/W) metal particles by evaporation, and processed by milling to generate a 1 nm thick metal film with holes of the same periodicity as the SL template. Mertig *et al.* [49] have utilized SL of *Sporosarcina (S.) ureae* with tetragonal lattice symmetry and 13.2 nm lattice spacing as a protein template to chemically deposit platinum clusters leading to the formation of highly ordered Pt arrays. The unit cell of resulting metal clusters has a size of 13.2 nm x 13.2 nm. It was stated that not only the localization and size of the Pt particles, but also the metal lattice growth is determined by the underlying SL protein template.

Besides the chemical deposition of metal nanoparticles or ions on SLs, one can also apply electrodeposition. Allred *et al.* [51] reported isolation and recrystallization of SLs from different microorganisms on platinum coated gold surfaces, and subsequent electrodeposition of cuprous oxide as a step towards electrochemical nano-device fabrication. Recently, Wahl *et al.* [72] have investigated the electron-beam induced formation of nanoparticle arrays of platinum (Pt) and palladium (Pd) on the SL of *B. sphaericus* NCTC 9602. They obtained regular arrays of metal nanoparticles placed inside the pores of SL sheets.

Genetic engineering provides a promising tool to generate tailored functional SLs that maintain their ability to self-assemble and have some novel functions due to fused tags. Recently, Liu *et al.* [52] expressed a truncated version of SbsC protein from *G.*

*stearothermophilus* (exhibiting a hexagonal lattice symmetry and a 20 nm unit cell dimension) in *E. coli*. Recrystallization of the purified protein on Si wafers led to a reassembled 2D SL lattice with identical pore sizes of 9 nm. Metal oxide based materials, *e.g.* hafnium oxide, were first deposited on octadecyltrichlorosilane (ODTS) modified SL by area-specific atomic layer deposition and after the removal of SL proteins; periodic nano hafnium oxide patterns (~9 nm) were fabricated. Therefore SLs have the potential as future templates of sub-10 nm patterning that can be applied in downscaling of logic and memory devices in nanoelectronics. Badelt-Lichtblau *et al.* [53] have expressed, purified and recrystallized a chimeric protein composed of truncated versions of SbpA fused with a short affinity tag *Strep*-tag II and a cysteine residue. The tags and truncations had no effect on reassembly of SL. This self-assembly product exposed the free cysteine residue on the outer surface at defined and regular positions making it accessible to gold nanoparticles, thus providing a perfect template for patterning.

## **1.6. Expression of SL Proteins in Eukaryotic Systems**

Although heterologous expression of SL proteins has been widely studied in various prokaryotic host cells such as *E. coli* [67] and *Bacillus* species [94], there are only a few publications reported on SL expression in eukaryotic systems such as yeast and human cell lines [29, 57]. In this section, I wanted to concentrate on yeast *S. cerevisiae* as a eukaryotic model system for heterologous protein expression and on specific SL proteins used in this study.

### **1.6.1. *Saccharomyces cerevisiae* as a Host Organism in Protein Expression**

Yeasts are the ideal tools in experimental molecular biology. They were the first eukaryotic organisms whose whole genome was fully investigated and explored. The yeast genome project was conducted between 1992 and 1996, and the sequence of all 16 chromosomes was determined. Since many eukaryotic cellular functions are preserved in yeasts, they are the model organisms for investigating the eukaryotic cell structures and events. Since they are unicellular, they can be grown on simple media with defined composition in a controllable manner and since they can easily be manipulated genetically, yeasts are one of the most popular host organisms used in genomic researches and protein expression studies [54].

The yeast *S. cerevisiae* is the most extensively investigated eukaryote under cellular, molecular and genetic aspects. *S. cerevisiae* is a remarkable tool in large-scale production of

foreign proteins for medical, experimental and technological purposes. Unlike *E. coli* cells, which have toxic cell wall components and mammalian cells that can contain viral or oncogenic DNA, *S. cerevisiae* cells are generally recognized as safe (GRAS) and easy to handle since they can grow to high densities in short time on simple media [55]. Until now many intracellular and extracellular proteins of different organisms have been expressed and produced in large-scales in *S. cerevisiae* [56]. Some examples of foreign proteins being expressed in the host *S. cerevisiae* are shown in Table 2.

**Table 2.** Some proteins from different organisms expressed in yeast *S. cerevisiae*

Foreign Protein	Source Organism	Observation in Yeast	Reference
mSbsC-eGFP (bacterial SL protein)	<i>Bacillus</i>	Expression resulted in formation of tube-like network structures.	[57]
Cathepsin S (enzyme)	Human	Active forms of enzyme have been expressed and purified.	[58]
SspA (bacterial virulence protein)	<i>Salmonella</i>	SspA interacts with yeast actin.	[59]
Cre (recombinase)	Coliphage	Expressed foreign recombinase was functional.	[60]
L1 (major capsid protein)	Papillomavirus	Capsid proteins self-assembled into virus-like structures <i>in vivo</i> .	[61]
CP (coat protein)	Tobacco mosaic virus	The coat proteins self-assembled into rod-like structures <i>in vivo</i> .	[62]

*S. cerevisiae* cells can be found in three categories according to their mating types: *MAT a* (haploid), *MAT A* (haploid) and *MAT a/a* (diploid). Each haploid cell type can go into the mitotic cell cycle or budding yielding haploid daughter cells. Cells with different mating types can mate or fuse forming the diploid cells. Each diploid cell can go through meiosis and

sporulation yielding asci composed of 4 haploid spores [63]. The schematic representation of *S. cerevisiae* life cycle can be seen in Fig. 11.

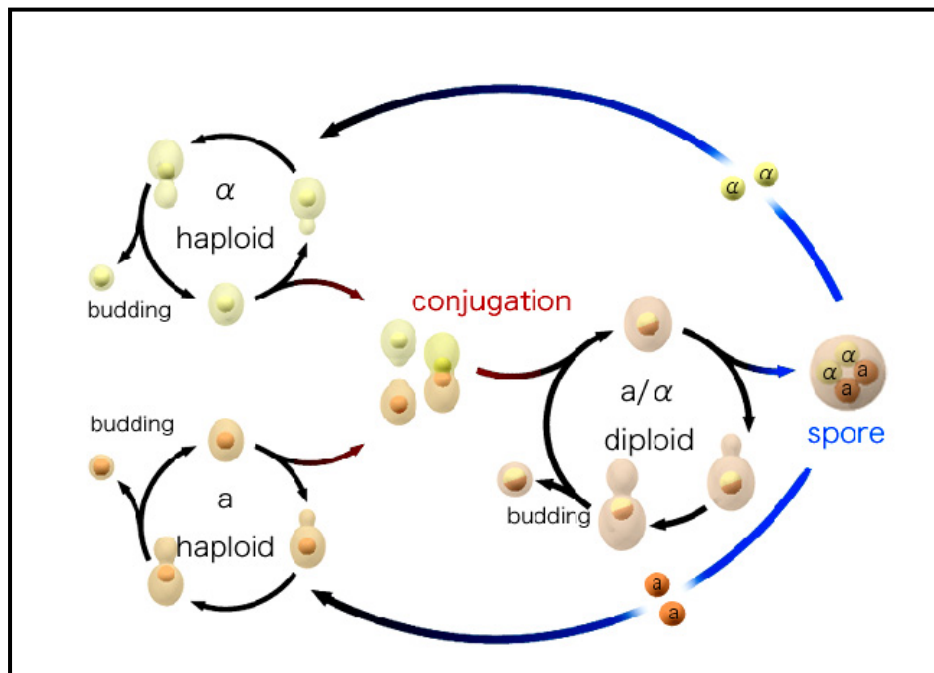


**Figure 11.** *S. cerevisiae* cell cycle ([http://en.wikipedia.org/wiki/File:Yeast\\_lifecycle.svg](http://en.wikipedia.org/wiki/File:Yeast_lifecycle.svg))

The cytoskeleton of *S. cerevisiae* cells consists of two types of elements: tubulin-based microtubules ( $\alpha$ -tubulin,  $\beta$ - tubulin and  $\gamma$ - tubulin) and actin-based microfilaments (Fig. 12). Actin networking is necessary for the cell polarization and transportation of the cell compartments during the cell cycle, while microtubules take role in forming the growth axis and positioning the mitochondria, Golgi apparatus and nucleus [64].

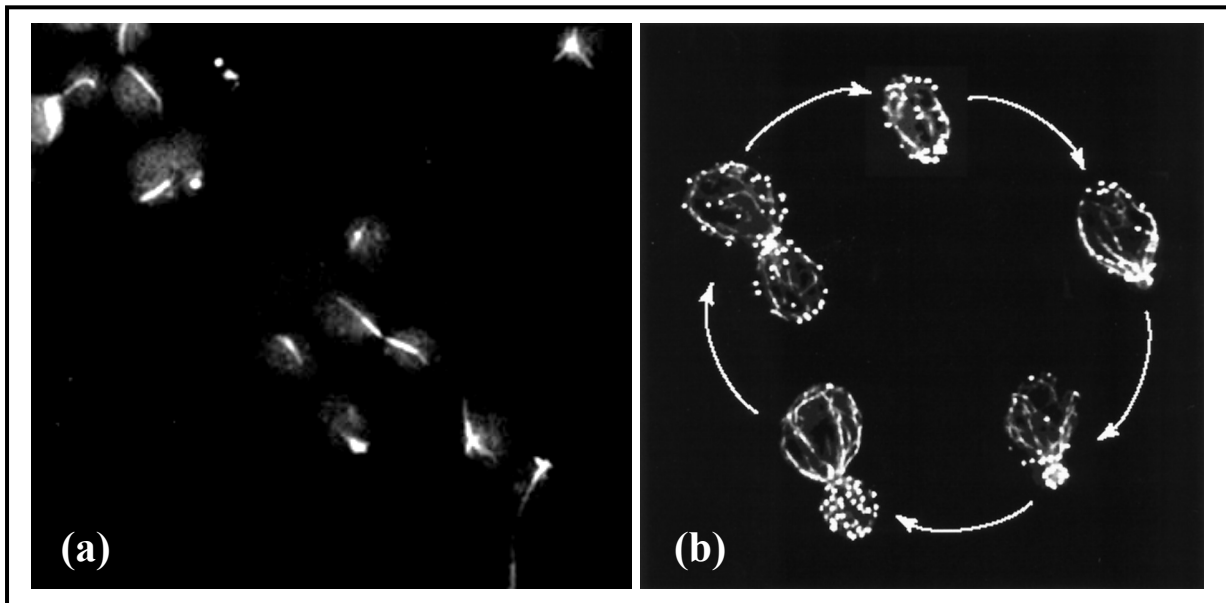


**Figure 12.** *S. cerevisiae* cytoskeletal elements. a) Microtubule localization in *S. cerevisiae* [65] b) Actin cytoskeleton dynamics during the cell cycle [66] (Detailed explanations of images can be found in indicated citations.)

### 1.6.2. SL Proteins Investigated in This Study

In this study we investigated the heterologous expression of three different SL proteins in yeast *S. cerevisiae* BY4741. SLs of interest were SbsC of *B. stearotherophilus* ATCC 12980 [69], s13240 of *B. stearotherophilus* DSM 13240 [8] and SslA of *S. ureae* ATCC 13881 [71] (Fig. 13).

*B. stearotherophilus* is an aerobic, endospore forming Gram-positive bacteria. Until now, SLs have been identified in 40 *Bacillus* species, but only a few of them have been genetically characterized, e.g. SbsA of *B. stearotherophilus* PV72/p6, SbsB of *B. stearotherophilus* PV72/p2 and SbsC of *B. stearotherophilus* ATCC 12980 [67]. SbsC possesses oblique lattice symmetry and is composed of 1099 aa with an N-terminal signal peptide of 30 aa. SbsC is a non-glycosylated polypeptide under optimal cell cultivation temperatures (55°C) [68]. It has been shown that the N-terminal region (aa 31-257), which is responsible for cell wall anchoring, and the C-terminal region (aa 920-1099) of this 112 kDa protein are not necessary for the oblique lattice structure formation [10]. S13240 is the SL protein of *B. stearotherophilus* DSM 13240. 113 kDa S13240 protein is composed of 1069 aa with a signal peptide of 30 aa. S13240 shows an oblique symmetrical structure like SbsC. It has been demonstrated that the two SLs have 95.6% homology for 270 aa of the N-terminal region [69]. Native and genetically engineered SLs have been studied for possible

applications in the field of biotechnology. For example, they were used to investigate immunotherapy of type I allergies by conjugating them with Bet v1 which is known to be the major allergen of birch pollen. It has been shown that a fusion construct of recombinant SbsC and Bet v1 (rSbsC-Bet v 1) displayed some important features making it an ideal allergy vaccine: less IgE binding and less mediator release, immune stimulatory effects, immune modulatory effects and the convincing constant ratio between allergen and adjuvant [40]. Blecha [69] has expressed an SL-eGFP fusion protein (SbsC-eGFP) in the yeast *S. cerevisiae* and in human HeLa cells that self-assemble into green fluorescent cylindrical tubular structures both *in vitro* and *in vivo*. He also investigated the mature and genetically engineered forms of S13240. The protein was expressed in *E. coli* and in the yeast *S. cerevisiae*. *In vitro* recrystallization studies showed again tube-like structures. This findings led us to investigate the large-scale production of such tubes and possible ways of metalizing them in order to get conducting materials for bionanotechnological applications. Recently, Liu *et al.* [52] expressed a truncated version of SbsC in *E. coli*. Recrystallization of the purified protein on Si wafers resulted in a reassembled 2D SL lattice with identical pore sizes of 9 nm. Metal oxide based materials were first deposited on the recrystallized SL leading to the formation of periodic nanoparticles of ~9 nm.

*S. ureae* is a Gram-positive bacterium intimately related to *B. pasteurii* and *B. sphaericus* having an SL protein called SslA which has a tetragonal symmetry. The three-dimensional structure of the regular outermost layer of *S. ureae* was first investigated in 1986 [70]. According to that study, SslA has a tetragonal symmetry with a lattice constant of 12.9 nm and a minimum thickness of 6.6 nm. The latest findings showed that this SL protein has a lattice spacing of 13.2 nm and a pore diameter of 2 nm [49]. The *sslA* gene structure has recently been explored, and it was found that the encoded 116 kDa protein is composed of 1097 aa with a signal peptide of 30 aa [44]. Mertig *et al.* [49] have utilized SslA as a protein template to chemically deposit platinum clusters. They observed the formation of highly ordered Pt arrays. The resulting metal arrays showed lattices with a unit cell size of 13.2 nm x 13.2 nm. They concluded that the localization, size and the metal lattice growth of Pt particles were determined by the underlying SslA protein template.



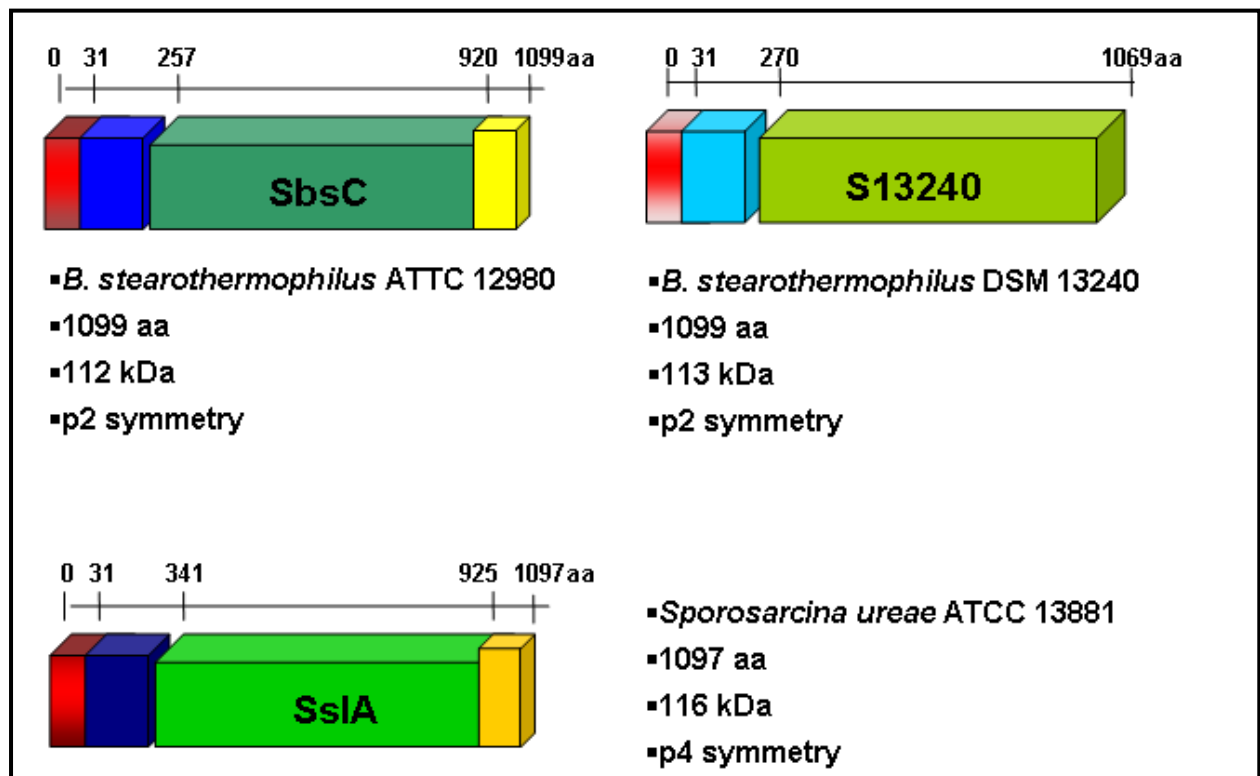


**Figure 13.** SL proteins investigated in this study. Red, blue, green and yellow areas stand for signal peptides, cell wall binding sites, domains required for self-assembly and domains not necessary for self-assembly respectively.

## II. Materials and Methods

### 2.1. Materials

Equipments, kits and similar products, chemicals, buffer and solutions, media, cell strains, primers and plasmids used in this study are listed in this section.

#### 2.1.1. Equipments

Equipment	Model	Company
Agarose gel electrophoresis System	B2/B1A	PeqLab
Blotter	-	PeqLab
Centrifuge	Avanti™ J25	Beckman-Coulter
Centrifuge	Biofuge fresco	Heraeus
Centrifuge	Biofuge pico	Heraeus
Centrifuge	5417 R	Eppendorf
Centrifuge	Sigma 3K 30	Sigma
DNA/protein gel chambers	-	PeqLab / Hoefer
Electroporation device	Gene pulser II	Bio-Rad
Fluorostar microplate reader	Fluorostar Omega	BMG Labtech
Fluorescence microscope	Axio imager	Zeiss
Fluorescence microscope	BZ-8100E	Keyence
Fluorescence microscope 4D Imaging System	Axiowert 200M	Zeiss
Heating blocks	-	Eppendorf / Kleinfeld
Herring Sperm DNA	-	Invitrogen
Incubators	-	WTB Binder / Heraeus
Laser scanning confocal microscope	DM 6000B	Leica
Magnet steering system	Combimag RCT	IKA
Nephelometer	Nephelostar galaxy	BMG Labtech
pH meter	766 Calimatic	Knick
Power supplies	-	Bio-Rad / Pharmacia

		Biotech
Scanning electron microscope	LEO DSM 982	Gemini
Spectrophotometer	Ultrospec 3000	Pharmacia Biotech
Thermocycler	Cyclone 96	PeqLab
Thermocycler	Primus	MWG-Biotech
Ultracentrifuge	Optima™ MAX	Beckman-Coulter
Vortexers	-	IKA

### 2.1.2. Kits and Similar Products

Product	Company
NucleoBond® plasmid purification	Macherey-Nagel
Invisorb® fragment cleanup kit	Invitek
Dc protein assay	Bio-Rad
ECLPlus western blotting detection system	Amersham Biosciences
Immobilon-P PVDF transfer membrane	Amersham Biosciences
96-well plates	Nunc
96-well plates with transparent bottom	Brand
Easybreathe membrane	Roth
VS dialysis membrane	Millipore

### 2.1.3. Chemicals

Chemical	Company
Acetic acid	AppliChem
Acetone	Prolabo
Acrylamide / Bisacrylamide	Sigma
Adenine	Serva
4-(2-aminoethyl)-benzenesulfonyl fluoride (AEBSF)	AppliChem
Agar	Formedium
Agarose	BioZym
Ammonium persulfate (APS)	Merck
Ampicillin (Amp)	AppliChem

Anti-GFP antibody	Roche
Anti-mouse antibody	GE Healthcare
BODIPY 650/665 phalloidin	Molecular Probes
Boric acid (H <sub>3</sub> BO <sub>3</sub> )	Roth
Bovine serum albumin (BSA)	Sigma
Bromophenol blue	Serva
Calcium chloride (CaCl <sub>2</sub> )	Roth
4, 6-diamidino-2-phenylindole dihydrochloride (DAPI)	AppliChem
dNTPs	NEB
Dithiothreitol (DTT)	AppliChem
Ethanol	Merck
Ethidium bromide (EB)	Sigma
Ethylendiamine-tetraacetic acid (EDTA)	Roth
Formaldehyde	Roth
Glycerol	Roth
Glycine	Roth
Glucose	Roth
Guanidine hydrochloride (GuHCl)	Roth
Herring sperm DNA	Invitrogen
Isopropanol	Roth
L-Histidine HCl	Roth
Lithium acetate (LiAc)	Roth
L-Leucine	Roth
L-Lysine HCl	Roth
L-Methionine	Roth
L-Tryptophan	Roth
Methanol	Fisher Chemicals
Magnesium chloride-anhydrous (MgCl <sub>2</sub> .6H <sub>2</sub> O)	AppliChem
Magnesium sulphate-anhydrous (MgSO <sub>4</sub> .7H <sub>2</sub> O)	Roth
N, N, N', N'-tetramethylethylenediamine (TEMED)	AppliChem
Peptone / Tryptone	Formedium
PEG 6000	Roth
Potassium acetate (CH <sub>3</sub> COOK)(KOAc)	Merck

Potassium chloride (KCl)	Roth
K <sub>2</sub> PtCl <sub>4</sub>	Aldrich
Potassium dihydrogenphosphate (KH <sub>2</sub> PO <sub>4</sub> )	Merck
Protease inhibitor cocktail	Roche
Skimmed milk powder	AppliChem
Sodium azide (NaN <sub>3</sub> )	Aldrich
Sodium chloride (NaCl)	Roth
Sodium dodecyl sulphate (SDS)	AppliChem
Sodium carbonate (Na <sub>2</sub> CO <sub>3</sub> )	Roth
Sodium hydroxide (NaOH)	AppliChem
Sodium phosphate (NaHPO <sub>4</sub> )	AppliChem
Disodium hydrogen phosphate (Na <sub>2</sub> HPO <sub>4</sub> )	AppliChem
Sorbitol	AppliChem
Tris(hydroxymethyl)aminometane (Tris) base	AppliChem
Triton X-100	Sigma
Tween 20	Roth
Uracil	Calbiochem
Yeast extract	Formedium
Yeast Nitrogen Base (YNB)	Formedium

#### 2.1.4. Enzymes

Enzyme	Company
Phusion DNA polymerase	Finnzymes
Restriction enzymes	NEB
Ribonuclease (RNase) A	Macherey-Nagel
T4 DNA ligase	Promega
Zymolyase 20T (20,000 U/mg)	Seikagaku Biobusiness Co

#### 2.1.5. Buffers and Solutions

Buffer and solutions used in this study can be grouped in two parts: commercial and self-made buffers and solution which were listed below.

**2.1.5.1. Commercial Buffers and Stock Solutions**

<b>Buffer</b>	<b>Company</b>
DNA loading buffer 6X	Fermentas
PBS	PAA
Phusion HF buffer	Finnzymes
Restriction enzyme buffers	NEB
T4 DNA ligase buffer 10X	Promega

**2.1.5.2. Self-made Buffers and Solutions**

<b>Buffer/Solution</b>	<b>Application</b>	<b>Components</b>	
TBE buffer (10x)	Agarose gel electrophoresis	Tris	89 mM
		Boric acid	89 mM
		in EDTA	2 mM (pH 8.0)
Tubing preparation buffer I	Dialysis	Na <sub>2</sub> CO <sub>3</sub>	2% (w/v)
		in EDTA	1 mM (pH 8.0)
Tubing preparation buffer II	Dialysis	EDTA	1 mM (pH 8.0)
Sorbitol solution	<i>In situ</i> protein extraction	Sorbitol	1.2 M
		in Tris-HCl	10 mM (pH 7.2)
Spheroplastic buffer	<i>In situ</i> protein extraction	Zymolyase 20T	10 mg/ml
			in sorbitol solution
Metallization buffer	Metallization	NaN <sub>3</sub>	3 mM
		MgCl <sub>2</sub>	1 mM
		in NaHPO <sub>4</sub> /	
		Na <sub>2</sub> HPO <sub>4</sub>	50 mM
GTE solution	Plasmid isolation	Tris-HCl	1 M (pH 8.0)
		EDTA	0.5 M
		Glucose	40% (w/v)

KOAc solution	Plasmid isolation	KOAc Glacial acetic acid dH <sub>2</sub> O	60 ml (5 M) 11.5 ml 28.5 ml
Solution I	Plasmid isolation	NaOH SDS	0.2 M 0.1% (w/v)
<i>Separating gel (12%)</i>	SDS-PAGE	Acrylamide Bisacrylamide SDS APS TEMED Tris-HCl	12 % (w/v) 0.1% 0.1% (w/v) 0.1% (w/v) 0.1% (v/v) 125 mM (pH 6.8)
Stacking gel (4%)	SDS-PAGE	Acrylamide Bisacrylamide SDS APS TEMED Tris-HCl	12% (w/v) 0.32% 0.1% (w/v) 0.1% (w/v) 0.1% (v/v) 375 mM (pH 8.8)
Running buffer	SDS-PAGE	Tris-base Glycine SDS	25 mM 192 mM 0.1% (w/v)
Protein loading buffer (6x)	SDS-PAGE	Glycerol SDS Bromophenol blue DTT Tris-HCl	30% (w/v) 10% (w/v) 0.1% (w/v) 600 mM (freshly added) 300 mM(pH 6.8)
LiAc solution	Yeast transformation	LiAc	1 M
PEG solution	Yeast transformation	PEG	50%

TBS buffer (10X)	Western blot	NaCl	137 mM
		Tris-HCl	20 mM (pH 7,4)
TBS-T buffer	Western blot	1 x TBS	
		Tween 20	0.1% (v/v)
Transfer buffer	Western blot	Glycine	192 mM
		Tris-base	25 mM
		Methanol	5% (v/v)
		SDS	0.1% (w/v)
Blocking solution	Western blot	5% (w/v) Skimmed milk powder dissolved in TBS-T buffer	

### 2.1.6. Media

Media	Components
LB (Luria-Bertani) broth/agar	Yeast extract 0.5% (w/v) Peptone 1% (w/v) NaCl 0.5% (w/v) (Agar) 2.5% (w/v)
YNB (Yeast Nitrogen Base) broth/agar	YNB 1.7 g/l (NH <sub>4</sub> ) <sub>2</sub> SO <sub>4</sub> 5 g/l Aminoacids (1x) Glucose 2% (w/v) (Agar) 2% (w/v)
Aminoacids (100x)	Adenine 2 g/l Histidine 10 g/l Leucine 10 g/l Lysine 10 g/l Methionine 10 g/l Uracil 2 g/l
YPD (Yeast extract-Peptone-Dextrose) broth/agar	Yeast extract 1% (w/v) Peptone 2% (w/v) Glucose 2% (w/v) (Agar) 2% (w/v)



SOC (Super Optimal Broth) medium	Yeast extract	0.5% (w/v)
	Peptone	2.0% (w/v)
	NaCl	10 mM
	CH <sub>3</sub> COOK	2.5 mM
	MgCl <sub>2</sub> x 6H <sub>2</sub> O	10 mM
	MgSO <sub>4</sub> x 7H <sub>2</sub> O	10 mM
	Glucose	20 mM
Sporulation medium	KCH <sub>3</sub> COOH	10 g/l
	Ade	0.01 g/l
	Lys	0.01 g/l
	Leu	0.01 g/l
	Trp	0.01 g/l
	His	0.01 g/l

### 2.1.7. Strains

Strain	Genotype	Source
<i>E. coli</i> Top10	<i>F mcrA</i> Δ( <i>mrr-hsdRMS-mcrBC</i> ) Φ80 <i>lacZ</i> Δ <i>M15</i> , Δ <i>lacX74</i> , <i>deoR</i> , <i>recA1</i> , <i>araD319</i> Δ( <i>araA-leu</i> ), 7697 <i>galU</i> , <i>galK</i> , <i>rpsL</i> ( <i>Str<sup>R</sup></i> ), <i>endA1</i> , <i>nupG</i>	INVITROGEN
<i>S. cerevisiae</i> BY4741	<i>MATa</i> , <i>his3Δ1</i> , <i>leu2Δ0</i> , <i>met15Δ0</i> , <i>ura3Δ0</i>	EUROSCARF
<i>S. cerevisiae</i> BY4742	<i>MATα</i> , <i>his3Δ1</i> , <i>leu2Δ0</i> , <i>lys2Δ0</i> , <i>ura3Δ0</i>	EUROSCARF
<i>S. cerevisiae</i> W303	<i>MATa</i> , <i>trp1::YFP-TUB1::TRP1</i> , <i>ura3-1</i> , <i>his3-11,15</i> , <i>leu2-3,112</i> , <i>ade2-1</i> , <i>can1-100</i>	[90]

### 2.1.8. Primers

Primer	Sequence	Restriction enzyme
SslAforBamATG	TATATATAGGATCCATGGCTGAATTACAGAT GTAAAAGA	<u>Bam</u> HI
SslArevXho	TATATATACTCGAGCGAACTAATACTAATGC ATTTGC	<u>Xho</u> I

SslArevXhoArgTEV	ATATATA <u>CTCGAGAC</u> CTTGAAAATAAAGGTTT TCGCGTCGGCGTCGGCGTCGCGAACTAATAAC TAATGCATTTGC	<u>XhoI</u>
SslArevXhoHisTEV	ATATATA <u>CTCGAGAC</u> CTTGAAAATAAAGGTTT TCGTGATGGTGATGGTGATGCGAACTAATAAC TA ATGCATTTGC	<u>XhoI</u>
SslArevXhoLysTEV	ATATATA <u>CTCGAGAC</u> CTTGAAAATAAAGGTTT TCCTTTTTCTTTTTCTTTTTTCGAACTAATAACTA ATGCATTTGC	<u>XhoI</u>
matS13240forBamATG	TATATATA <u>GGATCC</u> ATGGCAACGGACGTTGCG ACG	<u>BamHI</u>
matS13240revXho	TATATATA <u>CTCGAGG</u> TTTTTAACTACAGTTGTA GCATTATCGGCAA	<u>XhoI</u>
S13240revXhoArgTEV	TATATATA <u>CTCGAGAC</u> CTTGAAAATAAAGGTT TTCGCGTCGGCGTCGGCGTCGGTTTTTAACTAC AGTTGTAGCATTATC	<u>XhoI</u>
S13240revXhoHisTEV	TATATATA <u>CTCGAGAC</u> CTTGAAAATAAAGGTT TTCGTGATGGTGATGGTGATGGTTTTTAACTAC AGTTGTAGCATTATC	<u>XhoI</u>
S13240revXhoLysTEV	TATATATA <u>CTCGAGAC</u> CTTGAAAATAAAGGTT TTCCTTTTTCTTTTTCTTTTTGTTTTTAACTACA GTTGTAGCATTATCGGCAA	<u>XhoI</u>
matSbsCforBamATG	TATATATA <u>GGATCC</u> ATGGCAACGGACGTGGCG AC	<u>BamHI</u>
matSbsCrevXho	TATATATA <u>CTCGAG</u> TTTGGCCAGCATTTCAG CAAC	<u>XhoI</u>
tRFP-XhoI-for	TATATATA <u>CTCGAG</u> ATGAGCGAGCTGATCAAG GAGAAC	<u>XhoI</u>

tRFP-KpnI-rev	TATATATAGGTACCTTATCTGTGCCCCAGTTTG CTAGG	<i>KpnI</i>
---------------	--	-------------

### 2.1.9. Plasmids

Plasmid	Source
p426GPD-SslA(aa31-925)-eGFP	This study
p426GPD-SslA(aa31-925)-Arg-TEV-eGFP	This study
p426GPD-SslA(aa31-925)-His-TEV-eGFP	This study
p426GPD-SslA(aa31-925)-Lys-TEV-eGFP	This study
p426GPD-S13240(aa31-1069)-eGFP	[69]
p426GPD-S13240(aa31-1069)-Arg-TEV-eGFP	This study
p426GPD-S13240(aa31-1069)-His-TEV-eGFP	This study
p426GPD-S13240(aa31-1069)-Lys-TEV-eGFP	This study
p426GPD-eGFP	[69]
p426GPD-mSbsC(aa31-1099)-eGFP	[69]
p426GPD-mSbsC(aa31-1099)-TurboRFP	This study

## 2.2. Methods

In this section, methods of DNA and protein techniques with other experimental works like growth and fluorescence measurements, live cell imaging, sporulation, colocalization, recrystallization of SL monomers, metallization studies and microscopy were presented.

### 2.2.1. DNA Techniques

Applied DNA methods were mainly composed of DNA gel electrophoresis, plasmid DNA isolation, polymerase chain reaction, DNA purification, restriction enzyme digestion, ligation and transformation which are listed below.

#### 2.2.1.1. DNA Gel Electrophoresis

0.8% or 1% (w/v) agarose was dissolved in 1x TBE buffer (section 2.1.5.2). After boiling the mixture in the microwave oven, the solution was let to cool down. EB was added to the solution with the final concentration of 0.1 µg/ml before the gel was poured to the chamber. After polymerization, the gel was loaded with DNA samples. Fragments were separated in 1x

TBE buffer at constant voltage of 80 to 120 V. Detection was performed with the UV-light of the wavelength of 312 nm. Separated fragments were compared by size with the DNA fragments of the standard ladder, obtained upon digestion of  $\lambda$  phage DNA with *Bam*HI and *Hind*III restriction enzymes.

### 2.2.1.2. Isolation of Plasmid DNA from *E. coli* Cells

Alkaline lysis method was applied for the isolation of plasmid DNA. *E. coli* cultures were grown overnight. 2-4 ml of culture were poured into microfuge tubes and centrifuged at 4,000– 5,000 x g for 5 min. After the pellet was resuspended in 200  $\mu$ l of GTE solution, the 400  $\mu$ l of Solution I was added. The suspension was mixed by turning the tubes 6 times upside down and incubated on ice for 5 min. After the addition of 300  $\mu$ l of KOAc solution, the mixture was vortexed and incubated on ice for 5 min. Following the centrifugation for at 13,000 x g for 5 min, 600  $\mu$ l of isopropanol was added. After the centrifugation at 13,000 x g for 5 min at 4 °C, the pellet was washed twice with ice-cold 70% ethanol (after each wash step the suspension was centrifuged for 5 min at 13,000 x g). The pellet was dried for 5 - 10 min in the Eppendorf concentrator and resuspended in 50  $\mu$ l of distilled water. Alternatively, NucleoBond<sup>®</sup> Plasmid Purification kit was used according to the manufacturer instruction to obtain highly purified DNA e.g. for sequencing and cloning methods.

### 2.2.1.3. Polymerase Chain Reaction (PCR)

The genes of interest were amplified by standard PCR from the corresponding plasmid sources with the primers listed in section 2.1.8. The following formula was used in order to calculate the annealing temperatures of the primers:

$$T_m = 69,4^{\circ}\text{C} + 0,41 \times (\text{GC-Percent}) - 650 / \text{Primer length} - 6^{\circ}\text{C} \text{ (MWG-BIOTECH)}$$

The PCR mix was composed of:

Component	Final concentration
PCR-buffer (10x)	1 x
Template (x ng/ $\mu$ l)	1 ng/ $\mu$ l
dNTP mix (each dNTP 10 mM)	0,2 mM
Forward primer (100 pmol/ $\mu$ l)	1,5 pmol/ $\mu$ l
Reverse primer (100 pmol/ $\mu$ l)	1,5 pmol/ $\mu$ l

DNA polymerase (5 U/μl)	2,5 U
Total volume (H <sub>2</sub> O up to :)	100 μl

The following PCR program was used:

4 min 95°C	Initial denaturation	1x
1 min 94°C	Denaturation	30x
1 min Ta	Annealing	
n min 72°C	Elongation	
10 min 72°C	Final elongation	1x

#### ***2.2.1.4. DNA purification techniques***

Purification of PCR products and the DNA fragments of interest from agarose gel were the two methods applied.

##### ***2.2.1.4.1. Purification of PCR Products***

Invisorb® Fragment Cleanup kit was used for purifying the amplified PCR products according to the manufacturer's instructions.

##### ***2.2.1.4.2. DNA Fragment Purification from Gel***

A gel purification step was performed to purify the fragments with the size of interest. For this purpose, the DNA mixture was run on an agarose gel and a quick picture was made by a short-term UV irradiation. Fragments of interest were cut out of the gel and purified by Invisorb® Fragment Cleanup kit according to the manufacturer's instructions.

##### ***2.2.1.5. Digestion of DNA with Restriction Endonucleases***

1 μg of DNA was digested with 1 U of the corresponding restriction enzyme for 3-4 h at the permissive temperatures e.g. 37 °C in the appropriate buffer in a reaction volume of 50 μl. In double digestion reaction reactions, the buffer having the maximum activity for both enzymes was used.

##### ***2.2.1.6. Ligation***

In the ligation reaction, the target vector and the DNA fragment were mixed with a molar ratio of 1:3 with T4 DNA ligase (2U) and T4 DNA ligase buffer (1X) in a final volume of 10 μl and incubated at 4 °C or 16 °C overnight.

### ***2.2.1.7. Transformation***

Transformation of *E. coli* cells was performed by electroporation after preparing the electrocompetent cells. Yeast cells were transformed by LiAc method. Both methods are explained below.

#### **2.2.1.7.1. Preparation of Electrocompetent Cells**

An overnight *E. coli* culture was diluted 1:100 with LB medium to a final volume of 400 ml and grown until OD<sub>600</sub> of 0.5 at 37 °C. Cells were harvested by centrifugation at 4,000 x g for 10 min at 4 °C. Next, pellets were washed twice in 200 ml of ice-cold ddH<sub>2</sub>O and centrifuged at 4,000 x g for 10 min at 4 °C. Then, each pellet was resuspended in 40 ml of ice-cold 10% (v/v) glycerol and centrifuged at 4,000 x g for 10 min at 4 °C. Cells were subsequently resuspended in 1 to 2 ml of ice-cold 10% (v/v) glycerol and aliquoted per 40 µl into sterile microfuge tubes. Obtained aliquotes were stored at –80 °C and thawed on ice prior to use.

#### **2.2.1.7.2. Transformation of *E. coli* Cells by Electroporation**

For transformation, 5-8 µl of ligation mixture which were dialyzed in a sterile petri dish against ddH<sub>2</sub>O using a piece of Millipore VS membrane in order to get rid of the salts was gently mixed with 40 µl of electrocompetent *E. coli* cells and transferred into the prechilled (in ice) electroporation cuvette. Electroporation was performed by the Gene pulser II setup (voltage: 2,5 kV; capacity: 25 µF; resistance: 200 Ω ). An optimal pulse duration of 4.5 – 5 ms was estimated for a cuvette with 2 mm gap between the electrodes. After the pulse, 1 ml of pre-warmed (37 °C) SOC medium was immediately added to the transformation mixture. The cell suspension was taken into a microfuge tube and incubated at 37 °C for 1 hour. Next, the suspension was centrifuged at 2,500 x g for 1 min, 900 µl of the supernatant was discarded and the pellet was resuspended in the remaining solution. 10 µl of the final suspension was spreaded on an LB agar supplemented with Amp and Tet and incubated at 37 °C overnight.

#### **2.2.1.7.3. Transformation of Yeast Cells**

Yeast cells were transformed using the LiAc procedure [91]. Shortly, an overnight grown *S. cerevisiae* culture was diluted to OD<sub>600</sub> of 0.5 with YPD to a final volume of 20-50 ml and grown until OD<sub>600</sub> of 2.0 at 30 °C 140-170 rpm for 3-5 h. 1 ml of cells was harvested by centrifugation at 3,000 x g for 5 min. The pellet was first washed with 1ml of ddH<sub>2</sub>O and then with 1ml of 100 mM LiAc solution (after each wash step the suspension was centrifuged

at 3,000 x g for 5 min). To the resulting pellet these components were added to a final volume of 360  $\mu$ l in this order:

1. 240  $\mu$ l 50% PEG
2. 36  $\mu$ l 1 M LiAc
3. 10  $\mu$ l ssDNA (Herring Sperm DNA which was denatured at 95 °C for 5 min during the last centrifugation step)
4. 1  $\mu$ g plasmid
5. sddH<sub>2</sub>O

This suspension was incubated at 42 °C for 40 min (heat shock), centrifuged at maximum speed for 15 s and resuspended in 50-100  $\mu$ l sddH<sub>2</sub>O which were then spread on a YNB agar supplemented with required aa to be incubated at 30 °C for 2-3 days until the colonies would appear.

### **2.2.2. Protein Techniques**

Proteins were detected by SDS-PAGE and Western blot analyses as explained below.

#### ***2.2.2.1. SDS-PAGE and Western Blot Analysis***

Electrophoretic separation of the proteins on polyacrylamide gel under denaturing conditions (in presence of SDS) was performed according to Laemmli [92]. Protein gels consisting of 4% stacking gel and 12% separating gel were prepared. First, the separating gel was prepared by pouring the gel solution into the vertically aligned protein gel chamber and layered with isopropanol. After polymerization at room temperature (RT) for approximately 1 hour, isopropanol was removed and the stacking gel solution was pored onto the polymerized separating gel. A comb was inserted and the chamber was left for the polymerization of stacking gel. Next, the chamber was placed into the Mighty small II vertical gel electrophoresis system and filled with 1x Running buffer. To prepare the samples, yeast cells were grown overnight to OD<sub>600</sub> of 2.0 at 30°C in supplemented YNB medium with glucose as the carbon source. Cell extracts were obtained by breaking the cells with glass beads by vigorous vortexing in the presence of protease inhibitors (1 mM AEBSF, and 1x Protease Inhibitor Cocktail). 10  $\mu$ g of total protein was loaded to the gel. SDS-PAGE was performed first at 80V (for the stacking gel) and then at 120 V (for the separation gel). Gels were stained in Coomassie blue solution (section 2.1.4.4.) for 30 – 60 min at RT and washed subsequently with destaining solution (section 2.1.4.4.) until an optimal signal contrast was achieved. Proteins were transferred to a PVDF membrane using the semi-dry method for 2.5 h at RT at

1.5 mA/cm<sup>2</sup>. Protein marker was signed with a pen on the membrane and the membrane was blocked at least 1h at RT or over night at 4°C with 5% (w/v) non-fat dry milk in TBS-T. Membrane was incubated with monoclonal mouse anti-GFP antibody (1:1,000) in 5% (w/v) non-fat dry milk in TBS-T for 1h at RT and then washed three times for 5-10 minutes in TBS-T. Horseradish peroxidase-conjugated anti-mouse antibody (1:5,000) in milk was added to the membrane and incubated for 45 min at RT. Before the antigen-antibody complexes were visualised by enhanced chemiluminescence (ECL plus), the membranes were washed three times for 5-10 minutes with TBS-T.

#### **2.2.2.2. Protein Concentration Assay and Cell lysis**

Protein concentration was determined with the Lowry assay based Bio-Rad Dc protein assay system according to the manufacturer's instructions. Different concentrations of BSA were used for the preparation of the standard curve.

#### **2.2.3. Growth and Fluorescence Measurements**

Growth characteristics of yeast cells expressing S-layer proteins were determined by measuring the optical density in 96-well plates in the Nephelometer. 250 µl of cells were inoculated per well in YNB medium with an initial OD<sub>600</sub> of 0.1. Plates were closed with an "easybreathe"-membrane and incubated at 30°C with shaking. Data were evaluated with the NEPHELOstar control software.

For the fluorescence measurements, 250 µl of cells with OD<sub>600</sub> of 0.1 were inoculated in 96-well black plates with transparent bottom. Plates were incubated at 30°C with shaking in the Fluorostar microplate reader (FLUOROstar Omega, BMG Labtech) with a high energy xenon flashlamp as the light source. Fluorescence reading was performed in top reading measurement mode at excitation of 485 nm and emission of 520 nm. Data were evaluated by the FLUOROstar software.

#### **2.2.4. In vivo Protein Structure Investigation**

*S. cerevisiae* BY4741 cells expressing mSbsC-eGFP were grown overnight at 30°C in YNB medium supplemented with Leu, His, Met and glucose as the carbon source. 1 ml of the culture was centrifuged (3,500 x g, 5 min), resuspended in YNB medium and investigated with a fluorescence microscope (see below).



### **2.2.5. Live Cell Imaging**

For time lapse microscopy of budding cells, yeast cells were immobilized in an agar block as described [93]. Cells were grown in supplemented YNB medium with glucose as the carbon source to OD<sub>600</sub> of 1.0-1.5. 1 ml culture was centrifuged (3,500 x g, 5 min) and resuspended in YNB broth. 5 µl of the suspension was pipetted on a glass coverslip and covered with a piece of YNB agar. In order to prevent drying, the agar slice was sealed with nail polish, and 10 µl of YNB medium was dropped on top of it before placing the glass slide on the agar. Time-lapse experiments were conducted with temperature control at 30°C in 10 min intervals for 6-10 h with the 4D live imaging system.

Live mating experiments were performed similarly. *S. cerevisiae* BY4741 (*MATa*) cells expressing SbsC-eGFP and the mating partner *S. cerevisiae* BY4742 (*MATα*) cells were grown overnight on YNB medium supplemented with Leu, His, Met (BY4741) / Lys (BY4742) and glucose as the carbon source. From each plate, with the help of sterile toothpicks, equal amounts of cells were taken, mixed in an eppendorf tube and resuspended in YNB medium. 5 µl of the suspension were pipetted onto a glass coverslip and a piece of YPD agar was laid over the drop of cells. In order to prevent evaporation, the agar slice was sealed with nail polish and 10 µl of YNB medium was dropped onto it before placing the glass slide over the agar. Mating of cells was investigated at RT with a fluorescence microscopy (ZEISS). Time-lapse experiments were conducted for 2-3 h.

### **2.2.6. Sporulation**

*S. cerevisiae* BY4741 (*MATa*) cells expressing mSbsC-eGFP and BY4742 (*MATα*) cells were crossed and diploids were selected on YNB agar containing Leu and His. A single colony was taken and grown overnight in 20 ml YNB broth with Leu and His. Upon centrifugation, the cells were resuspended in 20 ml sporulation medium and incubated at 25°C for 20-30 days.

### **2.2.7. Colocalization Investigation Techniques**

#### **2.2.7.1. $\alpha$ -tubulin Staining**

*S. cerevisiae* W303 cells expressing YFP-TUB1 (kindly provided by Prof. T. U. Tanaka, University of Dundee, Wellcome Trust Biocentre, UK) were transformed with plasmid p426-

GPD-mSbsC-tRFP, grown overnight in YNB broth at 30°C to OD<sub>600</sub> of 2.0, and investigated with a confocal fluorescence microscope.

#### **2.2.7.2. Phalloidin Staining of Fixed Cells**

Phalloidin staining was done as reported [66] with slight modifications. BY4741 cells expressing mSbsC-eGFP were grown to OD<sub>600</sub> of 0.3-0.6 in 20 ml supplemented YNB broth and glucose as the carbon source, fixed for 5 min with formaldehyde (4% final concentration), centrifuged (3,500 x g for 5 min), and resuspended in 4% formaldehyde in PBS. After 30 min at 25°C, cells were washed twice with PBS and resuspended in 500 µl PBS. 100 µl of the cell suspension was mixed with 10 µl of BODIPY 650/665 phalloidin, which was prepared in methanol according to the instruction of the manufacturer and kept in the dark for 1 h. After washing the cells 3-5 times with PBS, they were investigated with the fluorescence microscope.

#### **2.2.7.3. DAPI Staining**

BY4741 cells expressing mSbsC-eGFP were grown overnight to OD<sub>600</sub> of 2.0 in 20 ml YNB broth supplemented with the essential amino acids and glucose as the carbon source. 1 ml of the culture was mixed with 5 µl of DAPI to a final concentration of 2.0 µg/ml and incubated for 2-5 min at RT. Cells were centrifuged at 5,000 x g for 3 min, and the pellet was resuspended in 30-50 µl. 1.5-3 µl of this suspension was investigated with the fluorescence microscope.

#### **2.2.8. *In situ* SL Protein Extraction**

*In situ* protein extraction was done as described by Blecha *et al.* [57] with slight modifications. Shortly, *S. cerevisiae* BY4741 cells expressing mSbsC-eGFP were grown overnight at 30°C in 500-1,000 ml YNB medium supplemented with Leu, His, Met and glucose as the carbon source. Cells were centrifuged (5,000 x g, 3 min) and washed twice with 25 ml sterile distilled water (sdH<sub>2</sub>O) and once with sorbitol solution. Cells were spheroplasted with zymolase in 25 ml spheroplasting buffer for 1 h. Spheroplasted cells were centrifuged (3,000 x g, 5 min), washed with 20 ml sorbitol solution and resuspended in 25 ml sdH<sub>2</sub>O containing plasmid inhibitors (1mM AEBSF and PI cocktail). After 10 min incubation on ice, *in situ* SL assemblies were collected in the pellet after centrifugation (20,000 x g, 30min, 4°C) and investigated with the fluorescence microscope (see below).

### 2.2.9 *In vitro* recrystallization of SL Monomers

*S. cerevisiae* BY4741 cells expressing mSbsC-eGFP were spheroplasted and *in situ* protein structures were obtained as described above. Obtained SL containing pellets were resuspended in 10 times pellet volume of 5M freshly prepared GuHCl. Monomerization of SL structures was performed at RT by shaking for 1-2h. Monomers were collected in supernatant by centrifuging the denatured samples at 100,000 x g for 1h at 4°C with Optima™ Max Ultracentrifuge. *In vitro* recrystallization was performed by dialyzing 1-2 ml of monomer solution against 10 mM CaCl<sub>2</sub> (pH 5.5, pH 7.5 and pH 9.0) in 6 - 8 KDa cut-off dialysis tubings (Spectrum) for at least 24h at 4°C and the resulting self-assembly products were stored at 4°C. In order to investigate the effect of Ca<sup>2+</sup> concentration on *in vitro* recrystallization process, we dialyzed the monomers against 0 mM, 1 mM, 10 mM and 20 mM CaCl<sub>2</sub> at pH 9.0 for 24 - 48 h.

### 2.2.10. Metallization

Metallization of SL tubes was performed according to Wahl *et al.* [72] with some modifications. Dialysis buffer containing 50 µg of recrystallized protein was centrifuged (20,000 x g, 4°C, 15 min) and resuspended in 50 µl freshly prepared metallization buffer (3 mM NaN<sub>3</sub>, 1 mM MgCl<sub>2</sub> in 50 mM NaHPO<sub>4</sub>/Na<sub>2</sub>HPO<sub>4</sub>, pH 7.4). 1 ml of 30 mM K<sub>2</sub>PtCl<sub>4</sub> salt solution (prepared 20-24 h before and kept in dark until the next day) was immediately added and the mixture was shortly vortexed. The suspension was incubated in the dark at RT on a rolling drum (6 rpm) for 4 hours. After centrifugation at 20,000 x g 4°C for 15 min, the pellet was resuspended in 100-200 µl of the buffer. 20-50 µl of the final suspension was immediately dropped on a SiO<sub>2</sub> wafer that was cleaned by sonication for 15 min first in acetone, then in isopropanol, and finally in sterile double distilled water. After 30 min incubation at RT, excess liquid was removed with tissue paper and the same amount of sterile double distilled water was dropped on the wafer. After 15-30 min, the excess water was removed and the wafer was left to dry. The control sample was prepared with the same procedure in the absence of Pt salt.

### 2.2.11. Fluorescence Microscopy

The 4D live cell imaging system was a Zeiss Axiovert 200M microscope with a CCD detector, a Plan-Apochromat 63x/1.4 oil immersion objective, and the filter set FS 31001 (Excitation Band Pass (Ex-BP) 480/30, Beam Splitter (BS) Long Pass 505, Emission Band

Pass (Em-BP) 535/40), and a HBO 100W Mercury arc lamp. MetaMorph 6.2v2 software was used as the imaging program.

Analysis of sporulating yeasts was performed with a Carl Zeiss Axio Imager microscope with a CCD camera, a Plan-Neofluar 100x/1.30 oil immersion objective and the FITC filter set 44 (Ex-BP 475/40, BSFT 500, Em-BP 530/50). Pictures were evaluated with the Carl Zeiss Axio Vision Product Suite.

Colocalization of mSbsC-tRFP structures with  $\alpha$ -tubulin was investigated with the laser scanning confocal microscope Leica DM 6000B with a Plan-Apochromat 63x/1.2 water immersion objective and a HBO 100 W mercury arc lamp and laser power sources. Excitation was performed with the 514 nm (YFP) or 561 nm laser (TRITC), and the emission was monitored with the detectors BP 560/50 (YFP) and BP 610/70 (TRITC). Picture evaluation was performed with the LAS AF Lite software program.

Investigation of *in vivo* mSbsC-eGFP structures, DAPI staining and colocalization with the actin cytoskeleton were conducted with the Keyence Fluorescence Microscope (BZ-8100E) with a 120 W mercury lamp, a CCD camera and a Plan-Apochromat 100x/1.4 oil immersion objective, and the following filter sets: GFP: Ex-BP 472.5/30, BS DM 495, Em-BP 520/35, FS TxRed: Ex-BP 562/40, BS DM 593, Em-BP 624/40 and FS DAPI: Ex-BP 377/50, SB DM 409, Em-BP 447/60. Deconvolution analyses of z-stack pictures with 0.1-0.2  $\mu\text{m}$  intervals were performed with the BZ analyzer software.

Length distribution analysis was conducted by measuring the tube lengths of fluorescent mSbsC-eGFP structures with ImageJ (<http://rsbweb.nih.gov/ij/>).

### **2.2.12. Electron Microscopy**

Scanning electron microscopy (SEM) imaging was carried out with the LEO DSM 982 Gemini SEM at a low voltage (2 kV) in high-vacuum ( $10^{-6}$  Pa). Energy dispersive X-ray spectroscopy (EDX) analysis was performed at 15 kV for the elemental analysis of metallized and unmetallized mSbsC-eGFP samples.

### III. Results

The aim of this study was to investigate the structure, thermal stability, *in vivo* self-assembly, recrystallization and metallization of three different recombinant SL proteins (SslA-eGFP, mSbsC-eGFP and S13240-eGFP) expressed in yeast *S. cerevisiae* BY4741 which could be further used in nanobiotechnological applications. For this purpose, the heterologous expression of SL fusion proteins was characterized with growth and fluorescence measurements coupled with Western blot analyses. Construction of 3D images by taking z-stack images with a fluorescence microscope provided better characterization of SL-eGFP assemblies. Thermal stabilities of *in vivo* expressed SL-eGFP fusion proteins were investigated by fluorescence microscopy and immunodetection. *In vivo* self-assembly kinetics during mitosis and meiosis was the second main issue. In parallel, association of *in vivo* SL-eGFP structures with the cellular components was of interest. Cell disruption experiments were conducted in order to free *in vivo* SL assemblies stably outside the cells (*in situ*). Monomerization of *in situ* SL-eGFP fusion proteins and subsequent recrystallization processes were resulted in the formation of fluorescent SL tubes or patches. Dialysis of monomerized fusion peptides at different conditions such as different ionic strengths, pH values and dialysis times provided information to understand the underlying *in vitro* recrystallization process better. Lastly, the metallization capacities of *in vitro* reassembled SL tubes for the possible applications in nanobiotechnology were studied.

#### 3.1. Expression of Recombinant SL Proteins in Yeast

In order to express the SLs of interest (SslA (aa31-925), SbsC (aa31-1099) and S13240 (aa31-1069) lacking the authentic signal peptides) tagged with eGFP (239 aa), *S. cerevisiae* strain BY4741 cells were transformed with plasmids p426-GPD-SslA-eGFP, p426-GPD-mSbsC\_oT-eGFP, p426-GPD-S13240-eGFP or p426-GPD-eGFP as a control. Growth analysis showed no significant impact of SL-eGFP expression on cell growth (Fig. 14 upper graph). Fluorescence measurements revealed that fluorescence increased until the stationary phase, before it strongly declined (Fig. 14 lower graph).

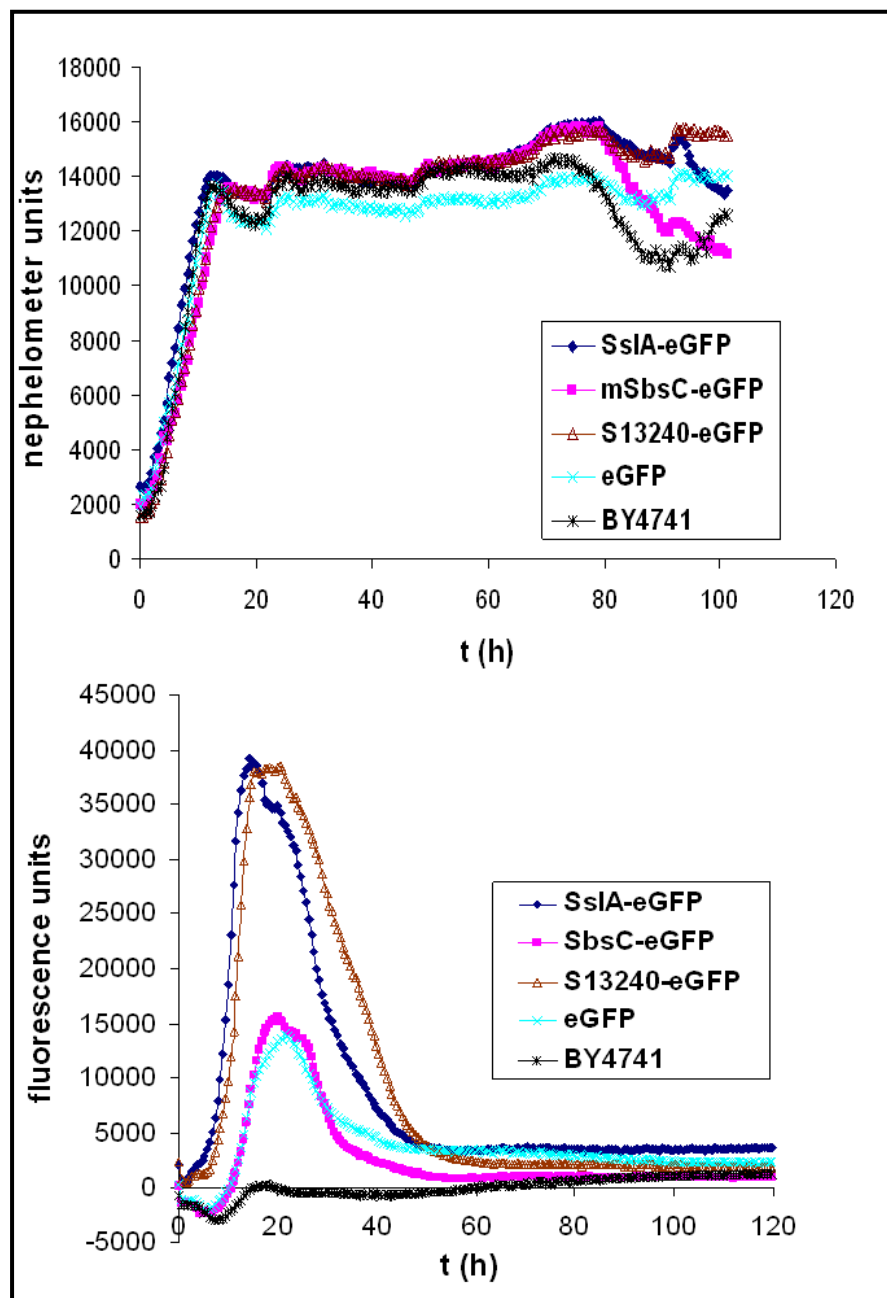


**Figure 14.** Growth and fluorescence curves throughout the cell cultivation. Upper curve: Nephelometer measurements show that S-layer expression slightly interferes with the wild type growth. Lower curve: Fluorostar measurements demonstrate that fluorescence intensity increases exponentially until the end of logarithmic phase whereas it starts to drop dramatically during the stationary phase showing the effect of decrease in cell duplication rate on fluorescence intensity. Dark blue, pink, yellow, turquoise and black curves are representing the *S. cerevisiae* BY4741 cells expressing SslA-eGFP, mSbsC-eGFP, S13240-eGFP, eGFP and wild type cells respectively. Cells were incubated in YNB media in 96 well plates with a starting OD (600nm) of 0.1 at 30°C with shaking.

Western blot analysis of cell lysates of overnight grown cultures with eGFP-antibody showed bands of 123 kDa, 139 kDa, 137 kDa and 27 kDa in accordance with the calculated theoretical molecular masses of SslA-eGFP, mSbsC-eGFP, S13240-eGFP and eGFP

respectively (Fig. 15). Putative degradation products (Fig. 15, right) were observed after Western blotting although protease inhibitors were used during the sample preparation. Fluorescence microscopy investigations of overnight grown cultures showed that SslA-eGFP fusion protein was expressed as fluorescent patches (Fig. 15a), mSbsC-eGFP (Fig. 15b) as tubular networks and S13240-eGFP (Fig. 15c) as hollow-like fibrillar network structures while eGFP did not show any distinct structure (Fig. 15d).

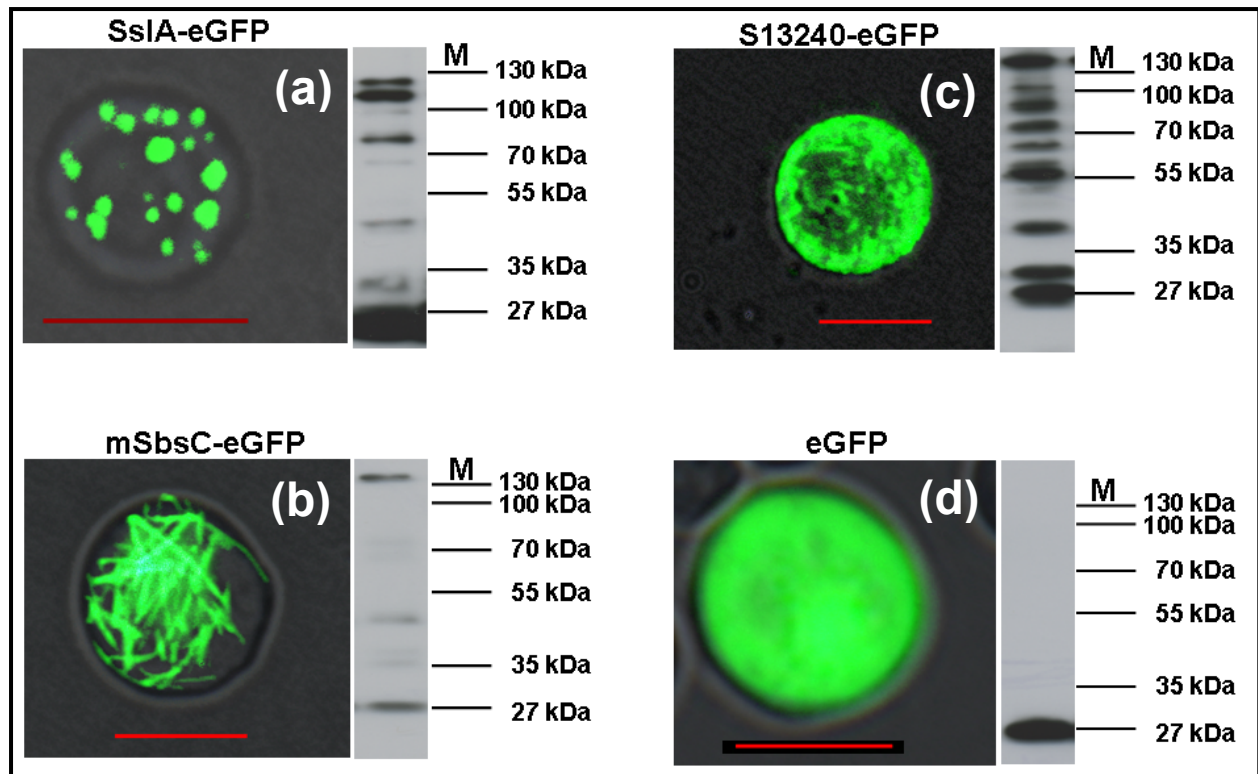


**Figure 15.** Fluorescence images of *S. cerevisiae* BY4741 cells expressing (a) SslA-eGFP patches, (b) SbsC-eGFP tubular networks, (c) S13240-eGFP hollow-like fibrillar network structures and (d) eGFP. z-stack pictures with 0.1-0.2  $\mu\text{m}$  intervals were taken and deconvolved. Western blot analysis with anti-GFP antibody revealed bands of 123 kDa (SslA-eGFP), 139 kDa (mSbsC-eGFP), 137 kDa (S13240-eGFP) and 27 kDa (eGFP) as can be seen on the right hand side of each picture. Cells were disrupted with glass beads and 10  $\mu\text{g}$  of the cell lysates were separated on a 12% SDS gel. All experiments were conducted in the presence of protease inhibitors. M: Protein marker. Scale bar = 5  $\mu\text{m}$

For a more detailed characterization of *in vivo* SL-eGFP structures, z-stack pictures of cells expressing the corresponding SL fusion proteins were taken with 0.1-0.2  $\mu\text{m}$  intervals and 3D reconstruction images were developed by deconvolution analysis. Still frame pictures of 3D reconstruction images are shown as top and side views in Fig. 16 where tubular blocks of different lengths ranging between 1.3-4.3  $\mu\text{m}$  can be identified for mSbsC-eGFP (Fig. 16 upper row). Fluorescent patches with diameters shorter than 1  $\mu\text{m}$  were observed for SslA-

eGFP (Fig. 16 second row). S13240-eGFP structures were seen as hollow network assemblies with a depth of  $\sim 2 \mu\text{m}$  (Fig. 16 lower row).

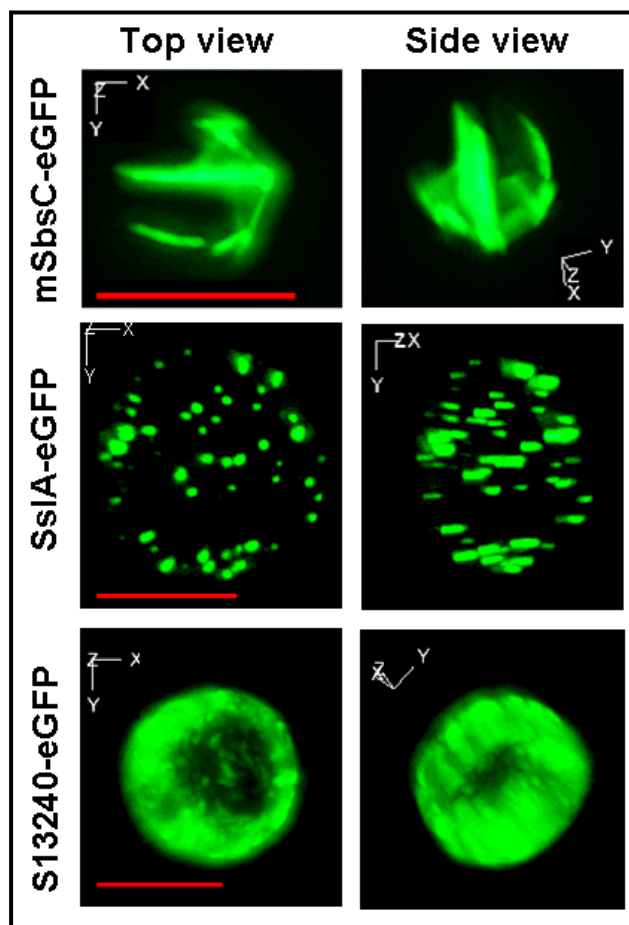


**Figure 16.** Fluorescent still frame pictures of 3D reconstruction images of *in vivo* mSbsC-eGFP in *S. cerevisiae* BY4741 cells. Upper row: top and side views of *in vivo* mSbsC-eGFP structures consisting of at least 5 tube-like assemblies having lengths in the range of 1.3-4.3  $\mu\text{m}$ . Second row: top and side views of *in vivo* SslA-eGFP patches with diameters shorter than 1  $\mu\text{m}$ . Lower row: top and side views of S13240-eGFP *in vivo* hollow structure with a depth of  $\sim 2 \mu\text{m}$ . z-stack pictures with 0.1-0.2  $\mu\text{m}$  intervals were taken and deconvolved into 3D reconstruction images. Scale bar = 5  $\mu\text{m}$

For the expression of SL proteins (SslA (aa31-925), SbsC (aa31-1099) and S13240 (aa31-1069)) tagged with positively charged aa (Arg, His or Lys, 6 aa), a TEV protease cleavage site (TEV, 7 aa) and eGFP (720 aa) which would further find applications in anion binding studies or in waste water treatment researches, p426-GPD-SL-3xArg/His/Lys-TEV-eGFP plasmids (Section 2.1.9) were generated, cloned and expressed in yeast *S. cerevisiae* BY4741. Fluorescence microscopy images of overnight grown cultures showed no structural differences from the corresponding *in vivo* SL-eGFP structures (Fig. 17). Western blot analysis of total cell lysates (in the absence of protease inhibitors) of overnight grown



cultures demonstrated the expected molecular weights of fusion proteins with some degradation products (Fig. 18).

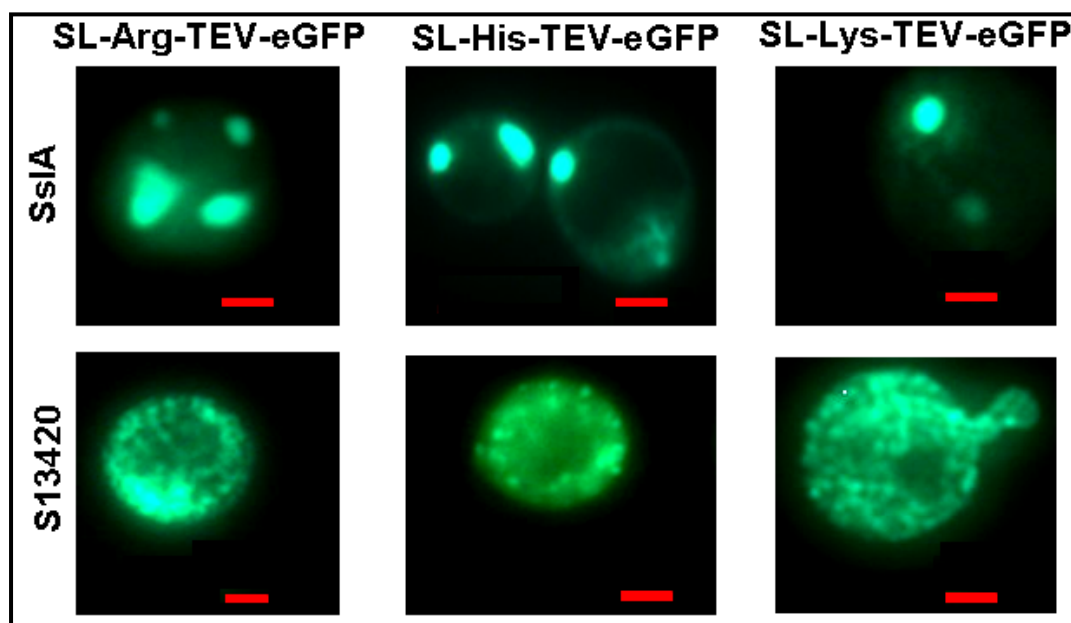


**Figure 17.** Fluorescence images of overnight grown *S. cerevisiae* BY4741 cells expressing SsIA-Arg/His/Lys-TEV-eGFP patches (first row) and S13240-Arg/His/Lys-TEV-eGFP hollow-like network structures (second row). Scale bar = 1  $\mu$ m

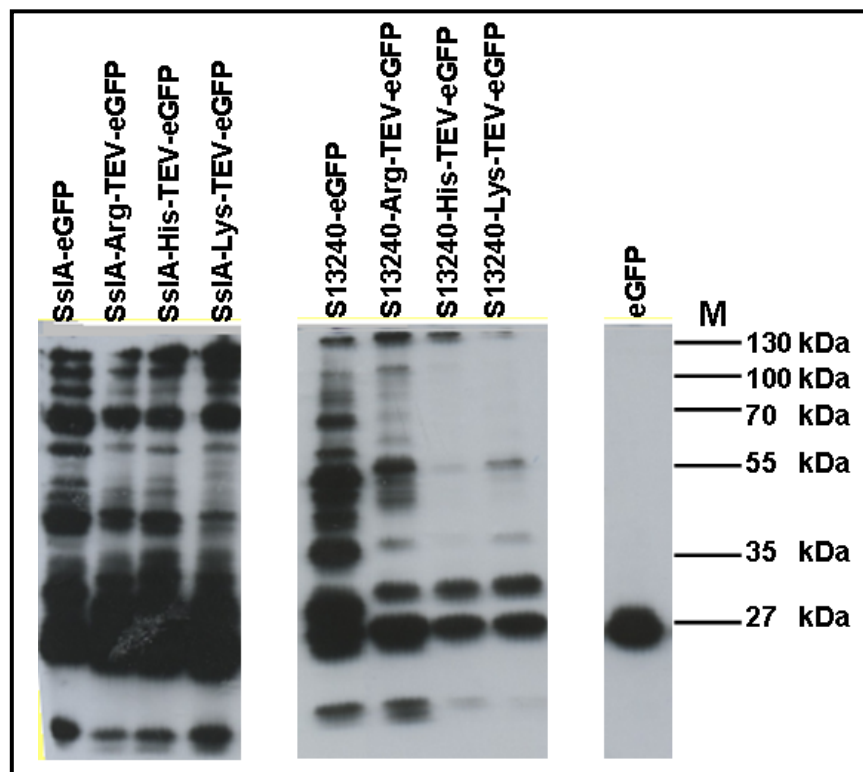


**Figure 18.** Western blot analysis of overnight grown SL-Arg/His/Lys-TEV-eGFP expressing *S. cerevisiae* BY4741 cells. Western blot analysis with anti-GFP antibody showed bands of 124 kDa for SslA- Arg/His/Lys-TEV-eGFP, 138 kDa for S13240-Arg/His/Lys-TEV-eGFP and 27 kDa for eGFP which was the control. Cells were disrupted with glass beads and 10  $\mu$ g of the cell lysates were separated on a 12% SDS gel in the absence of protease inhibitors. M: Protein marker

Since many degradation products were observed in early western blot analyses, an expression analysis experiment was performed at later time points of cell cultivation in order to see the progression of degradation. Cells were incubated with an  $OD_{600}$  of 0.1 in YNB media supplemented with the essential aa and glucose. Samples were collected at certain time points, disrupted with glass beads and total cell lysates were analyzed by Western blotting in the presence of protease inhibitors. Results indicated an increase of degradation products with the cultivation time (Fig. 19). The least degradation was observed in mSbsC-eGFP expressing cells with a few remarkable additional bands detected at 45 kDa and 27 kDa which was corresponding to the eGFP band appeared after 8 h of incubation. No degradation product was observed in eGFP expressing cells.

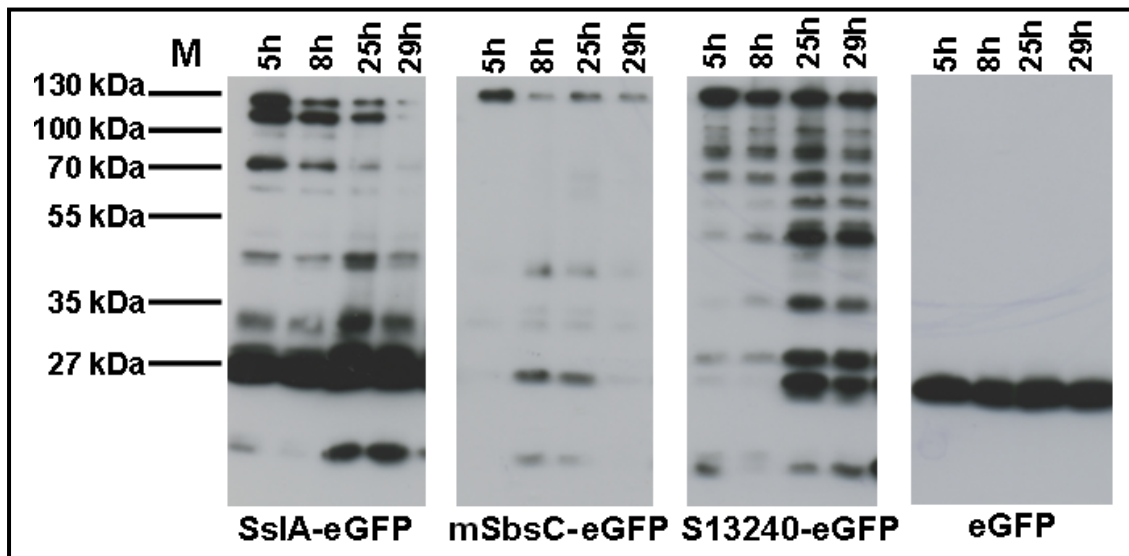


**Figure 19.** Time course detection of SslA-eGFP (123 kDa), mSbsC-eGFP (139 kDa), S13240-eGFP (137 kDa) and eGFP (27 kDa) with anti-GFP antibodies during cultivation. Cells were incubated with an  $OD_{600}$  of 0.1 in YNB media. Cells were collected at the indicated time points, disrupted with glass beads and 7  $\mu$ g of the cell lysates were separated on a 12% SDS gel. All experiments were conducted in the presence of protease inhibitors. M: Protein marker

### 3.2. *In vivo* Thermal Stability of SL-eGFP Proteins

With the aim of testing the *in vivo* stability of SL fusion proteins against high temperatures, overnight grown *S. cerevisiae* BY4741 cells expressing SL-eGFP with  $OD_{600}$  of 1.0-2.0 were centrifuged (3,500xg 5 min) and pellets were incubated at 80°C for 2 days and for additional 2 days at 100°C. Corresponding bands for SslA-eGFP (123 kDa), S13240-eGFP (137 kDa) and eGFP (27 kDa) were detected by Western blot analysis (Fig. 20 right) after disrupting the pellets with glass beads. Some *in vivo* SslA-eGFP structures (in 8% of the observed cells) could be visualized by fluorescence microscopy (Fig. 20 upper row) after 4 days of heat treatment. However, no signal was detected from mSbsC-eGFP expressing cells neither after Western blotting nor fluorescence microscopy showing that this fusion construct was the least stable protein. The strongest bands were obtained for S13240-eGFP implying that this fusion protein is the most stable construct at these experimental conditions.

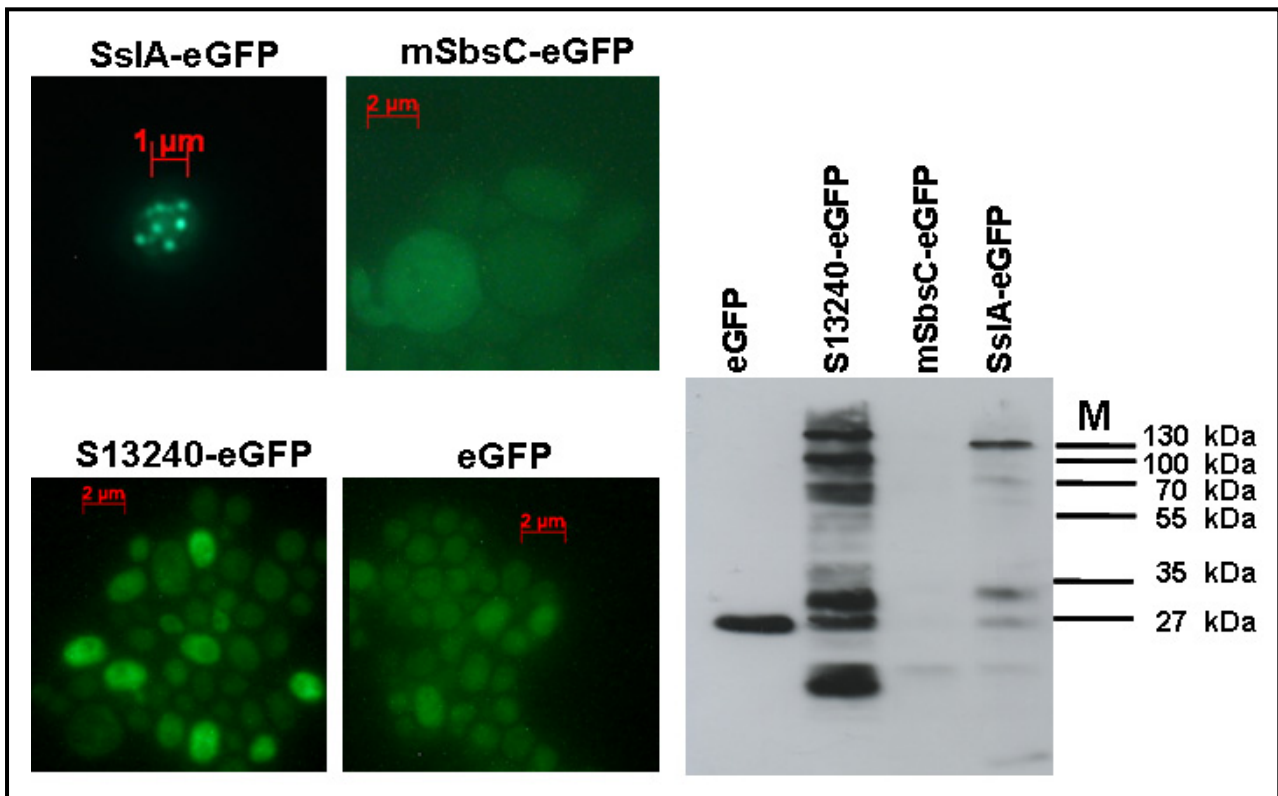


**Figure 20.** Temperature stability analysis of *in vivo* expressed SslA-eGFP (123 kDa), mSbsC-eGFP (139 kDa), S13240-eGFP (137 kDa) and eGFP (27 kDa) at combined temperatures of 80°C and 100°C. Left: Fluorescence images of cells after the heat treatment. Right: The most stable fusion protein was S13240-eGFP with the strongest detected bands. The least stable protein was mSbsC-eGFP. Cells were cultivated overnight, centrifuged (4,000 x g, 5 min), pelleted in microfuge tubes and incubated at 80°C for 2 days and at 100°C for additional 2 days. Dried cells were disrupted with glass beads and 10 μg of the cell lysates were separated on a 12% SDS gel. Proteins were detected with anti-GFP antibodies. All experiments were conducted in the presence of protease inhibitors. M: Protein marker

Next set of experiments were performed by incubating the cell pellets at 100°C for 2, 6 and 8 days or by autoclaving them at 121°C for 20 min (please refer to Fig. 15 for the corresponding fluorescence images and Western blot pictures of recombinant cells before heat treatment). Western Blot analysis showed that S13240-eGFP was the most stable fusion protein (Fig. 21). Some protein bands of S13240-eGFP could even be detected after 6 days of incubation at 100°C. None of the cells survived after 2, 6, and 8 days of incubation at 100 °C or after the autoclaving which were tested by cultivating the cells on YPD agar after each drying step. No yeast cell growth was observed. The second most stable protein was seemed to be SslA-eGFP which showed a band of 123 kDa with degradation products at the end of 2 days. For mSbsC-eGFP I could just obtain very weak signals suggesting that most of this fusion protein was degraded during the heat treatment. Interestingly, eGFP was quite stable in that at the end of both 2 and 6 days I could detect signals at 27 kDa (Fig. 21).

After autoclaving the pellets at 121°C for 20 min, we obtained similar results. S13240-eGFP was the most stable protein showing the strongest signal. The weakest signal was detected for mSbsC-eGFP among the other SL-eGFP constructs.

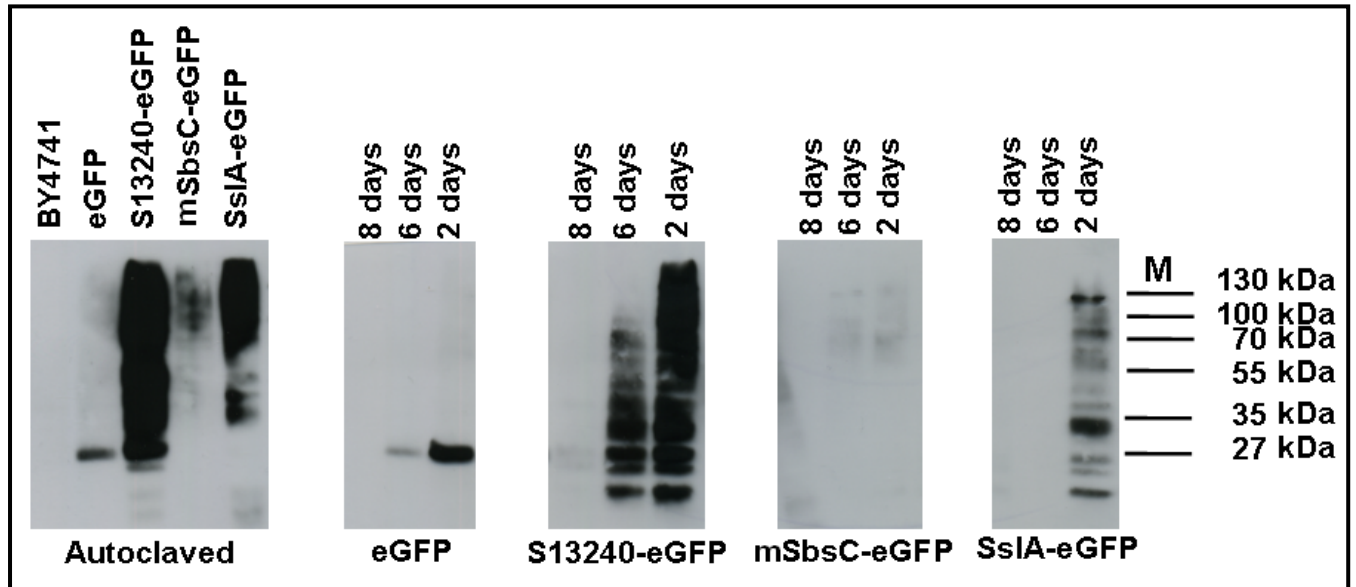


**Figure 21.** Temperature stability analysis of *in vivo* expressed SslA-eGFP (123 kDa), mSbsC-eGFP (139 kDa), S13240-eGFP (137 kDa) and eGFP (27 kDa) at 100°C. The most stable fusion protein was S13240-eGFP. Some S13240-eGFP bands could even be detected after 6 days of incubation. The least temperature stable protein was mSbsC-eGFP. After autoclaving the samples at 121°C for 20 min, signals from each construct could be detected. Cells were cultivated overnight at 30°C in 50 mL YNB medium, collected in 4 tubes (4X12.5 ml), centrifuged (4,000 x g, 5 min), pelleted in microfuge tubes and the pellets were either incubated at 100°C for 2, 6 and 8 days or autoclaved at 121°C. Dried cells were disrupted with glass beads and 15 µl of the cell lysates were separated on a 12% SDS gel. Proteins were detected with anti-GFP antibodies. All experiments were conducted in the presence of protease inhibitors. M: Protein marker

After each heat treatment the dried samples were analyzed with a fluorescence microscope. At the end of 2 days of incubation at 100°C, I could observe the characteristic *in vivo* SL-eGFP structures just for mSbsC (only 6% of the cells had the tubular assemblies, Fig. 22 second row). The negative control (untransformed *S. cerevisiae* BY4741 cells) showed weak autofluorescence (Fig. 22). Although the characteristic SslA-eGFP and S13240-eGFP *in vivo* structures could not be visualized by fluorescence microscopy (Fig. 22), Western blot analysis showed protein bands (Fig. 21). After 2 days of incubation only 7% of the cells expressing SslA-eGFP were fluorescent but not showing the patch-like structures (Fig. 22). After 8 days of incubation at 100°C, I could observe neither protein bands with Western blotting nor any strong fluorescence signal with fluorescence microscopy. Although the autofluorescence can not be excluded, the absence of characteristic SL-eGFP structures can be explained by conformational changes of SL fusion proteins due to the heat treatment. This

could lead disassembly of SL monomers so that no distinct structure was visualized but eGFP like plain fluorescence was observed (Fig. 22). After autoclaving the pelleted cells at 121°C for 15 min, strong fluorescence signal was observed in some of the cells showing that the SL-eGFP proteins were maintained without the characteristic *in vivo* structures (Fig. 22) but in the form of monomers which could have been detected with anti-GFP antibodies (Fig. 21).

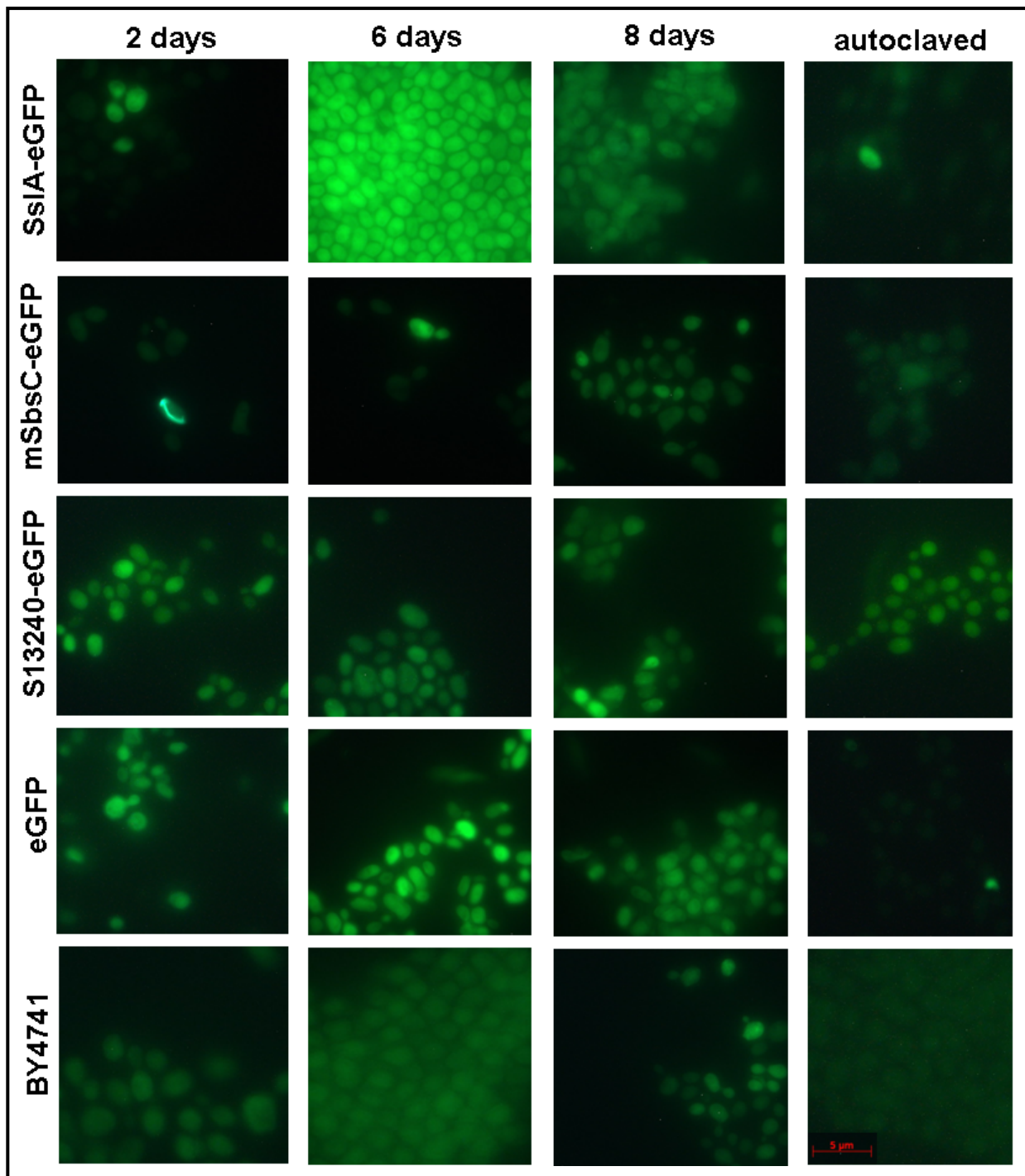


**Figure 22.** Fluorescence images of SL-eGFP expressing cells after the heat treatment. Columns from left to right: cells incubated for 2 days, 6 days, 8 days at 100 °C and cells autoclaved at 121°C for 20 min. Scale bar = 5 µm



### 3.3. *In vivo* Self-assembly Kinetics of mSbsC-eGFP

While investigating the *in vivo* SL-eGFP structures, it was observed that during mitosis, buds emerging from SslA-eGFP, S13240-eGFP and eGFP expressing cells got fluorescent right after the newly developed bud appeared. But, for the mSbsC-eGFP expressing cells, the situation was different. The newly appearing buds were never fluorescent. This case raised the question how the mSbsC-eGFP structures are formed *in vivo* and how such tubular assemblies are transmitted to the buds during mitosis and meiosis. In this section *in vivo* mSbsC-eGFP formation during mitosis and meiosis was analyzed with live cell imaging.

#### 3.3.1. Formation of SL Assemblies during Mitosis

Formation of SL assemblies during mitotic divisions was analyzed by live fluorescence imaging of 10 vegetative cells of *S. cerevisiae* BY4741 strain expressing mSbsC-eGFP. The duration of mitosis in this strain was about 180 min. On average, SL assemblies became visible in the buds 126 min after the appearance of the bud projection (defined as  $t = 0$  min). In no case, SL structures projected from the mother to the daughter cells. Instead, SL assemblies formed independently inside the daughter cells. This observation was made for both haploid (Fig. 23a) and diploid cells (Section 3.3.2). 100 min after the start of the observation, mSbsC-eGFP became visible as a single, very small (0.5-1.0  $\mu\text{m}$ ) dot-like structure (indicated by an arrow in Fig. 23a). This dot served as a nucleation center for the development of a short tube-like assembly. The growing tube changed its intracellular position and eventually bent to form a branched structure with two connected tubes. The further SL assembly proceeded *via* formation of triangular tubular network structure (Fig. 23b).



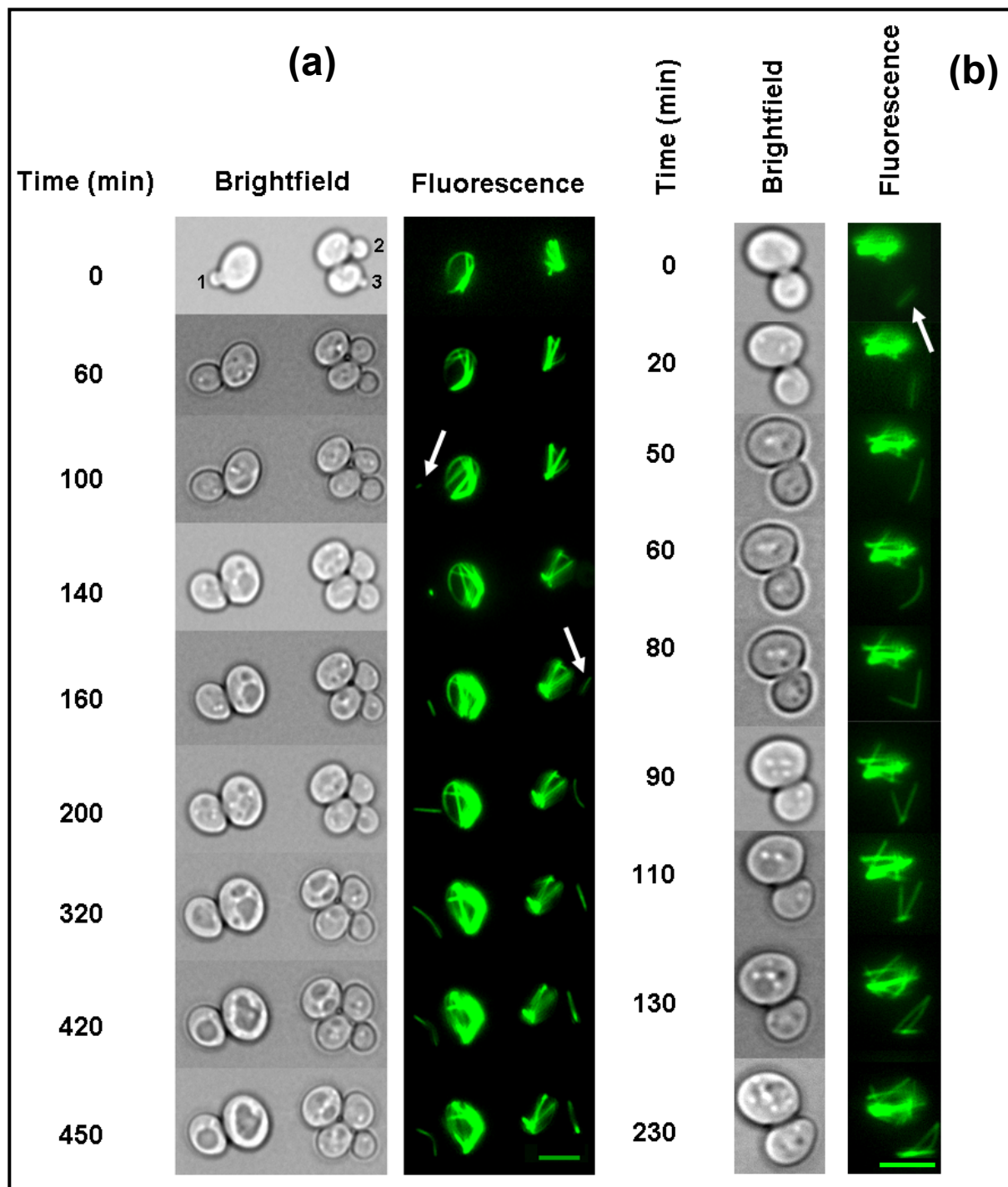


**Figure 23.** Imaging of *S. cerevisiae* BY4741 cells expressing mSbsC-eGFP during mitosis. Bright field (left column) and fluorescence microscopy images (right column) were taken from a time-lapse series at the indicated time points. (a) Appearance of SL structures. Buds are numbered (1-3). Buds 1 and 2 originate from fluorescent mother cells, while bud 3 stems from a non-fluorescent mother cell. Newly appearing SL structures are indicated with arrows. Bud emergence is defined as 0 min. (b) Branching of the SL structures. Progression of a SL tube-like structure (designated with the arrow) into a triangular tubular network is shown in different cells. Start of observation is defined as 0 min. Scale bar = 5  $\mu$ m

### 3.3.2. Formation of SL Assemblies during Meiosis

In order to see how mSbsC-eGFP assemblies are formed and transmitted during meiosis, crossing of *S. cerevisiae* BY4741 (*MATa*) cells expressing mSbsC-eGFP and the mating partner *S. cerevisiae* BY4742 (*MAT $\alpha$* ) cells was performed on YPD agar. The mating process was observed with a fluorescence microscope. The diploid bud of the zygote got fluorescent at the end of 50 min where the start of observation is defined as 0 min (Fig. 24, third row). Similar to the case of budding in haploid cells, the newly appeared diploid bud expressed mSbsC-eGFP fusion protein independently.

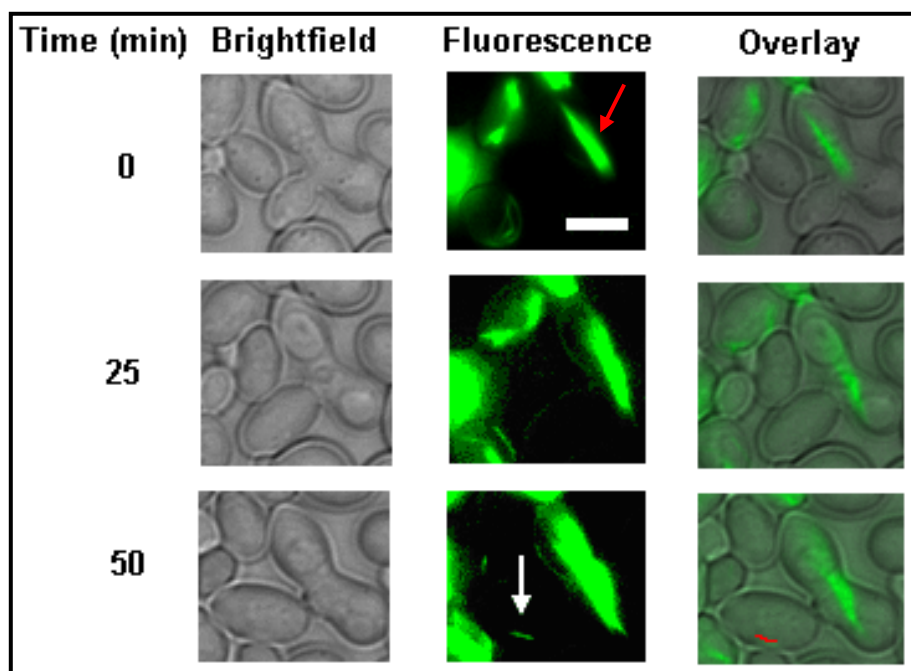


**Figure 24.** Live microscopy imaging of *S. cerevisiae* zygote cell expressing mSbsC-eGFP during meiosis. Bright field (left column), fluorescence (middle column) and overlay (right column) images were taken from a time-lapse series at the indicated time points. mSbsC-eGFP protein extended towards the mating partner that was not having the corresponding plasmid expressing mSbsC-eGFP (shown with the red arrow). 50 min after the start of the observation, mSbsC-eGFP became visible as a single tube-like structure (indicated by the white arrow). Start of observation is defined as 0 min. Scale bar = 5  $\mu$ m

Unlike the budding case in haploid cells where mSbsC-eGFP tubes were not projected to the newly developed bud, during the cell fusion in meiosis, SL fusion proteins expressed by *S. cerevisiae* BY4741 (*MATa*) extended towards the mating partner BY4742 (*MAT $\alpha$* ) that was not having the corresponding plasmid expressing mSbsC-eGFP (Fig. 24 & Fig. 25). In Fig. 25 at  $t = 0$  min a zygote with two mating partners, one showing the tube-like mSbsC-eGFP assemblies and the other expressing no mSbsC-eGFP protein can be seen. After 50 min of observation, a diploid bud emerged from the zygote; the tubular assemblies changed their

intracellular conformation and projected towards the mating partner without any fusion construct.

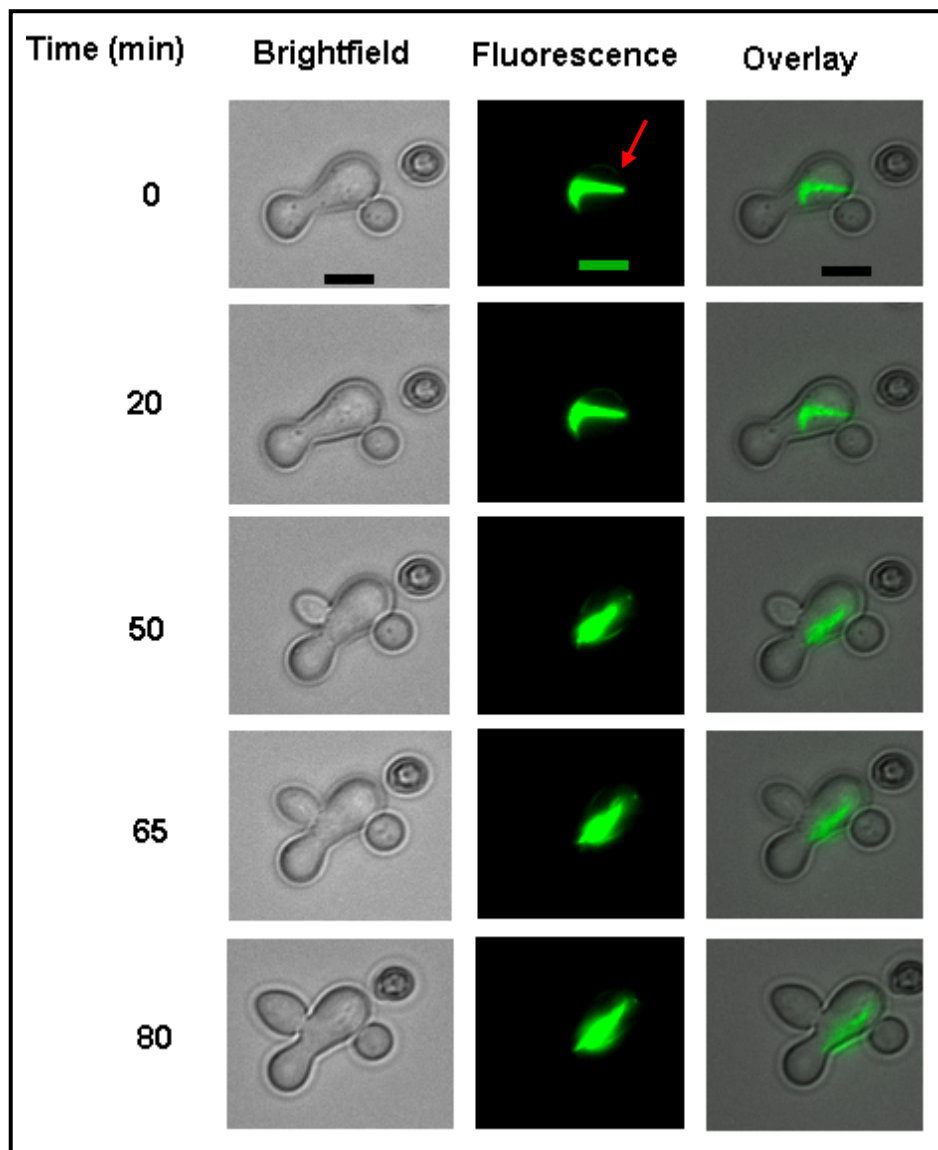


**Figure 25.** Projection of mSbsC-eGFP tube-like structures during the cell fusion. Bright field (left column), fluorescence (middle column) and overlay (right column) images were taken from a time-lapse series at the indicated time points. After 50 min of observation, a diploid bud emerged from the zygote meanwhile the tubular assemblies (showed with the red arrow) expressed by the mating partner on the right changed their intracellular position and projected towards the mating partner on the left lacking the fusion protein. Start of observation is defined as 0 min. Scale bar = 5  $\mu$ m

Live fluorescence microscopy investigations of *S. cerevisiae* cells expressing mSbsC-eGFP showed that the fusion protein was not transmitted to the daughter cells but the newly developed buds were expressing the SL proteins independently. Thus, I analyzed the diploid yeast cells after meiosis in order to investigate the SL expression or transmission pattern. Similar to the budding of haploid cells, the daughter cell of a diploid yeast cell got

fluorescent without any projection after 50 min of observation (Fig. 26, third row). mSbsC-eGFP appeared in the form of a short tube-like structure which elongated into a tubular assembly of  $\sim 5 \mu\text{m}$ .

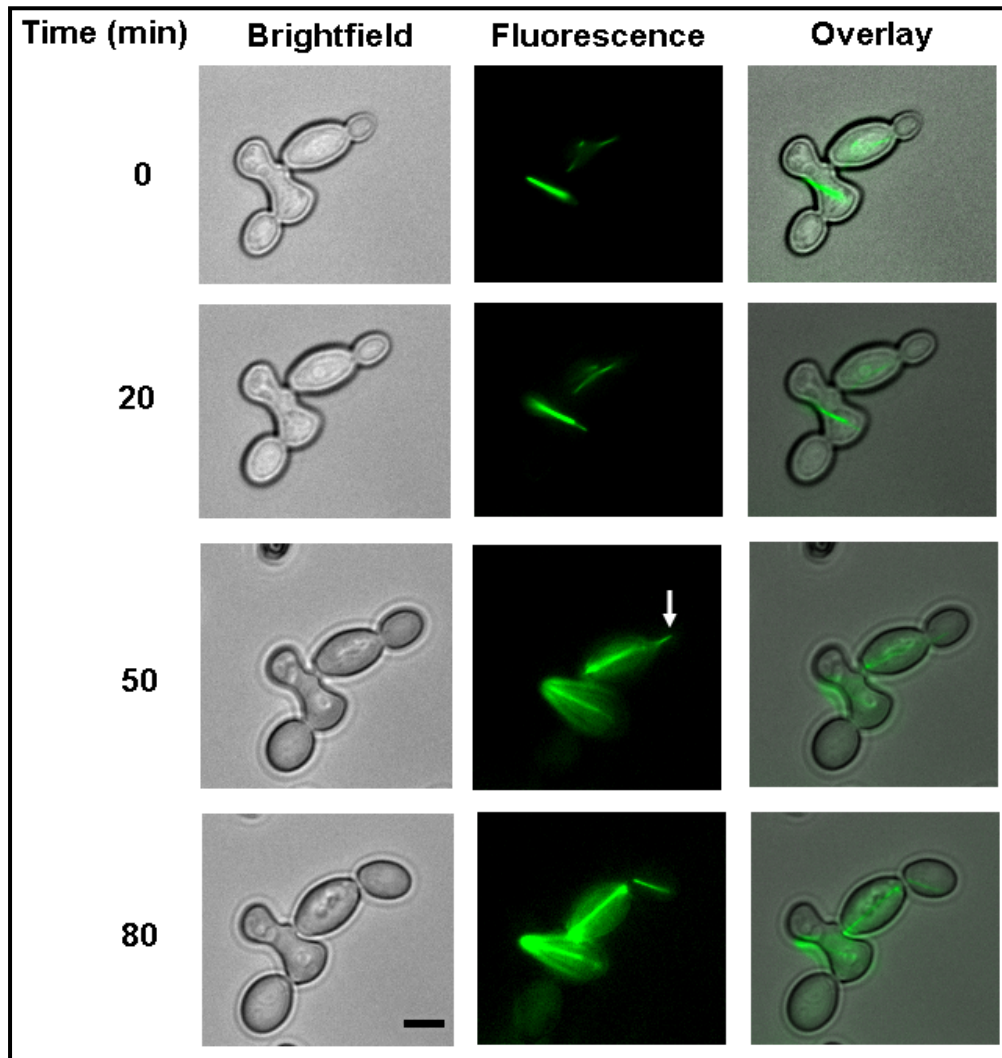


**Figure 26.** Imaging of diploid *S. cerevisiae* BY4741 cells expressing mSbsC-eGFP during mitosis. Bright field (left column) and fluorescence microscopy images (right column) were taken from a time-lapse series at the indicated time points. New SL structure was formed independently (indicated with the white arrow). Start of observation is 0 min. Scale bar =  $5 \mu\text{m}$

### 3.3.3. Formation of SL Assemblies during Sporulation

The next aim was to investigate the transmission of SL structures expressed by a diploid cell to ascospores during meiosis. Sporulation of diploid cells, obtained by mating of *S. cerevisiae* strain BY4742 (*MATa*) with BY4741 (*MATa*) expressing mSbsc-eGFP, was induced and 30 tetrads were analyzed by fluorescence microscopy (a representative example of analyzed tetrads can be seen in Fig. 27). In most of the tetrads (67%) all four spores exhibited

fluorescent SL assemblies. 13% of the tetrads had three and 20% had two fluorescent spores. In general, one of the spores presented a significantly denser network that exhibited a stronger fluorescence. These observations suggest that preformed SL assemblies of the diploid cells are distributed to ascospores during meiosis.

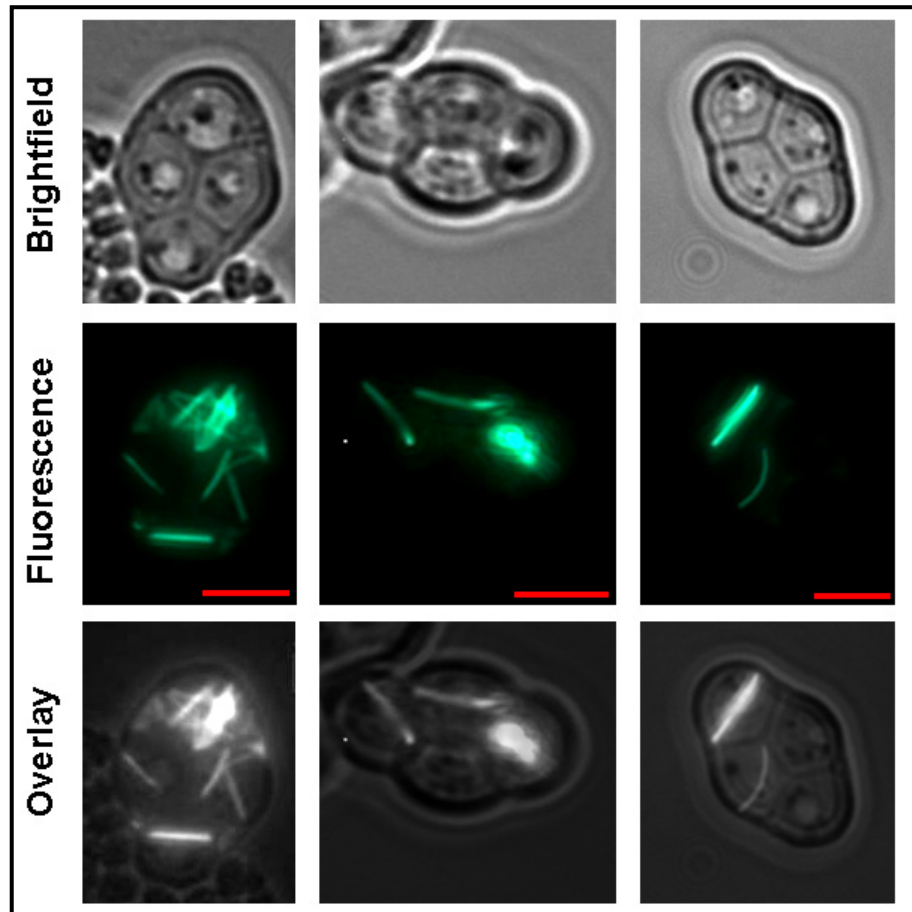


**Figure 27.** Fluorescence microscopy of tetrads. Diploid cells, obtained by mating of untransformed *S. cerevisiae* strain BY4742 (*MATa*) with BY4741 (*MATa*) expressing mSbsc-eGFP, were sporulated, and the resulting tetrads were analyzed by fluorescence microscopy. Scale bar = 2  $\mu$ m

### 3.4. Colocalization Studies

Live fluorescence microscopy imaging of yeast cells during mitosis and meiosis showed that mSbsC-eGFP tube-like structures were not projected from mother cells to the daughter cells. But, in the case of cell fusion, SL projection was observed from one mating partner to the other. After sporulation, it was observed that in most tetrads, all of the spores of an ascospore got fluorescent. These findings brought us to the topic of *in vivo* localization of SL structures and their interactions with the cytoplasmic elements. For this purpose, I studied first the association of mSbsC-tRFP assemblies with yeast microtubules which are forming the yeast

cytoskeleton with actin patches and filaments. Secondly, the interaction of mSbsC-eGFP structures with actin network was investigated. The last target was the nuclear region and mitochondrial network.

### **3.4.1. Colocalization with Microtubules**

Under the scope of investigation of *in vivo* mSbsC-tRFP colocalization with microtubular elements, *S. cerevisiae* W303 cells expressing YFP-tagged  $\alpha$ -tubulin (YFP-TUB1) were transformed with plasmid p426-GPD-mSbsC-tRFP, and transformants were analyzed by confocal fluorescence microscopy (Fig. 28). Microtubules were visualized as yellow (due to the easiness of visualizing green and red in one picture, yellow signal was converted to green) tubular structures (Fig. 28, right column). mSbsC-tRFP structures were observed as red tubular assemblies (Fig. 28, left column). No overlap between the green and the red fluorescence could be observed in budding or not budding cells, demonstrating that mSbsC-tRFP is not associated with microtubules.

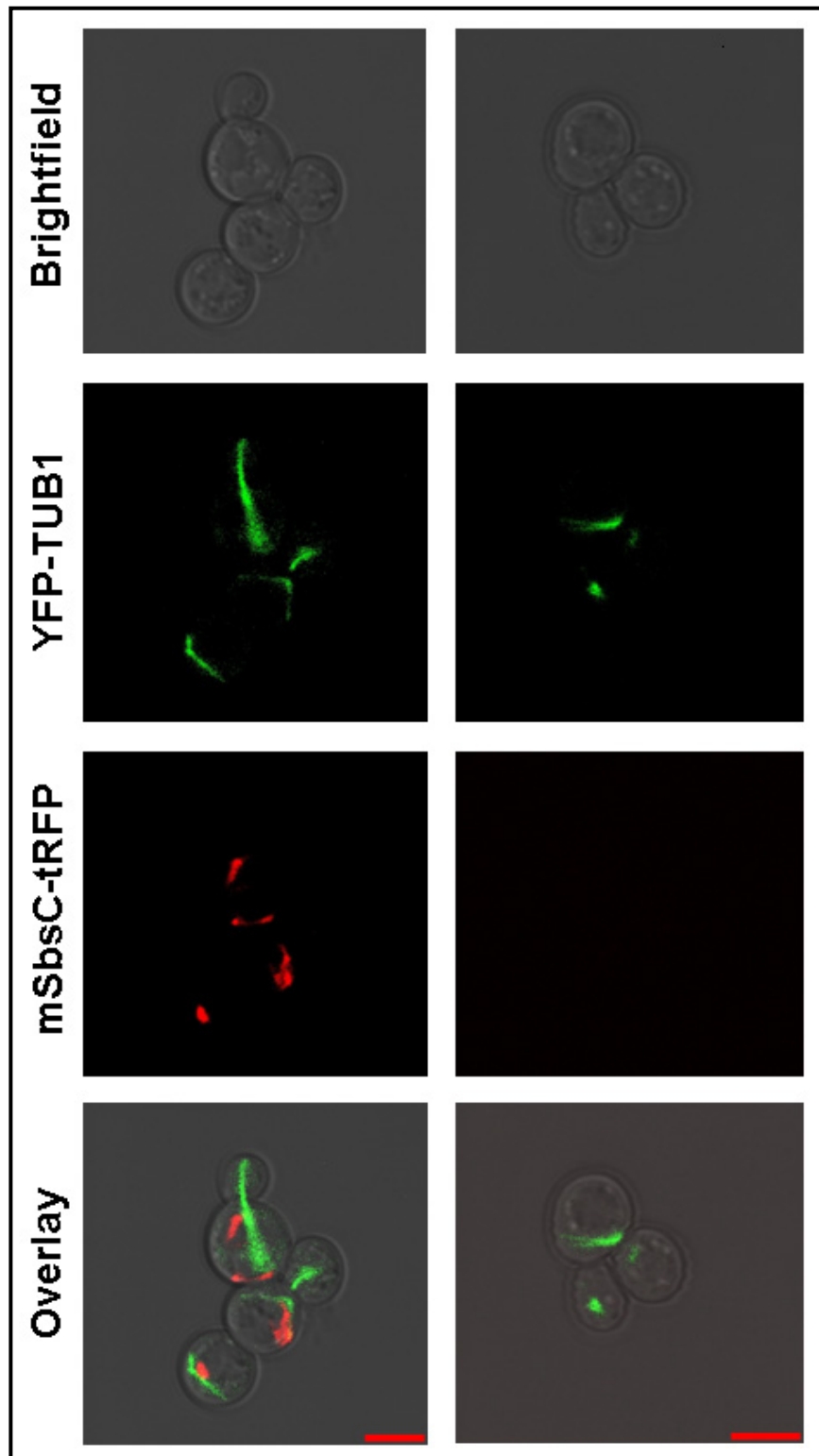


**Figure 28.** Microtubule cytoskeletal elements do not colocalize with mSbsC-tRFP. First column: *S. cerevisiae* W303 cells (with and without buds) expressing YFP-TUB1 and mSbsC-tRFP; second column: *S. cerevisiae* W303 cells expressing YFP-TUB1. Pictures were taken with a confocal fluorescence microscope. Scale bar = 5  $\mu$ m



### 3.4.2. Colocalization with Actin Network

To visualize the actin network, *S. cerevisiae* BY4741 cells expressing mSbsC-eGFP were stained with phalloidin and analyzed with the fluorescence microscope. Actin networks were observed as red patches and filaments (Fig. 29 right column) and mSbsC-eGFP as tube-like structures (Fig. 29 left and middle columns). Except for a few small patches I did not observe an overlap of mSbsC-eGFP assemblies with the actin network in cells with buds or without buds, indicating that mSbsC-eGFP is not associated with actin meshwork (Fig. 29).

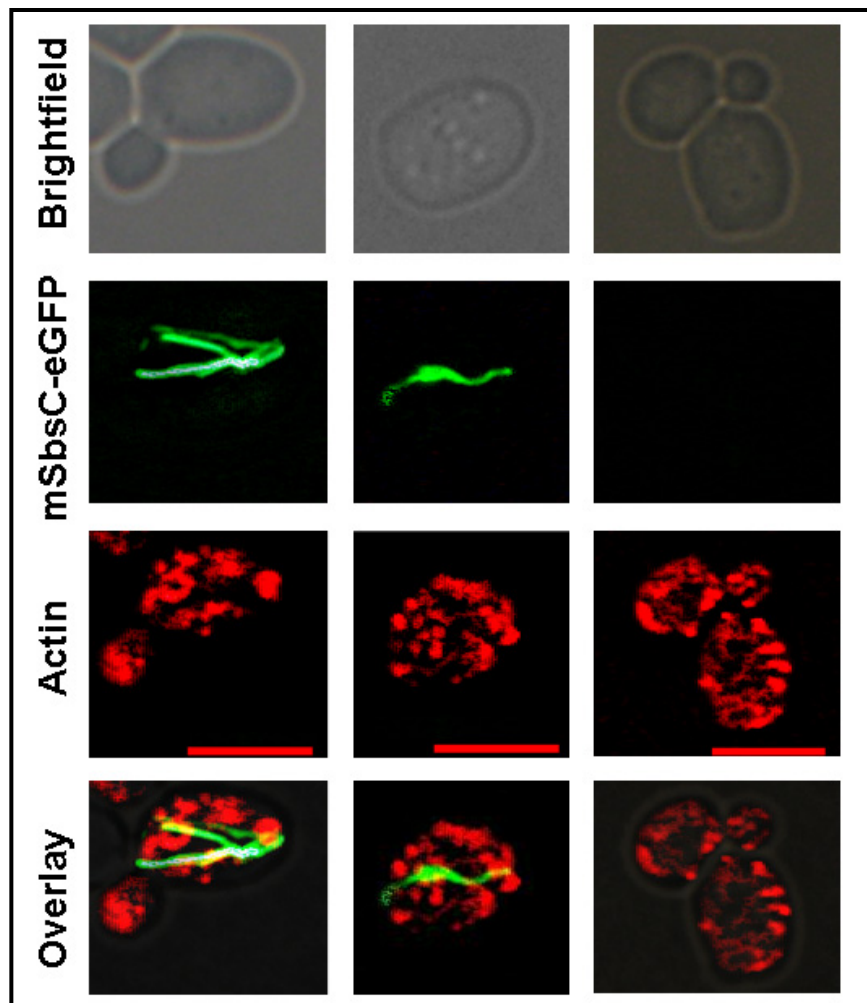


**Figure 29.** Phalloidin staining. *S. cerevisiae* BY4741 early log cells expressing mSbsC-eGFP were stained with phalloidin and analyzed with the fluorescence microscope. A *S. cerevisiae* BY4741 cell expressing SL with or without a bud (left and middle column, respectively) and untransformed control cells (right column) were stained with phalloidin and analyzed by fluorescence microscopy (25 - 34 z-stack pictures of 0.1  $\mu\text{m}$  intervals were taken and deconvolved). Scale bar = 5  $\mu\text{m}$



### 3.4.3. Colocalization with Nucleus and Mitochondrial Network

Lastly, I investigated the possible association of nuclear region and the mitochondrial network which were visualized by DAPI staining as blue (Fig. 30, right column) with mSbsC-eGFP tubes. Staining of DNA with DAPI gave no hint for association of the tubular SL structures with the nuclei or mitochondria (the staining was strong enough to detect the mitochondrial DNA with DAPI) in neither budding nor not budding cells (Fig. 30 left and middle columns).

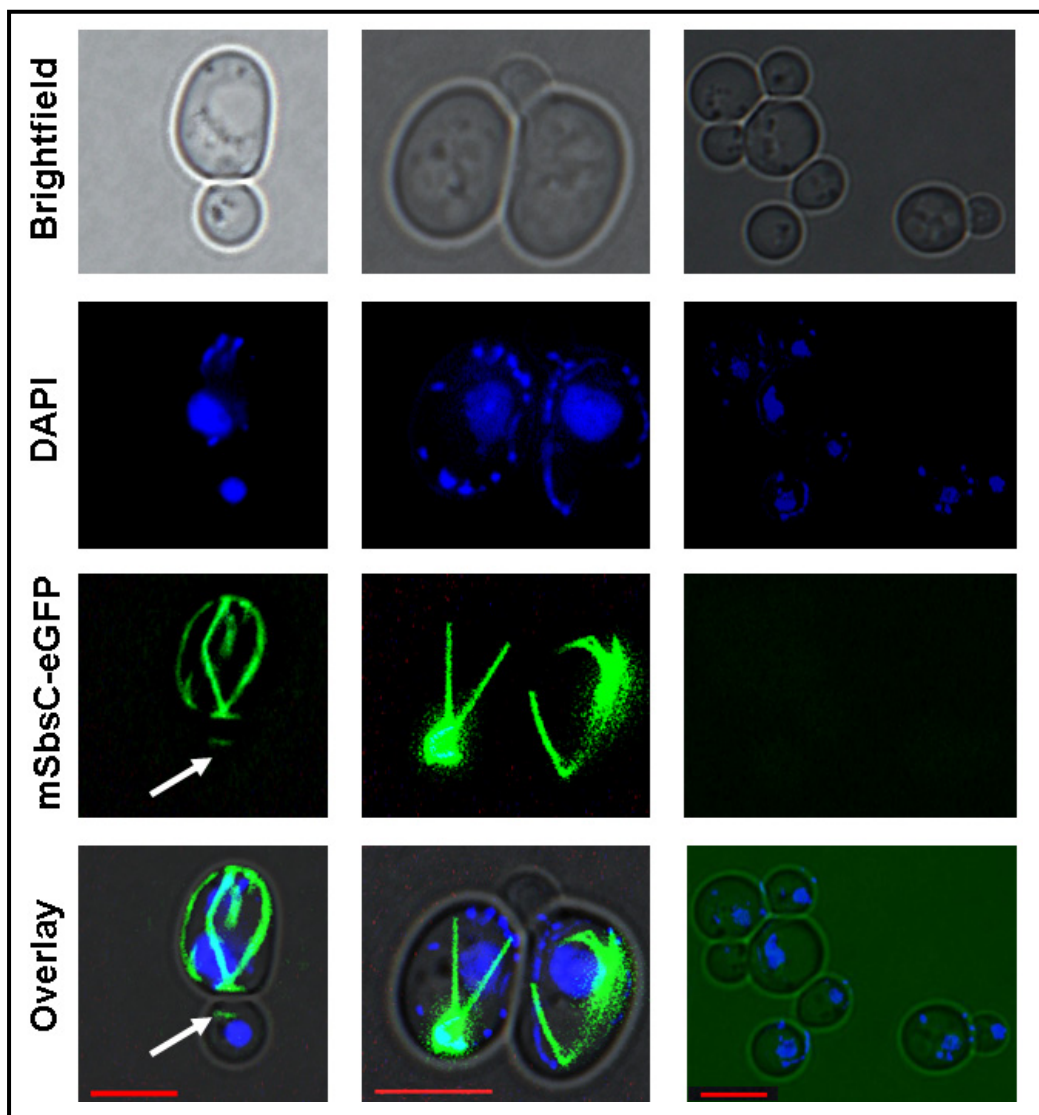


**Figure 30.** *S. cerevisiae* BY4741 cells (from exponential phase) expressing mSbsC-eGFP with (left column) and without a bud (middle column) were stained with DAPI and monitored with the fluorescence microscope. Untransformed *S. cerevisiae* BY4741 cells served as a control (right column). The newly formed SL structures (indicated by the white arrow) in the daughter cell are not associated with the nucleus or mitochondria (6-7 z-stack pictures of 0.3  $\mu\text{m}$  intervals were taken and deconvolved). Scale bar = 5  $\mu\text{m}$

### 3.5. *In vitro* Recrystallization

SL monomers can self-assemble into monomolecular arrays in suspensions, on solid surfaces, e.g. silicon, glass, carbon and synthetic polymers or lipid films [5]. In previous sections, it was demonstrated how *in vivo* SL tube-like structures formed (self-assembled) in yeast cytoplasm which is a fluidic environment during mitosis and meiosis. In this section, I investigated the *in situ* extraction, *in vitro* recrystallization of SL tubular structures and the factors affecting the recrystallization process.

#### 3.5.1. *In vitro* Recrystallization of mSbsC-eGFP

In order to see if *in vivo* tube-like mSbsC-eGFP structures would be maintained out side the cells (*in situ*), yeast cells expressing mSbsC-eGFP (Fig. 32-1) were converted to spheroplasts by treatment with zymolyase and eventually burst open by osmotic shock. The *in vivo* SL structures were retained in the spheroplasts (Fig. 32-2) and even after the burst (Fig. 32-3), indicating their high stability. The *in vivo* and *in situ* structures differed in terms of length. 50 of *in vivo* mSbsC-eGFP structures were randomly selected and their lengths were determined (Fig. 31a). Tube lengths varied from 0.78  $\mu\text{m}$  to 5.06  $\mu\text{m}$ , with an average of 2.49  $\mu\text{m}$ . 36% of the tubes were in the range of 2-3  $\mu\text{m}$  length. The average *in vivo* diameter was 0.3  $\mu\text{m}$ . After burst of the cells, the average *in situ* tube length was 1.69  $\mu\text{m}$  (Fig. 31b). The shortest tube was 0.66  $\mu\text{m}$  and the longest was 4.77  $\mu\text{m}$ . 63% of the tubes were in the range of 1-2  $\mu\text{m}$ . The average *in situ* diameter was 0.24  $\mu\text{m}$  which was in line with the *in vivo* situation. We observed shorter tubular structures than the *in vivo* case, most probably, due to the change of environmental conditions like ionic strength, *in vivo* structures disassembled from the networking into shorter tubes during the osmotic shock

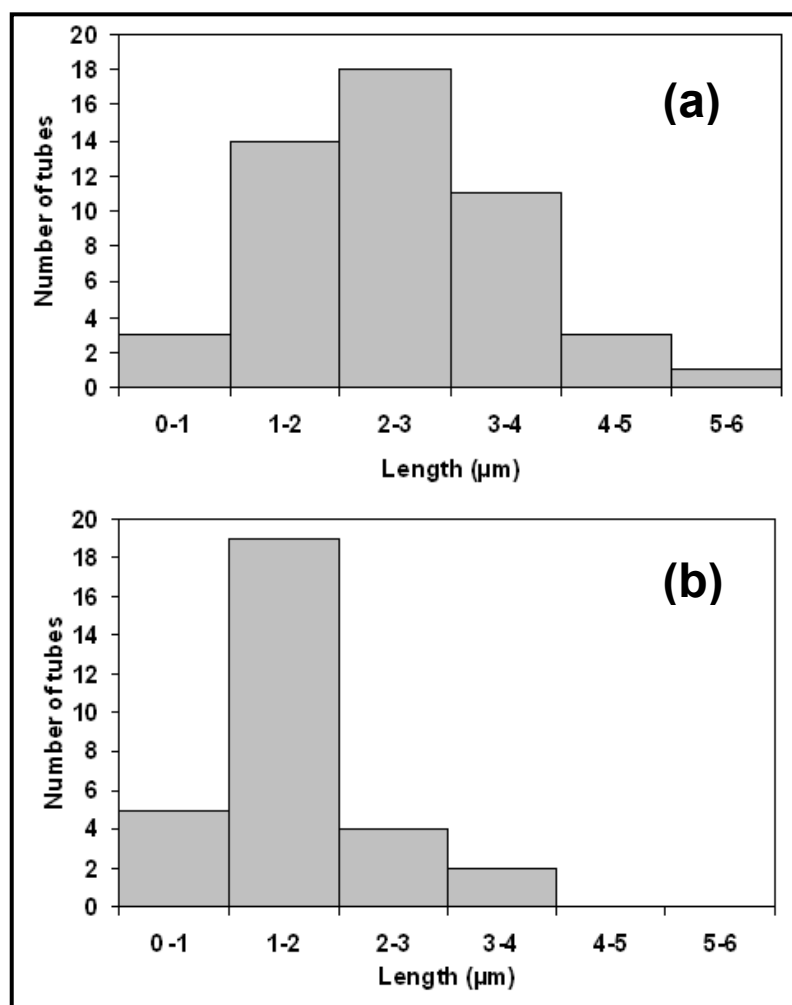


**Figure 31.** Length distribution analysis of *in vivo* and *in situ* mSbsC-eGFP structures **a)** Length distribution of 50 mSbsC-eGFP structures formed *in vivo*. Tube lengths varied from 0.78  $\mu\text{m}$  to 5.06  $\mu\text{m}$ , with an average of 2.49  $\mu\text{m}$ . **b)** *In situ* length distribution diagram of 30 mSbsC-eGFP structures. The average tube length was 1.69  $\mu\text{m}$ . The shortest tube was 0.66  $\mu\text{m}$  and the longest was 4.77  $\mu\text{m}$ . 63% of the tubes were in the range of 1-2  $\mu\text{m}$ .

After obtaining the tubular structures stably *in situ*, I monomerized them. Monomerization was performed by the treatment of *in situ* obtained proteins with a chaotropic agent (5 M GuHCl). Monomerized SL assemblies were no longer visible. Instead the image section showed a plain fluorescence without any structure (Fig. 32-4 & 32-5). Monomers were dialyzed in order to see if we would again obtain tubular fluorescent assemblies. Upon removal of GuHCl by 48 h of dialysis against 10 mM  $\text{CaCl}_2$  at pH 5.5 tubular SL structures formed again (Fig. 32-6). mSbsC-eGFP monomers were able to self-assemble *in vitro* into fluorescent tubes showing that eGFP did not interfere with the *in vitro* self-assembly process. Fluorescent *in vitro* recrystallized mSbsC-eGFP structures were investigated both with fluorescence microscopy and SEM (Fig. 36).

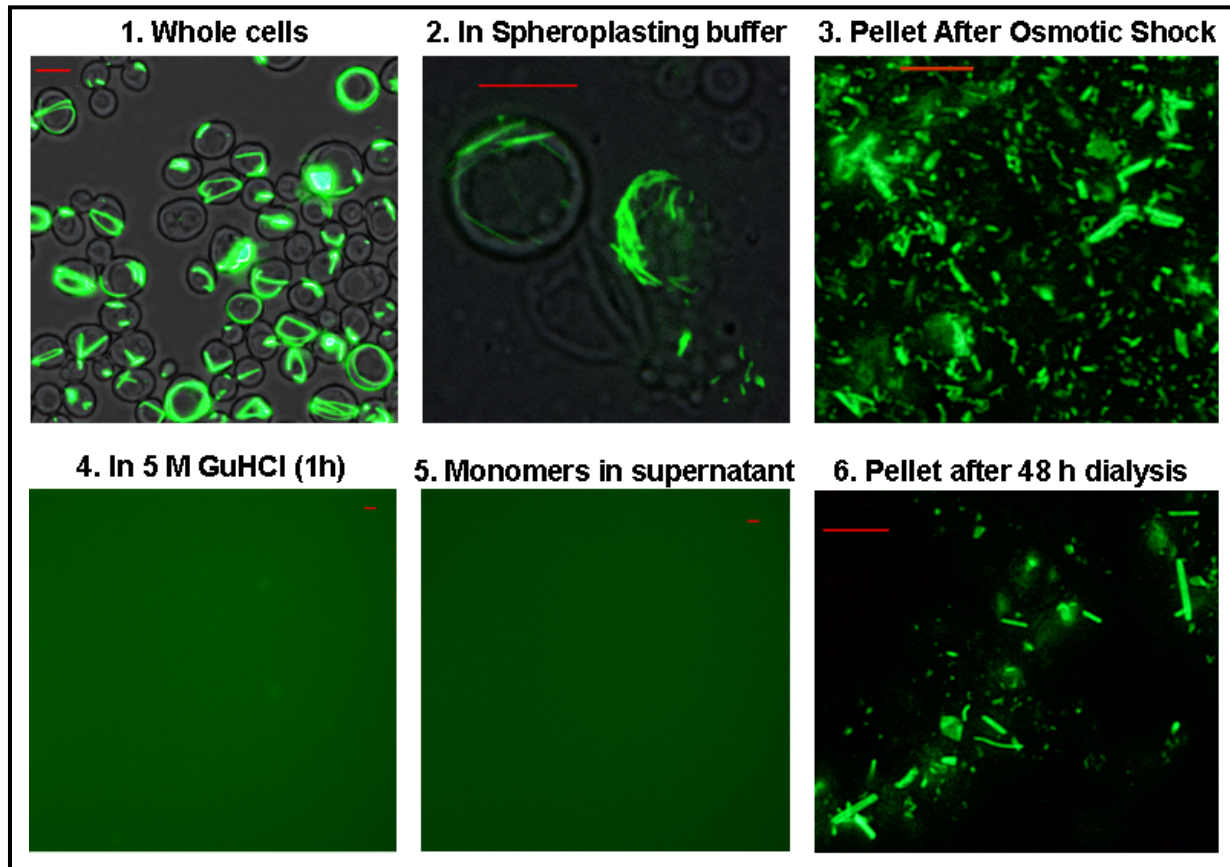


**Figure 32.** Fluorescence microscopy images of *in vitro* recrystallization of SbsC-eGFP. **1)** Cells expressing tubular SbsC-eGFP assemblies were grown overnight with shaking at 30°C in YNB media and centrifuged **2)** Pellet of cells was resuspended in spheroplasting buffer containing zymolase and incubated at 30°C for 1.5 h. *In vivo* tubular structures were maintained during the enzymatic disruption of the cell walls *in situ*. **3)** Spheroplasts were burst with osmotic shock and SL tubes were collected as a pellet. **4)** In order to obtain SL monomers, pellet was resuspended in 5 M GuHCl. After 1 h of incubation, no SL structure was observed. **5)** Monomers were collected in supernatant. **6)** Following the removal of the chaotropic agent GuHCl by dialysis against 10 mM CaCl<sub>2</sub> for 48 h, we obtained the successful reassembly of SbsC-monomers into fluorescent tubular structures in dialysis buffer. Scale Bar = 5 μm

### 3.5.2. *In vitro* Recrystallization of S13240-eGFP

The same procedure was followed for S13240-eGFP expressing cells. The corresponding cells were first spheroplasted and then burst with osmotic shock. Structures observed in spheroplasts and in pellets after the osmotic shock were similar (Fig. 33-1 & Fig. 33-2). Fibrillar network structures were obtained in the pellet after the osmotic shock. Following the monomerization, no specific SL structure was seen, instead only plain fluorescence without any structure was visualized (Fig. 33-3). Removal of GuHCl by dialysis for 48 h against 10 mM CaCl<sub>2</sub> at pH 5.5 resulted in the formation of fluorescent SL structures (Fig. 33-4). The obtained *in vitro* assemblies were similar to *in situ* case but the structures were more densely packed most probably due to the changed ionic strength of the environment.

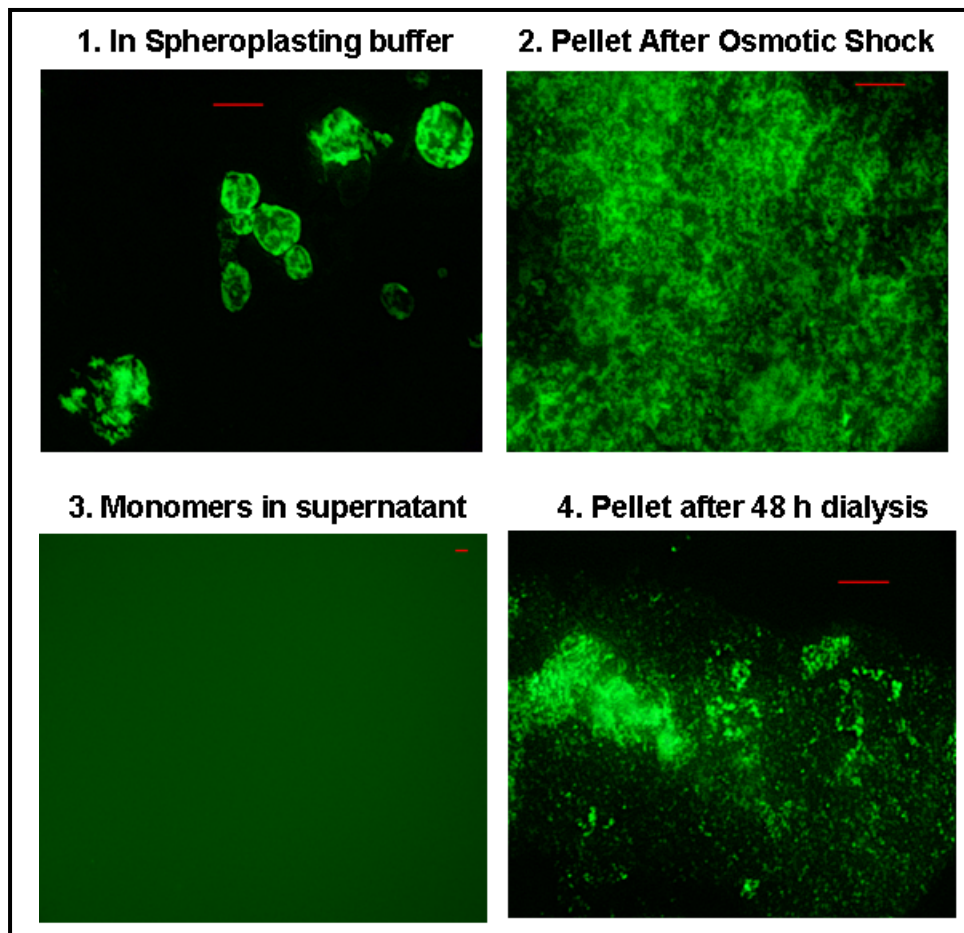


**Figure 33.** Fluorescence microscopy images of *in vitro* recrystallization of S13240-eGFP. Cells expressing tubular S13240-eGFP assemblies were grown overnight with shaking at 30°C in YNB media and centrifuged **1)** Pellet of cells was resuspended in spheroplasting buffer containing zymolase and incubated at 30°C for 1.5 h. *In vivo* network structures were maintained during the enzymatic disruption of the cell walls *in situ*. **2)** Spheroplasts were burst with osmotic shock and SL assemblies were collected as a pellet. **3)** Pellet was resuspended in 5 M GuHCl. After 1 h of incubation, no SL structure was observed. Monomers were collected in supernatant. **4)** Following the dialysis against 10 mM CaCl<sub>2</sub> for 48 h, the successful reassembly of S13240-monomers into fluorescent structures in dialysis buffer was observed. Scale Bar = 5 μm

### 3.5.3. *In vitro* Recrystallization of SslA-eGFP

*In vitro* recrystallization of SslA-eGFP assemblies was performed similar to other SL-eGFP preparations (Fig. 34). In spheroplasting buffer, I observed the cells expressing SslA-eGFP with fluorescent patches which were maintained after the osmotic shock as well (Fig. 34-2). Plain fluorescence lacking any distinct structure was obtained after the monomerization step (Fig. 34-3). Unlike mSbsC-eGFP and S13240-eGFP monomers for which 24 h of dialysis was enough for the formation of SL assemblies, SslA-eGFP monomers took 2 weeks to form fluorescent assemblies of finer patches and tube-like structures (Fig. 34-4). *In situ* and *in vitro*

SslA-eGFP structures were different. While these SL proteins formed fluorescent patches *in situ*, after recrystallization they self-assembled into finer patches together with tube-like assemblies *in vitro*.

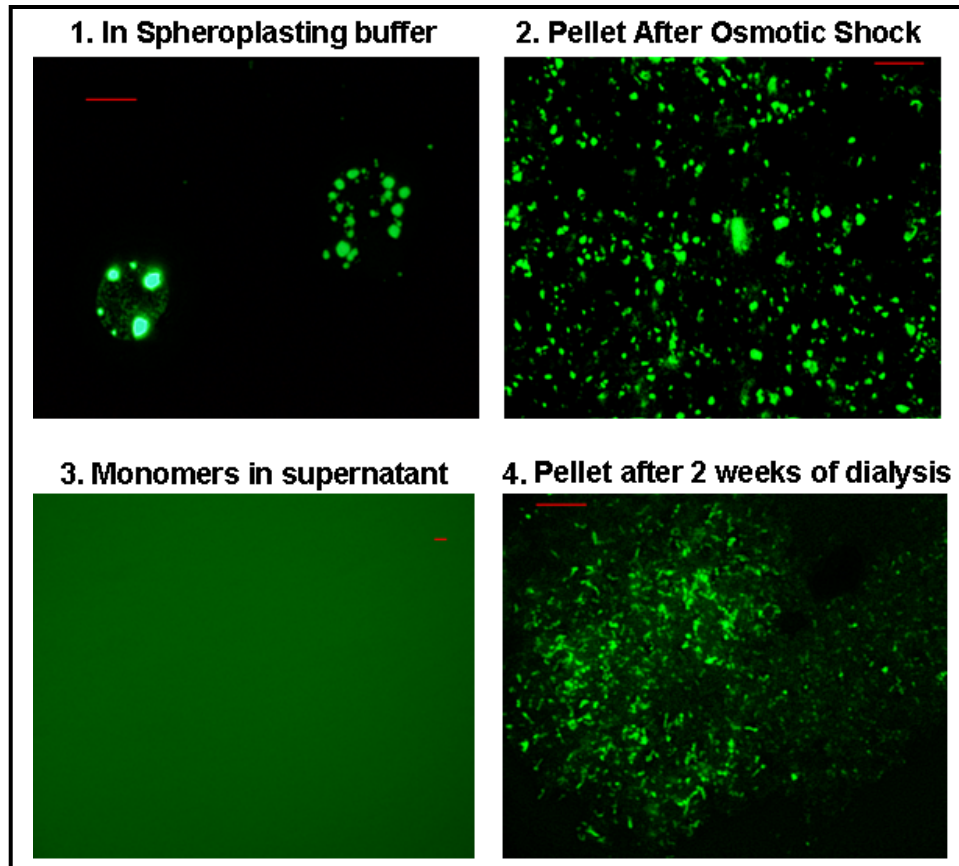


**Figure 34.** Fluorescence microscopy images of *in vitro* recrystallization of SslA-eGFP. Cells expressing SslA-eGFP were grown overnight with shaking at 30°C in YNB media and centrifuged down. **1)** Pellet of cells was resuspended in spheroplasting buffer containing zymolase and incubated at 30°C for 1.5 h. *In-vivo* tubular structures were maintained *in-situ* during the enzymatic disruption of the cell walls. **2)** Spheroplasts were burst with osmotic shock and S-layer patches were collected as a pellet. **3)** S-layers were monomerized in 5 M GuHCl solution. After 1 h of incubation, no S-layer structure was observed. Monomers were collected in supernatant. **4)** Following the dialysis against 10 mM CaCl<sub>2</sub> for 2 weeks, SslA-eGFP monomers self-assembled into fluorescent structures in dialysis buffer. Scale Bar = 5 μm

### 3.5.4. eGFP as Control

As a control the recrystallization experiment was conducted with only eGFP expressing yeast cells. After the enzymatic disruption of the cell walls, no distinct structure was observed (Fig. 35-1). Spheroplasts showed the same *in vivo* homogeneous fluorescence pattern. *In vitro* recrystallization resulted in the formation of plain fluorescence areas rather than any distinct structure (Fig. 35-4).



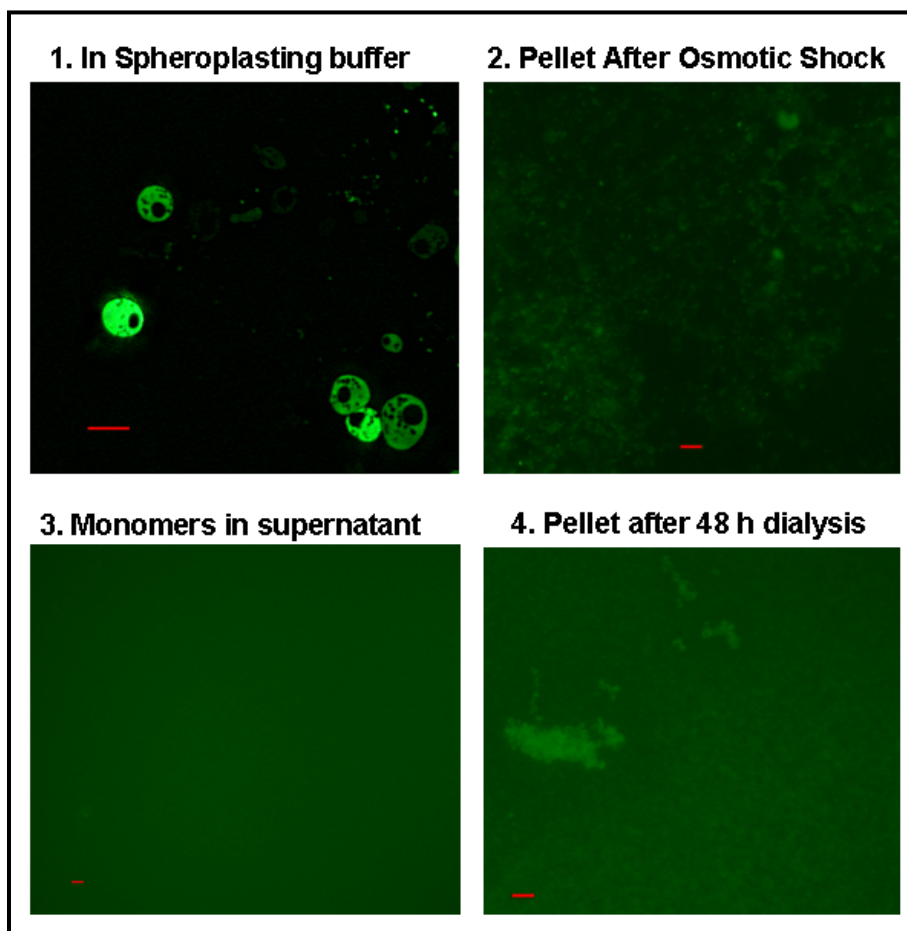


**Figure 35.** Fluorescence microscopy images of *in-vitro* recrystallization of eGFP. Cells expressing eGFP were grown overnight with shaking at 30°C in YNB media and centrifuged down. **1)** Pellet of cells was resuspended in spheroplasting buffer containing zymolase and incubated at 30°C for 1.5 h. **2)** Spheroplasts were burst with osmotic shock **3)** Proteins were monomerized in 5 M GuHCl **4)** Following the dialysis against 10 mM CaCl<sub>2</sub> for 48 h or longer, no specific structure was observed other than some coagulated eGFP proteins. Scale Bar = 5 μm

### 3.5.5. Characterization of *In vitro* Recrystallized SL-eGFP Structures

All of the SL-eGFP monomers were able to self-assemble into specific structures namely tubes, patches or networks after dialysis against 10 mM CaCl<sub>2</sub> at pH 5.5. These *in vitro* structures were investigated both with a fluorescence microscope and SEM. mSbsC-eGFP structures were composed of tubular assemblies (Fig. 36, second row). SslA-eGFP monomers self-assembled into either patches or tubular structures (Fig. 37, first column). However, the patches that were observed with SEM were larger than the ones observed with the fluorescence microscopy (Fig. 36, first row). Most probably, some of SslA-eGFP proteins failed to get fluorescent due to the misfolding of eGFP. *In vitro* S13240-eGFP assemblies were observed as oval surfaces with the fluorescence microscopy (Fig. 36, third row).

Although mSbsC-eGFP was mostly visualized as tubular assemblies, SslA-eGFP and S13240-eGFP were observed as either patches, folded layers or tube-like structures (Fig. 37).

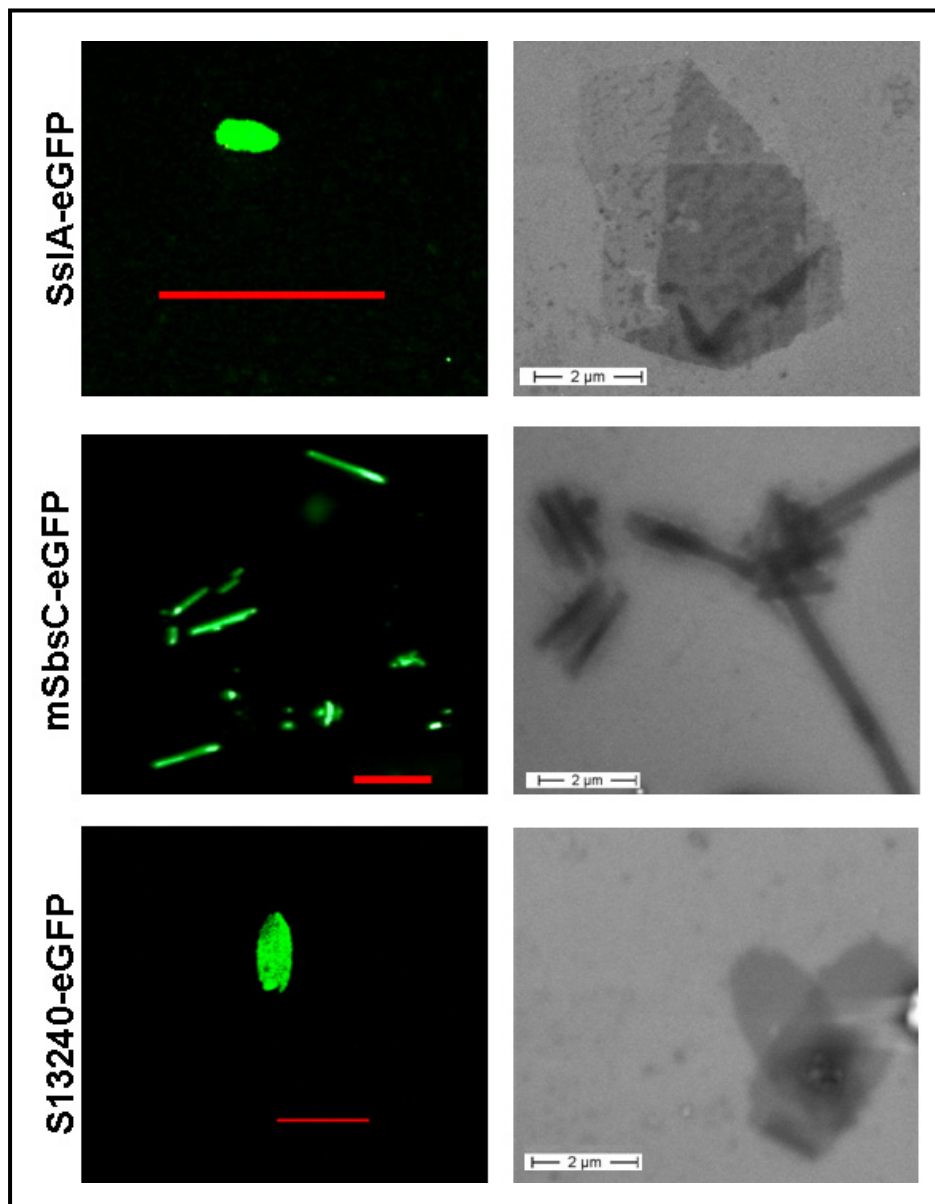


**Figure 36.** Fluorescence microscopy (a) and SEM (b) images of *in vitro* recrystallized recombinant mSbsC-eGFP from *S. cerevisiae* BY4741 cells. SL were isolated from osmotically lysed cells by centrifugation, monomerized with 5 M GuHCl, and dialyzed against 10 mM CaCl<sub>2</sub> at pH 5.5 for 48 h. SEM pictures were made at 2 kV. Red scale bar = 5 μm



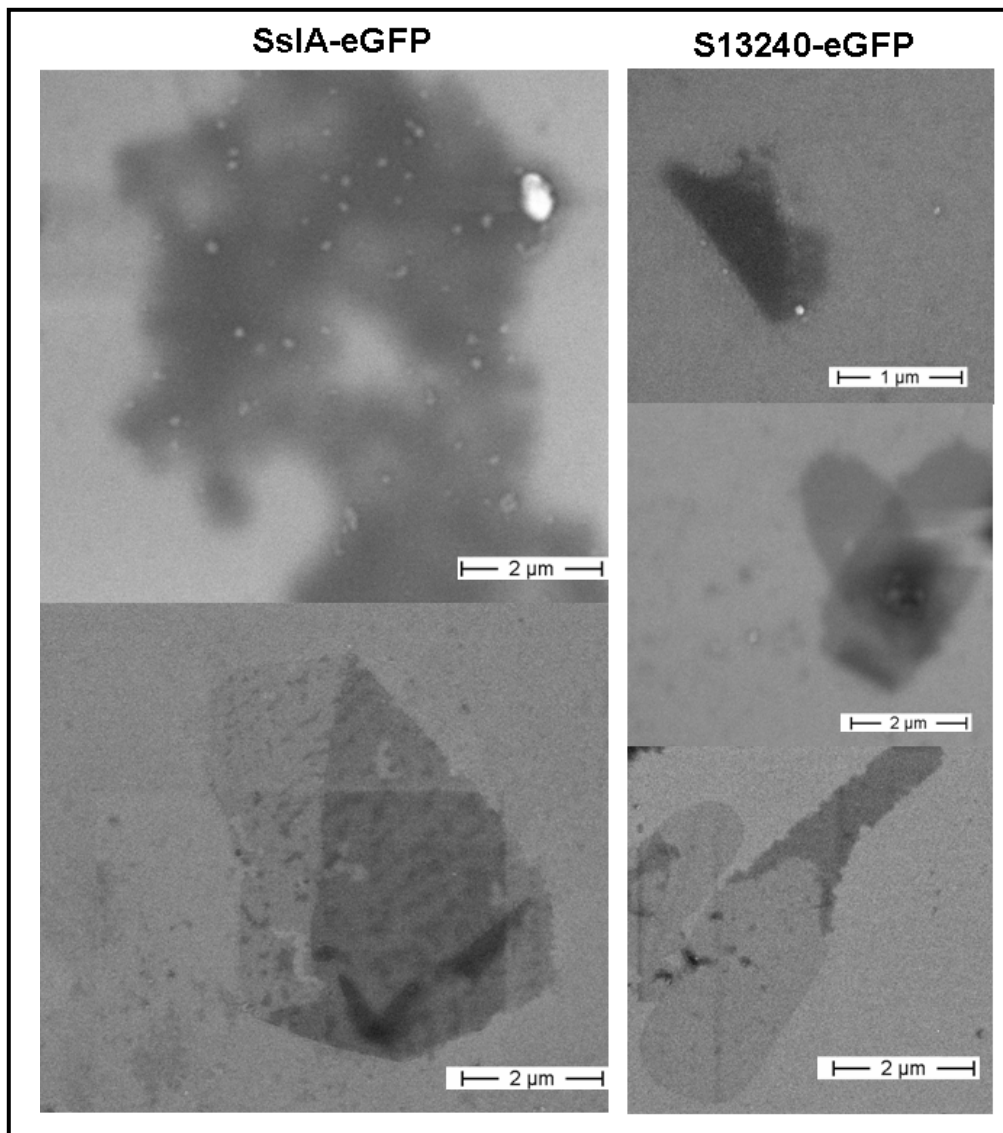


**Figure 37.** SEM images of different forms of *in vitro* recrystallized SslA-eGFP and S13240-eGFP proteins from *S. cerevisiae* BY4741 cells. SL were isolated from osmotically lysed cells by centrifugation, monomerized with 5 M GuHCl, and dialyzed against 10 mM CaCl<sub>2</sub> at pH 5.5 for 48 h. Pictures were made at 2 kV.

### 3.5.6. Recrystallization of mSbsC-eGFP on Surfaces

It has recently been reported that SL monomers can self-assemble into monomolecular arrays in suspensions, on solid surfaces e.g. silicon, glass, carbon and synthetic polymers or lipid films [5]. In previous sections, results regarding *in vivo* and *in vitro* reassembly of various SL-eGFP fusion proteins were presented. In all cases, recrystallization had taken place in solutions namely either in yeast cytoplasm (*in vivo*) or in dialysis buffer (*in vitro*). Reassembly products were mainly composed of fluorescent tube-like structures, patches or multi-layers. Thus, a set of experiments were performed to recrystallize mSbsC-eGFP monomers on solid surfaces. In fact, a glass cover slip was divided into pieces and placed into

the dialysis tubings containing the SL monomers. The tubing content was dialyzed against 10 mM CaCl<sub>2</sub> for 24 h at pH 5.5 and the pieces of glass were investigated with a fluorescence microscope. I could not observe any tube-like assemblies on the glass surfaces; instead, mSbsC-eGFP monomers self-assembled into fluorescent multi-layers (Fig. 38).

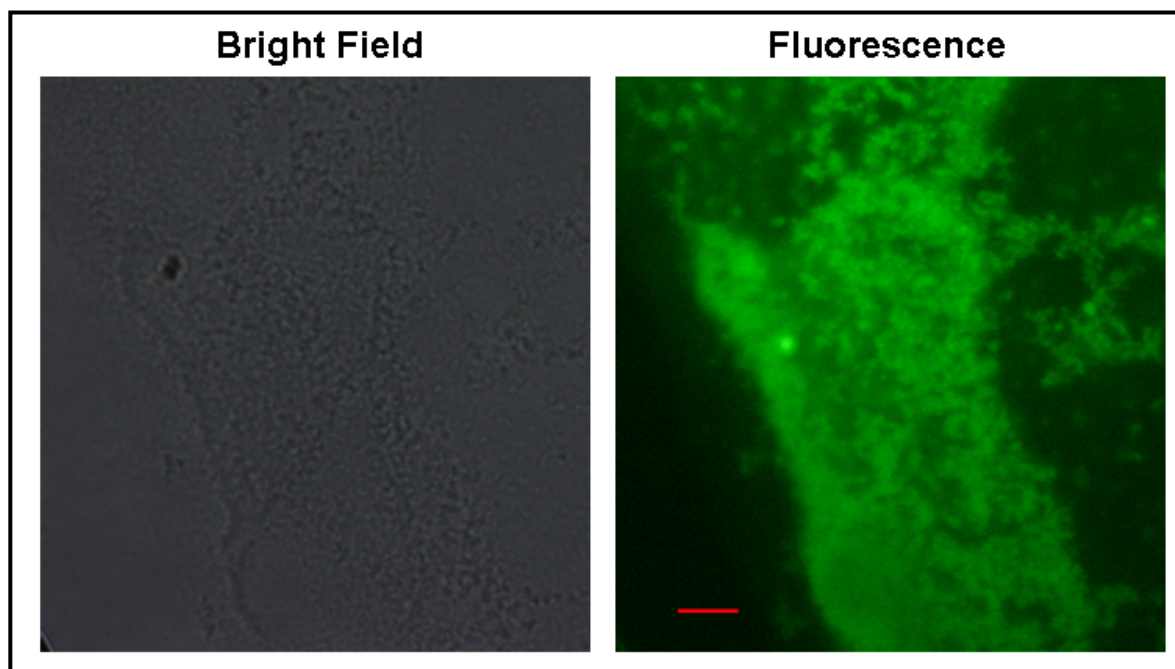


**Figure 38.** *In vitro* recrystallization of mSbsC-eGFP monomers on a glass surface. Pieces of glass were placed into the dialysis tubings containing the SL monomers. The tubing content was dialyzed against 10 mM CaCl<sub>2</sub> for 24 h at pH 5.5 and the pieces of glass were investigated with a fluorescence microscope. Scale Bar = 5  $\mu$ m

### 3.5.7. Influence of Calcium Concentration, pH and Dialysis Time on *in vitro* Recrystallization Process

All of the *in vitro* recrystallization experiments were conducted in the presence of 10 mM CaCl<sub>2</sub>. In this section, the factors affecting *in vitro* recrystallization process were investigated. The question was: Can we control the length and the diameter of *in vitro* formed mSbsC-eGFP tubes? For this purpose, effects of CaCl<sub>2</sub> concentration, pH and the dialysis time on the *in vitro* reassembly process of mSbsC-eGFP monomers were studied.

#### 3.5.7.1. Effect of Calcium Concentration

The first parameter to investigate the recrystallization process was the calcium concentration of the dialysis buffer. mSbsC-eGFP fusion protein monomers were analyzed by applying CaCl<sub>2</sub> concentrations of 0 mM, 1 mM, 10 mM, and 20 mM, respectively, in the dialysis

buffer. Dialysis was performed for 24 h and 48 h at pH 9.0. In the absence of calcium I observed aggregates of fluorescent proteins, but no tubular structures, neither after 24 h nor after 48 h (Fig. 39, top row). Likewise fluorescence aggregates formed in the presence of 1 mM CaCl<sub>2</sub>, however after 48 h I noticed short tubes of less than 1 μm length (Fig. 39, second row). Recrystallization of SL monomers into tubes longer than 3 μm was observed in the presence of 10 mM CaCl<sub>2</sub> (Fig. 39, third row). Further increase of the CaCl<sub>2</sub> concentration to 20 mM resulted in shorter tube structures and the concomitant appearance of multiple dot-like structures (Fig. 39, last row).

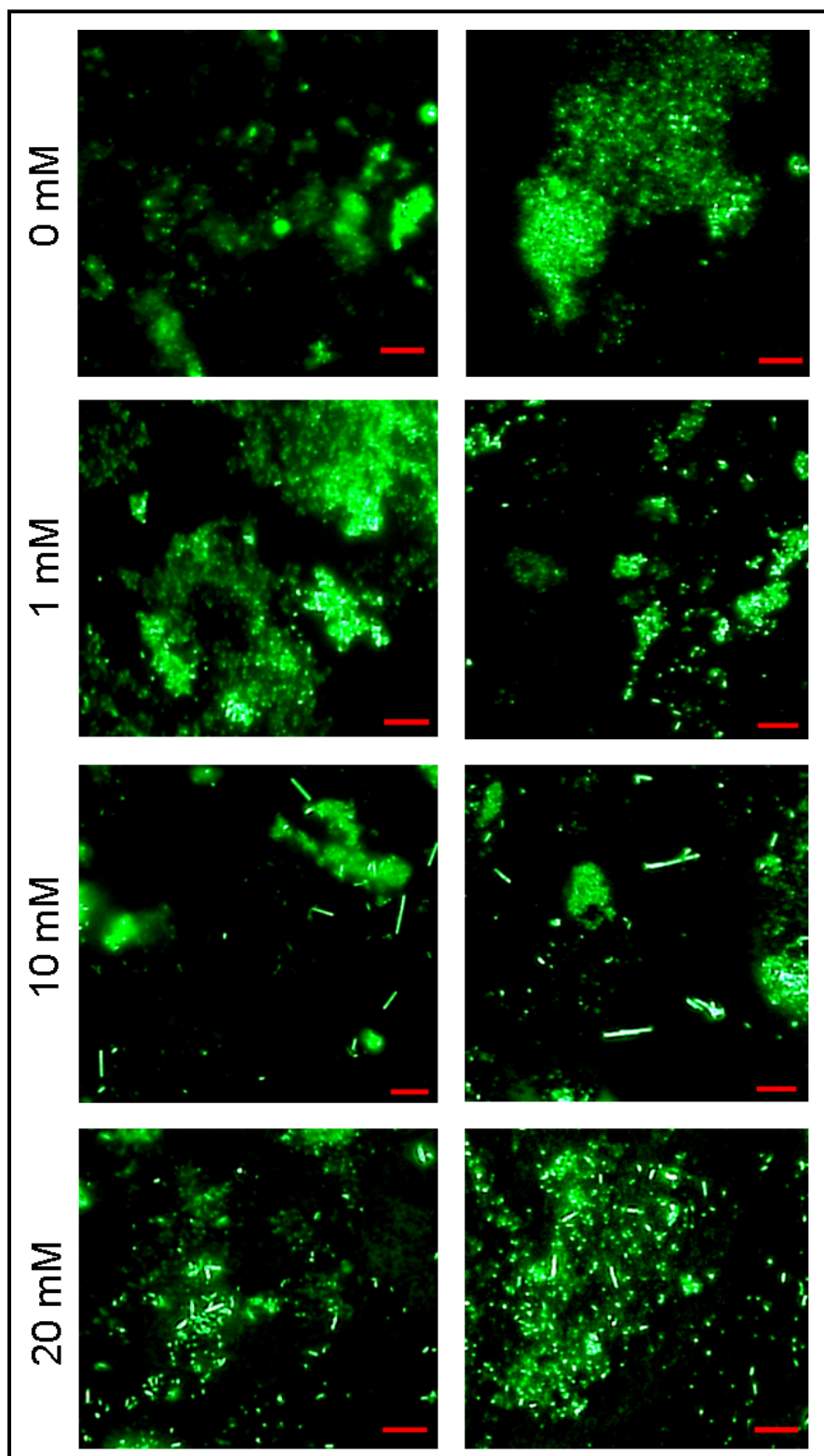


**Figure 39.** *In vitro* recrystallization of mSbsC-eGFP monomers at different  $\text{CaCl}_2$  concentrations. Tubular structures were obtained by dialyzing the monomers against 0 mM, 1 mM, 10 mM and 20 mM  $\text{CaCl}_2$  for 24 h (first column) and for 48 h (second column) at pH 9.0. Scale Bar = 5  $\mu\text{m}$

### 3.5.7.2. Effect of pH and Dialysis Time

The effect of the pH value on the recrystallization of mSbsC-eGFP was tested by varying the pH of the dialysis buffer which is mainly composed of 10 mM CaCl<sub>2</sub>. Three different pH values were analyzed: pH 5.5, pH 7.5, and pH 9.0 (Fig. 40). With higher pH values, the average length of the SL tubes increased from 2.5 μm (pH 5.5) and 2.96 μm (pH 7.5) to 3.34 μm (pH 9.0) after 24 h dialysis, and from 2.69 μm (pH 5.5), 3.61 μm (pH 7.5) to 4.13 μm (pH 9.0) after 48 h dialysis (Table 3). The longest tubes with 8.11 μm and 9.08 μm were obtained at pH 9.0 after 24 h and 48 h, respectively (Table 3). The average *in vitro* tube diameter was in the range of 0.3-0.5 μm as *in vivo* and *in situ*. Additionally, regardless of the pH of the dialysis buffer, when the dialysis was performed longer, it was observed that the average tube lengths got longer (Table 3). For example, at pH 9.0 the average tube length was 3.34 μm after 24 h of dialysis. At the end of 48 h, the average tube length increased to 4.13 μm. This observation was the same for other pH values.

**Table 3.** Effect of dialysis time and pH on maximum, minimum, and average lengths of *in vitro* recrystallized mSbsC-eGFP tubular structures

Dialysis time	mSbsC-eGFP length (μm)								
	pH 5.5			pH 7.5			pH 9.0		
	Max	Min	Avg	Max	Min	Avg	Max	Min	Avg
24 h	6.11	0.80	2.50	5.72	1.24	2.96	8.11	0.81	3.34
48 h	5.76	0.67	2.69	7.07	0.61	3.61	9.08	1.00	4.13

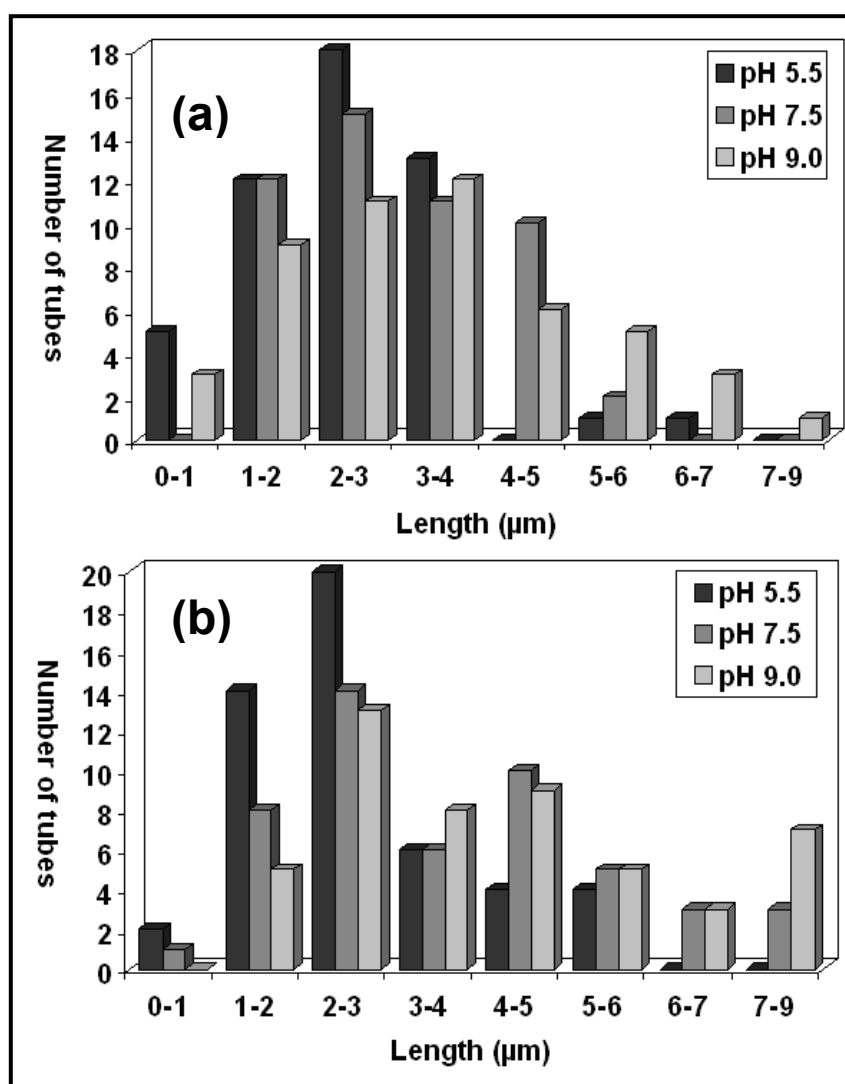


**Figure 40.** Length distribution diagram of 50 recrystallized mSbsC-eGFP proteins at different pH values. Tubular structures were obtained by dialyzing the monomers against 10 mM CaCl<sub>2</sub> for 24 h (a) and for 48 h (b) at pH 5.5, pH 7.5 and pH 9.0.

### 3.6. Metallization of mSbsC-eGFP Tubes

Metal deposition on SL structures has been widely studied. Mertig *et al.* [49] have utilized SL of *S. ureae* with tetragonal lattice symmetry and 13.2 nm lattice spacing as a protein template to chemically deposit platinum clusters leading to the formation of highly ordered arrays of platinum. Besides the chemical deposition of metal nanoparticles or ions on SLs, one can also apply electrodeposition. Allred *et al.* [51] reported isolation and recrystallization of SLs from different microorganisms on platinum coated gold surfaces, and subsequent electrodeposition of cuprous oxide as a step towards electrochemical nano-device fabrication. In this section, I

investigated the possibility to perform chemical deposition of platinum on *in vitro* recrystallized tubular mSbsC-eGFP structures and the factors influencing this process.

### 3.6.1. Effect of Temperature on Metallization

To this end, the SL assemblies formed upon dialysis were treated with  $\text{K}_2\text{PtCl}_4$  in the presence of a reducing agent ( $\text{NaN}_3$ ). I investigated the effect of reaction temperature on the reduction potential of  $\text{Pt}^{2+}$  ions. For this purpose metallization was performed at RT and at  $4^\circ\text{C}$ . I observed the accumulation of Pt particles on SL tubes after 4 h of reduction reaction at only RT as can be seen in Fig. 41a. The reaction conducted at  $4^\circ\text{C}$  for 4 h did not demonstrate any formation of metal particles due to the decreased reaction rate (Fig. 41b). The observed SL tubes were not covered with any metal particulates and they have the same physical appearance as the control sample which was containing the reducing agent but not  $\text{K}_2\text{PtCl}_4$  and which was incubated at RT for 4 hours.

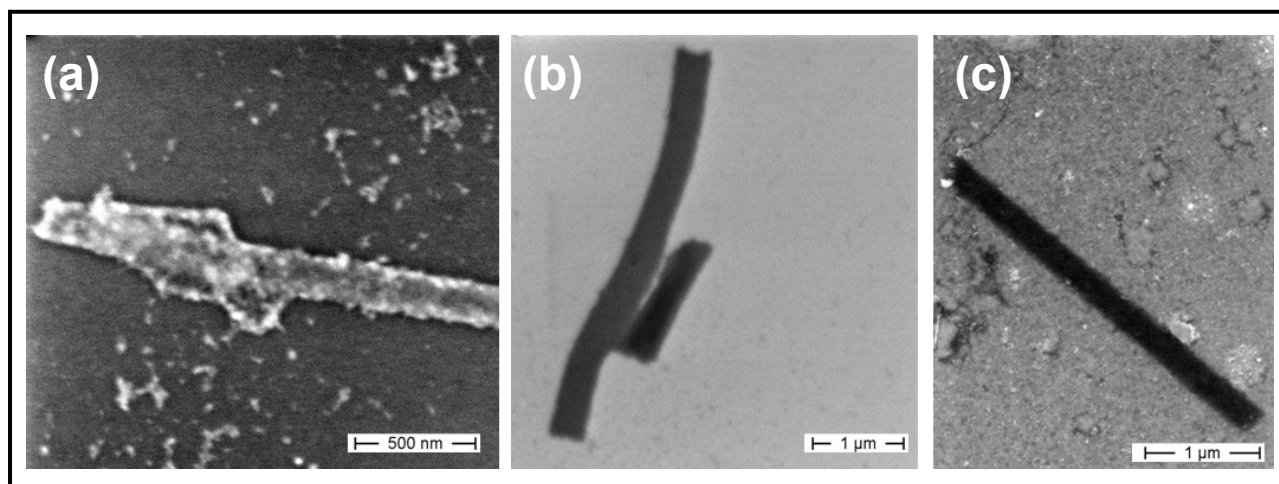


**Figure 41.** Metallization of *in vitro* recrystallized mSbsC-eGFP tubes at different temperatures. SLs resuspended in metallization buffer containing the reducing agent (3 mM  $\text{NaN}_3$ ) were incubated in 3 mM salt solution and incubated for 4 h at (a) RT and (b)  $4^\circ\text{C}$ . (c) SLs resuspended in metallization buffer without any  $\text{K}_2\text{PtCl}_4$  as control (after 4 h of incubation at RT). Pictures were made at 2 kV with SEM.

### 3.6.2. Effect of Platinum Concentration on Metallization

In order to optimize the amount of Pt required for the metallization process, I tested different combinations of  $\text{K}_2\text{PtCl}_4$  and protein concentrations. For this purpose, metallization was performed at RT for 4 h with three different  $\text{K}_2\text{PtCl}_4$  concentrations: 3 mM, 6 mM and 30 mM. I observed an increase in plasticity caused by the metal coat with SEM as  $\text{K}_2\text{PtCl}_4$  concentration was increased from 3 mM to 30 mM (Fig. 42, first row). Control samples were

visualized as 2D dark thin tubular layers (Fig. 42, second row). Metallized probes were brighter due to the increased contrast caused by bound metal particles so that I could make more detailed, better focused pictures where folded layers of SL tubes could be visualized (Fig. 42a & Fig. 44a).

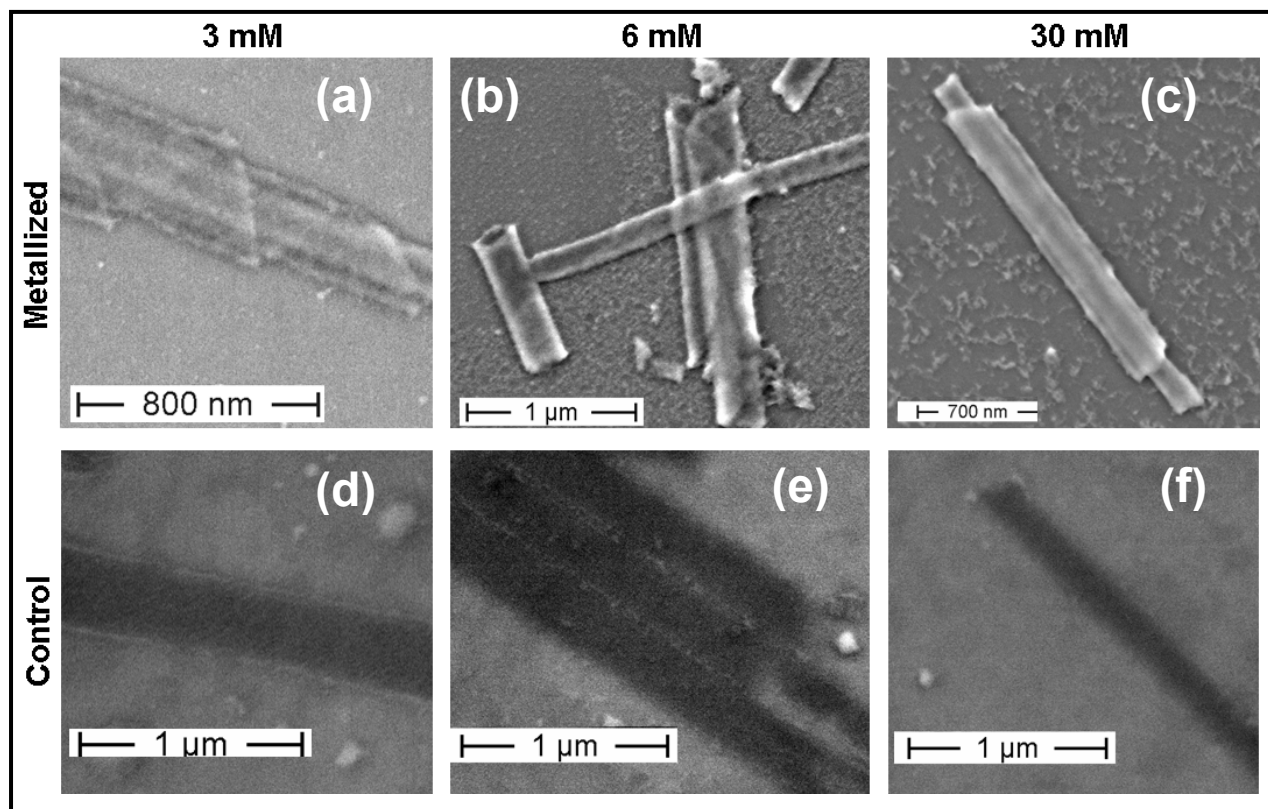


**Figure 42.** Metallization of *in vitro* recrystallized mSbsC-eGFP tubes at different  $K_2PtCl_4$  concentrations. SLs resuspended in metallization buffer containing the reducing agent ( $NaN_3$ ) were incubated in 3 mM (a), 6 mM (b) and 30 mM (c)  $K_2PtCl_4$  salt solution and incubated for 4 h at RT. Lower row represents the control SL samples resuspended in metallization buffer containing 3 mM (d), 6 mM (e) and 30 mM (f)  $NaN_3$  without any  $K_2PtCl_4$ . Pictures were made at 2 kV with SEM.

Samples metallized with 3 mM, 6 mM and 30 mM  $K_2PtCl_4$  at RT for 4 h were investigated with a fluorescence microscope. Control samples containing the reducing agent but not the metal salt solution showed fluorescent mSbsC-eGFP tubes showing that the reducing agent did not interfere with eGFP signal (Fig. 43). In the brightfield the tubular structures could not be observed due to their thinness (Fig. 43). Upon metallization, the tubes could be visualized in the brightfield due to the increased contrast and thickness caused by the metal coats. As the metal concentration increased, the brightfield signal was enhanced showing the effect of the metal coat (Fig. 43). Interestingly, I could not observe any fluorescence signal in metallized samples.



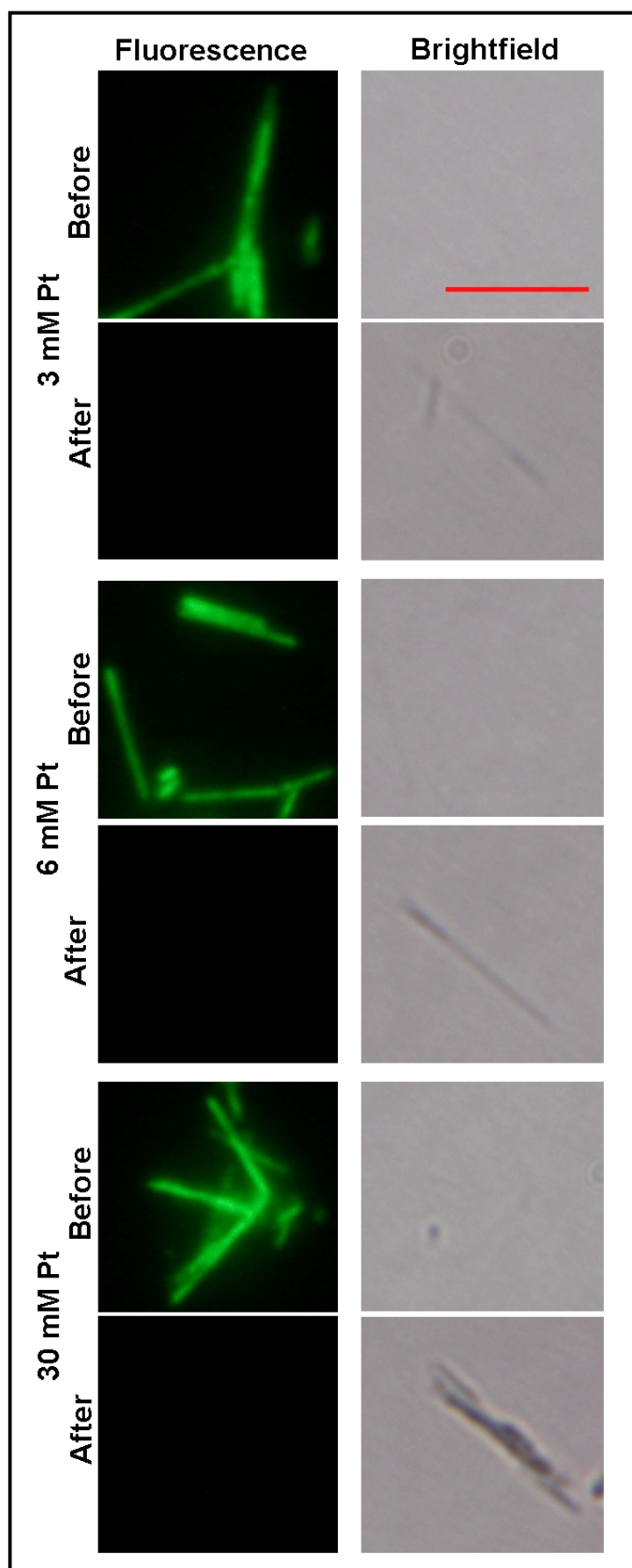


**Figure 43.** Fluorescence and brightfield images after and before metallization with different  $K_2PtCl_4$  concentrations. Samples were resuspended in  $NaN_3$  buffer without  $K_2PtCl_4$  as control (“before”). Metallization occurred by addition of 3 mM, 6 mM and 30 mM  $K_2PtCl_4$  in the presence of reducing agent  $NaN_3$  (“after”). The exposure times for brightfield and the fluorescence images are 1/9 s and 8 s, respectively. Scale bar = 5  $\mu m$

Optimal conditions for the regular deposition of Pt were obtained with 30 mM  $K_2PtCl_4$  and 50  $\mu g$  of protein. As can be seen in Fig. 44a (left), the SL tubes were coated under these conditions with Pt, as revealed by EDX analysis (Fig. 44a, right). The additional peaks for chlorine and potassium originate from the  $K_2PtCl_4$  salt solution. In the control sample, which was treated in the absence of platinum salt, no Pt peak was obtained (Fig. 44b). The metalized structure seen in Fig. 44a nicely demonstrates that the tube-like structures resulted from folded layers.

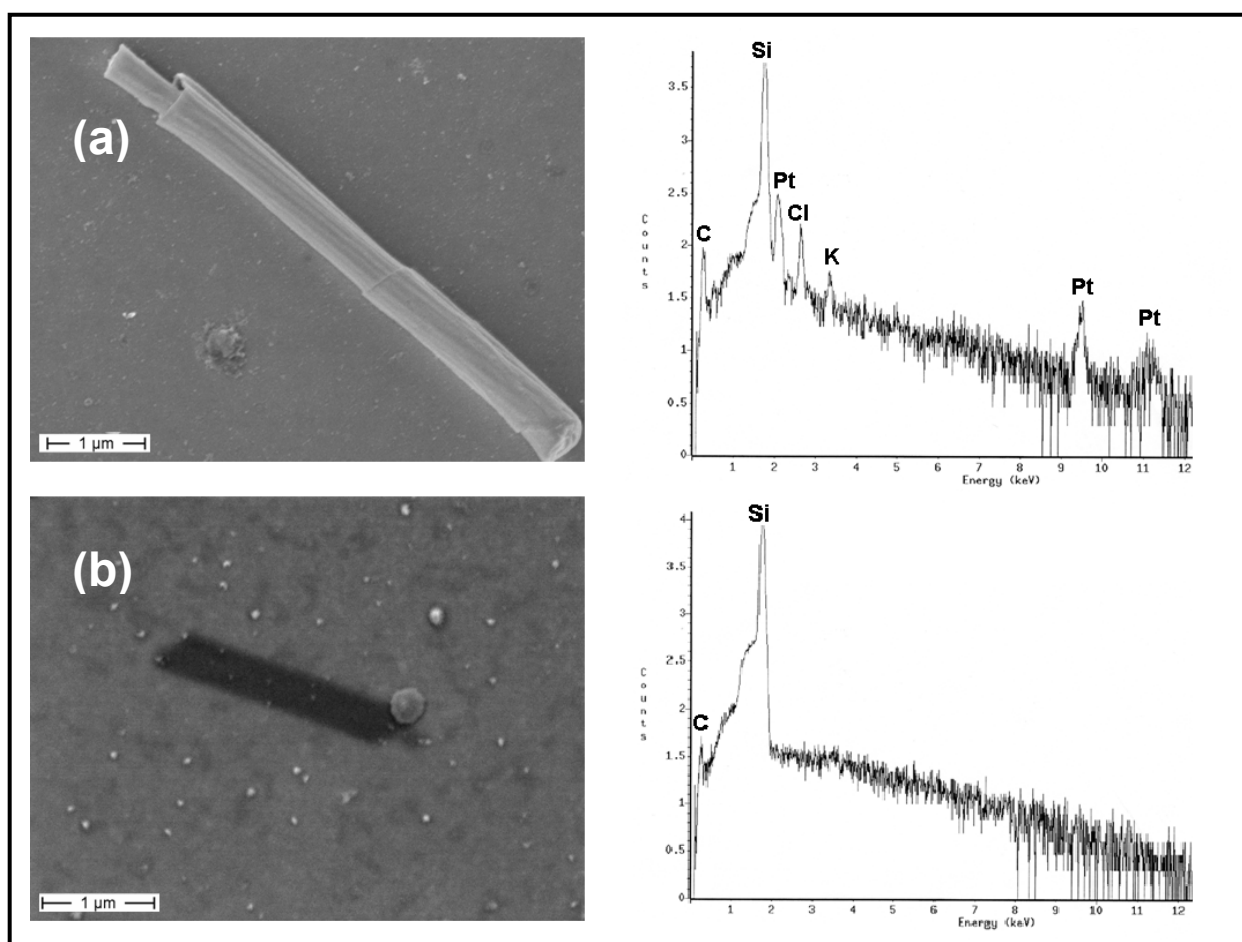


**Figure 44.** SEM images of tube-like structures from *in vitro* recrystallized mSbsC-eGFP. SL structures were treated with (a) or without (b)  $K_2PtCl_4$  in the presence of  $NaN_3$ . The regular deposition of Pt was obtained with 30 mM  $K_2PtCl_4$  and 50  $\mu g$  of protein. Pictures were made at 2 kV. The respective EDX graphs are shown on the right. Analysis was conducted at 15 kV.

## IV. Discussion

### 4.1. Expression Analyses of Recombinant SL Proteins in Yeast

SslA-eGFP (123 kDa), mSbsC-eGFP (139 kDa) and S13240-eGFP (137 kDa) fusion proteins were expressed in yeast *S. cerevisiae* BY4741 and it was observed that the recombinant protein expression did not interfere with the growth of the culture (Fig. 14) as it was already reported by Blecha *et al.* [57]. This showed that the heterologous expression of SL-eGFP proteins did not have any obvious side-effect on wild-type yeast metabolism and cell cycle mechanism.

Fluorescence measurements revealed that fluorescence signal increased during the exponential phase, but it decreased dramatically with the beginning of the stationary phase (Fig. 14). This was most probably caused by a combination of reduced protein expression level, elevated proteolysis, and decrease of the intracellular pH during the stationary phase. It was previously reported that activities of many proteolytic enzymes, i.e aminopeptidase yscCo, carboxypeptidase yscY, proteinase yscA and proteinase yscB, increased several folds when *S. cerevisiae* cells entered the stationary phase [95]. Western blot analyses were performed in the presence of protease inhibitors by collecting cell samples at certain time points throughout the cultivation. Protein degradation was already detected in mid-exponential cells (Fig. 19) showing that one of the reasons causing the fluorescence decrease was proteolysis. It is known that the fluorescence intensity of eGFP depends on various factors such as pH, temperature, protein concentration and preliminary illumination [73]. It was previously published that during the stationary phase, yeast cellular pH decreases. Imai *et al.* [74] have shown that the intracellular pH of *S. cerevisiae* cells was decreasing from pH 6.8 (exponential phase) to pH 5.5 (stationary phase) by using a fluorescence microscopic image processing technique. Tsien [73] has stated that wild-type GFP can be quenched at high (pH > 11) or low (pH < 5) pH values and the GFP variants such as eGFP which were designed to have enhanced spectral properties at pH 7.0 are more sensitive to pH changes. Patterson *et al.* [75] have reported that eGFP can be quenched 50% at pH 5.5 which was found to be the intracellular pH value of stationary yeast cells. This conclusion is in line with our results where I observed a sharp decrease in fluorescence intensities of stationary *S. cerevisiae* cells expressing SL-eGFP fusion proteins.

Fluorescence imaging revealed that SslA-eGFP fusion protein was expressed as fluorescent patches, mSbsC-eGFP as tubular networks and S13240-eGFP as hollow-like fibrillar network structures while eGFP did not show any distinct structure (Fig. 15). The *in vivo* SL-eGFP structures remarkably differed from that of the native bacterial envelope structures where SL monomers self-assembled into highly porous mono- or multi-layers [11]. Although SbsC and S13240 monomers can form assemblies with oblique symmetries [69], these two SL proteins self-assembled into different structures *in vivo*. This could have resulted from different patterns of monomer-monomer interactions which were most probably caused by the aa composition of SLs. It has been demonstrated that SbsC and S13240 have 95.6 % homology for 270 aa of the N-terminal region which is not necessary for the self-assembly process [69]. Recently, Pavkov *et al.* [25] have investigated the structure and binding characteristics of SbsC. They reported that SbsC is composed of six separate domains connected by short flexible linkers. Domain I (aa31-260) contains mostly positively charged and aromatic side chains, which mediate the binding to negatively charged Secondary Cell Wall Polymers (SCWP). The remaining domains together with the C-terminal part are responsible for the monomer-monomer interactions. Since the remaining domains' aa compositions differ in SbsC and S13240, it is possible to have altered monomer-monomer interactions resulting in the formation of different *in vivo* SL-eGFP structures. SslA, which was determined to have a tetragonal symmetry [70], was observed to form fluorescent patches *in vivo*.

Contrary to the findings of Blecha *et al.* [57] who did not observe any degradation products during the mSbsC-eGFP expression in *S. cerevisiae*, some degradation products were noticed in all of the SL-eGFP constructs during the cultivation despite the use of protease inhibitors during the cell lysis step (Fig. 15). Possibly, the time point and/or modifications of the sample preparation can account for the observed differences. It was seen that as the cultivation time increased, the level of degradation raised. Surprisingly, no degradation product was detected for eGFP. Since eGFP is composed of a barrel structure composed of 11  $\beta$ -strands [73], this makes the protein quite stable against proteolytic degradation. However, time course detection of SL-eGFP constructs with monoclonal anti-GFP antibodies showed the presence of degradation bands lower than 27 kDa implying that eGFP was degraded during the cultivation (Fig. 19). Most probably, fusion of SL proteins to eGFP altered the conformation of the fluorescence protein so that possible hidden proteolytic cleavage sites of the native protein became accessible for proteases. Among the SL-eGFP fusion proteins, mSbsC-eGFP was the most proteolysis resistant protein since less degradation bands were detected (Fig.

19). mSbsC-eGFP monomers form tube-like *in vivo* assemblies which can be found as a network as well. During the self-assembly process, protease binding sites could be located in such a way that this may make the SL fusion proteins less accessible to proteases, thus making them more stable to intracellular degradation.

Additionally, I investigated the heterologous expression of SL proteins (SslA, SbsC and S13240) tagged with positively charged aa (Arg, His or Lys), a TEV protease cleavage site (TEV) and eGFP. The aim was to construct SL proteins capable of binding toxic metals which are found as anionic compounds in wastewater such as selenium, arsenic, molybdenum and antimony [76]. For this purpose, p426-GPD-SL-3xArg/His/Lys-TEV-eGFP plasmids (Section 2.1.9) were generated, cloned and expressed in yeast *S. cerevisiae* BY4741. Fluorescence microscopy images of overnight grown cultures showed no structural differences from the corresponding *in vivo* SL-eGFP structures (Fig. 17) showing that the additional aa-TEV tags did not interfere with the *in vivo* fusion protein expression.

## 4.2. *In vivo* Thermal Stability of SL-eGFP Proteins

Proteins are programmed to function efficiently at the environmental temperatures of organisms to which they belong meaning that proteins are mainly functionally active in a specific temperature range. Outside this range, proteins can lose their structural integrity, denature and lose their functionalities [77]. In this study, thermal stabilities of *in vivo* expressed SL-eGFP constructs were investigated. Pellets of cells expressing the corresponding SL fusion proteins were incubated at 80°C for 2 days and for additional 2 days at 100°C. Corresponding protein bands for SslA-eGFP (123 kDa), S13240-eGFP (137 kDa) and eGFP (27 kDa) were detected by Western blotting. In contrast, no protein signal was detected for mSbsC-eGFP. The most and the least thermostable fusion constructs were S13240-eGFP and mSbsC-eGFP respectively according to the Western blot analyses where the strongest signals were detected from S13240-eGFP expressing cells. The same results were obtained with the second set of experiments conducted at 100°C for 2, 6 and 8 days.

SbsC and S13240 are SL proteins of two different strains of thermophilic *B. stearothermophilus* bacteria. These cells can be cultivated optimally at 55 °C and some of their proteins have been found to be stable at elevated temperatures, i.e.  $\alpha$ -Amylase from *B. stearothermophilus* was found to show activity even at 95°C [78]. It has been reported that

thermostable proteins are rather compact (well-packed), they have larger surface areas hidden upon oligomerization and they were composed of increased number of hydrogen bonds [79]. SL proteins are composed of monomeric subunits which interact with hydrogen bonds making them more thermostable. According to Western blot analyses, mSbsC-eGFP fusion protein was the weakest protein in terms of thermal stability because the regarding protein bands could not be detected after the heat treatment. This could be explained by the tertiary structure of the protein. Until now, only the tertiary structure of SbsC has been studied. Pavkov *et al.* [25] have reported on the structure and binding characteristics of SbsC. They stated that SbsC is formed of six domains connected by short flexible linkers and each domain is arranged in such a way that the whole protein has an elongated structure which looks like a string. This reveals that the SbsC monomers are not compact, but instead elongated, that makes them less thermostable. Lately, it has been reported on thermal and chemical denaturation of SL protein of *B. sphaericus* (SbpA) having a square lattice structure [80]. The authors have recrystallized the SbpA monomers on a silicon surface and after 10 min of heat treatment at 70°C, they observed the loss of SL structures by scanning force microscopy. The SL regular lattice arrangements were completely lost which was an irreversible denaturation process. In line with this publication, I observed the loss of *in vivo* fluorescent SL structures after the heat treatment.

eGFP was found to be quite stable after incubation at 100°C for 2 or 6 days. Since eGFP is composed of a barrel structure consisting of 11  $\beta$ -strands [73], this makes the protein compact and quite stable against proteolytic degradation as well as against heat treatment. Although I could not observe the *in-vivo* SL-eGFP structures any more, I could still detect the proteins with anti-GFP antibodies. Most probably, the heat treatment disturbed tertiary structures of SL-eGFP monomers and caused them to disassemble. Since eGFP is quite stable, it was still functional, intact and connected to the SL domain. This enabled us to detect the proteins with anti-GFP antibodies and to visualize the cells expressing SL-eGFP as plain fluorescent cells without any distinct structure comparable to only eGFP expressing cells (Fig 22). In order to understand the mechanism behind the thermal stabilities of SL fusion proteins, similar experiments can be conducted *in vitro* for the further investigations. Fluorescence and electron microscopy analyses of *in vitro* SL structures after and before the heat treatment can enable us to investigate the structural changes in micro and nano scales. If any change is observed, monomerization and subsequent recrystallization experiments can be conducted in

order to investigate whether SL proteins can recover their identical fluorescent *in vitro* structures after the heat treatment.

### 4.3. Formation of SL Assemblies during Mitosis and Meiosis

While investigating the *in vivo* SL-eGFP structures, it was observed that during mitosis, buds emerging from cells expressing SslA-eGFP, S13240-eGFP and eGFP got fluorescent right after the newly developed bud appeared. But, for mSbsC-eGFP expressing cells, the situation was different. The newly appearing buds were never fluorescent. This case brought us to the question how the mSbsC-eGFP structures are formed *in vivo* and how such tubular assemblies are transmitted to the buds during mitosis and meiosis.

With this study, we report for the first time on the kinetics of the formation of recombinant SL assemblies *in vivo* during yeast cell cycle by applying live fluorescence imaging. Our results show that mSbsC-eGFP assemblies do not project from the mother to the daughter cell during budding, instead novel assemblies form independently in the buds (Fig. 23a). In all cases, the new SL developed from a single dot-like structure. I did not observe the parallel formation of several assembly structures. Our data hint at the existence of a single nucleation center where the *in vivo* self-assembly process initiates unlike the case of *in vitro* recrystallization where the self-assembly starts at multiple nucleation sites and continues until the formed layer meets the other layers [81]. It has been reported on the native bacterial SL formation process of many prokaryotes. Like *in vitro* recrystallization, native SL propagation on the outermost layers of prokaryotes occurs at multiple nucleation sites which are random domains [31]. Recently, Pavkov *et al.* [25] have studied formation of SbsC layer on the outermost layer of *B. stearothermophilus*. They showed that SbsC consists of six domains connected with short flexible linkers which involve in introduction of dislocations and disclinations required for the continuous growth of SL arrays on the cell surface which starts at multiple nucleation points.

SL assemblies are composed of monomeric subunits. Monomers should interact with each other first to form dimmers, then oligomers, and finally a polymer. Time-lapse microscopy revealed that a focal assembly structure gave rise to a growing tube-like structure that eventually changed its position and bent, leading to a more complex branched structure (Fig. 23b). Recrystallization of the recombinant S-layer monomers *in vitro* resulted in the

synchronous formation of several tube-like structures of similar size and structure as *in vivo*. This different behavior under *in vivo* and *in vitro* conditions may result either from considerable differences in the concentration of recombinant SL proteins expressed by yeast cells (or available in the *in vitro* recrystallization environment) or from the presence/absence of cellular components that initiate SL-assembly. Understanding the molecular mechanisms underlying the nucleation, interaction of monomers and expansion of the SL assemblies in the yeast cytosol may offer novel strategies for applying recombinant SL in nanobiotechnology.

In order to see how mSbsC-eGFP assemblies are formed and transmitted during meiosis, I crossed *S. cerevisiae* BY4741 (*MATa*) cells expressing mSbsC-eGFP and the mating partner *S. cerevisiae* BY4742 (*MAT $\alpha$* ) cells. Similar to mitosis, diploid cells expressed mSbsC-eGFP fusion protein independently (Fig. 24). Unlike the budding case where mSbsC-eGFP tubes were not projected to the newly developed bud, during the cell fusion in meiosis, SL fusion protein expressed by *S. cerevisiae* BY4741 (*MATa*) extended towards the mating partner BY4742 (*MAT $\alpha$* ) that was not having the corresponding plasmid expressing mSbsC-eGFP (Fig. 24 & Fig. 25). In *S. cerevisiae*, cell fusion starts by the septum degradation which involves the decomposition of the cell wall mediated by  $\alpha$ -pheromone. Degradation of septum causes membrane conjugation and mixing of the cytoplasmic contents [82]. Thus, after the cell fusion, the resulting diploid zygotes continued to express mSbsC-eGFP fusion proteins by using the recombinant plasmids leading to the further progression of SL tubes towards the untransformed mating partner.

Contrary to the situation in vegetative yeast cells, our data indicate that SL assemblies can be transmitted from a sporulating diploid cell to the resulting ascospores. In the majority of tetrads, all four spores exhibited fluorescent SL assemblies, often with a denser network in one of the spores (Fig. 27). Only in a minority of the analyzed tetrads three or two of the spores possessed fluorescent structures. As spores are metabolically inert forms of yeasts [83], it is very unlikely that the SL structures originated from newly synthesized and assembled SL proteins. Instead I favor the idea that the pre-existing tubular network in the diploid cell is split during spore formation, with a high likelihood that all resulting spores obtain fragments.



#### 4.4. Colocalization Studies

Live fluorescence microscopy imaging of yeast cells during mitosis and meiosis showed that mSbsC-eGFP tube-like structures were not projected from mother cells to the daughter cells. We questioned how such assemblies were forming *in vivo*. If the monomers were using the cytoplasmic elements as templates or assembly surfaces as they use SCWP of the bacterial cell wall, what were these templates? These questions brought us to the topic of *in vivo* localization of SL structures and their interactions with the cytoplasmic elements. For this purpose, I studied first the association of mSbsC-tRFP assemblies with yeast microtubules which are forming the yeast cytoskeleton with actin patches and filaments. Secondly, I investigated the interaction of mSbsC-eGFP structures with actin network and the last target was the nuclear region and mitochondrial network.

Since microtubules are also tubular assemblies like *in vivo* mSbsC-tRFP structures, the first target for colocalization was microtubules which were visualized by expressing the  $\alpha$ -*tubulin* tagged with YFP. It has been recently reported on spindle microtubule dynamics in living budding yeast cells by visualizing the microtubules during mitosis [84]. Microtubules were observed during mitosis by expressing the major  $\alpha$ -*tubulin* (Tub1) with GFP tag. Spindle movement was watched at different stages of mitosis by live microscopy imaging, i.e. spindle elongation towards the daughter cell during the late anaphase. I could not observe any colocalization between SLs and microtubules neither in cells with buds nor without buds (Fig.28). This observation is in accordance with live cell imaging results where I did not observe any projection of SLs towards the daughter cells. On the other hand, microtubules were observed to elongate towards the newly born bud in order to provide chromosome segregation (Fig 28, second row).

Actin networking is necessary for the cell polarization and transportation of the cell compartments during the cell cycle [64]. Since they are composed of tube-like filaments (Fig. 12b), I investigated the possible association of mSbsC-eGFP structures with the actin cytoskeleton. The data provided no indication for an association of the SL structures with the actin filaments (Fig. 29). However, I noticed a few focal points, where mSbsC-eGFP and actin fluorescence overlap. While we can not exclude the possibility of a coincidental localization of the two structures, this observation could also hint at the possibility that SL self-assembly is initiated at a specific site along the actin cytoskeleton and proceeds in the

cytosol without any template. Staining of DNA with DAPI gave no hint for association of the tubular SL structures with the nuclei or mitochondria in either budding or not budding cells (Fig. 30).

It was previously reported that SL assembly takes place by the surface localization of previously synthesized SL monomers in many bacteria [85]. Doran *et al.* [85] showed that *Azotobacter vinelandii*, which are Gram-negative bacteria, could not form their native SL upon cultivation in media lacking  $\text{Ca}^{2+}$  ions; when the media were supplemented with  $\text{Ca}^{2+}$ , SL formation was mediated. These data demonstrated the necessity of  $\text{Ca}^{2+}$  ions for the *in vivo* SL monomer self-assembly process on native cells. Our colocalization results showed that *in vivo* expressed mSbsC-eGFP tube-like assemblies did not show any association with yeast cytoskeletal elements: actin and microtubules or mitochondrial network implying that the SL monomers did not use them as a template for self-assembly. In line with the previous findings of SL assembly dependence on  $\text{Ca}^{2+}$  ions, we can make such a hypothesis: Since yeast cytoplasm is rich in  $\text{Ca}^{2+}$  ions [86], mSbsC-eGFP monomers self-assembled first into monolayers, then they bend because the monolayers were not fixed onto a surface namely negatively charged SCWP which are the original templates of SbsC where the monomers are bound by electrostatic interactions [25]. However, the question still remains: what do mSbsC-eGFP monomers use as a template for the initiation of nucleation *in vivo*? In this study, it has been shown that *in vivo* self-assembly process of mSbsC-eGFP initiates at a possible single nucleation point. Moreover, colocalization experiments revealed that the SL fusion proteins were not associating with actin and tubulin cytoskeleton elements or with nucleus and mitochondria. Interaction of SL proteins with other cellular components and *in vitro* nucleation initiation of recrystallized SL proteins can be further investigated by analytical and microscopical techniques. Control over the nucleation initiation process could enable us to build regular SL arrays or tube-like structures on surfaces or in solutions with a programmed manner.

#### **4.5. *In vitro* Recrystallization**

SL proteins can self-assemble into flat sheets, open ended cylinders, or spheres on solid substrates or in solutions making them appealing for biotechnological applications [3]. These assemblies can be monomerized by chaotropic agents, and upon the removal of the chemical SL subunits can recrystallize into regular protein arrays [10]. The self-assembly process and

the resulting structures of SL proteins depend on various parameters like temperature, ionic strength, and protein concentration [18]. In this study, mSbsC-eGFP fusion protein was expressed in *S. cerevisiae* cells and, the self-assembly process and self-assembly products were investigated *in vivo* and *in vitro*.

In our case study, the average cell diameter of *S. cerevisiae* was in the range of 3-5  $\mu\text{m}$ . *In vivo* mSbsC-eGFP tube lengths varied from 0.78  $\mu\text{m}$  to 5.06  $\mu\text{m}$ , with an average of 2.49  $\mu\text{m}$ . The average *in vivo* diameter was 0.3  $\mu\text{m}$ . In order to see if *in vivo* tube-like mSbsC-eGFP structures would be maintained outside the cells (*in situ*), I burst the *S. cerevisiae* cells by osmotic shock. After burst of the cells, the average *in situ* tube length was 1.69  $\mu\text{m}$ . The shortest tube was 0.66  $\mu\text{m}$  and the longest was 4.77  $\mu\text{m}$ . Tubular structures were retained, however slightly shorter than those observed *in vivo*. Most probably, the change of the ionic strength upon the osmotic lysis of the cells leads to a partial disassembly of the *in vivo* structures from the network into shorter tubes. Following the monomerization process, SL proteins were dialyzed in order to see if tubular fluorescent assemblies would be obtained again. mSbsC-eGFP monomers were able to self-assemble *in vitro* into fluorescent tubes demonstrating that eGFP did not interfere with the *in vitro* self-assembly process (Fig. 32). When I conducted the same recrystallization experiment in the presence of glass surfaces, instead of tube-like assemblies, fluorescent multi-layers formed (Fig. 38). Most probably, monomers preferred binding on the glass surface and interact with each other to form layers of proteins attached to the solid substrate than forming free layers in solution which would bend by electrostatic or hydrophobic interactions resulting in the formation of tubes.

The same recrystallization experiment was performed for S13240-eGFP and SslA-eGFP expressing cells. The corresponding cells were first spheroplasted, burst with osmotic shock, monomerized and recrystallized *in vitro*. Hollow-like fibrillar *in vivo* network structures of S13240-eGFP were maintained *in situ* following the osmotic shock. *In vitro* recrystallization upon dialysis of SL monomers resulted in the formation of same fluorescent fibrillar aggregates (Fig. 33) as well as in the formation of folded layers (Fig. 37). Although SbsC and S13240 monomers can form assemblies with oblique symmetries [69], they formed different structures *in vivo* and *in vitro*. This could have resulted from differences in monomer-monomer interactions caused by the aa contents. Until now, only the tertiary structure of SbsC was explored [25]. Pavkov *et al.* [25] have reported that SbsC is composed of six separate domains. Domain I (aa31-260) contains mostly positively charged and aromatic side

chains, which mediate the binding to negatively charged SCWP. The remaining domains together with the C-terminal part are responsible for the monomer-monomer interactions. Since the remaining domains have different aa compositions in S13240 [69], it is possible to have altered monomer-monomer interactions resulting in the formation of fibrillar networks rather than tube-like assemblies *in vitro*. On the other hand, SslA forms assemblies with tetragonal symmetry [70]. *In vivo* expression of SslA-eGFP led to the formation of fluorescent patches which were maintained *in situ* after the osmotic shock (Fig. 34). Unlike the other SL-eGFP constructs, I could not observe the same patches after the *in vitro* recrystallization process. Rather, I observed finer patches and tube-like assemblies most probably because of changes in environmental conditions like ionic strength.

#### **4.6. Influence of Calcium Concentration, pH and Dialysis Time on *in vitro* Recrystallization Process of mSbsC-eGFP Monomers**

Doran *et al.* [85] showed that *Azotobacter vinelandii*, which are Gram-negative bacteria, did not form their native SL upon cultivation in media lacking  $\text{Ca}^{2+}$  ions. When the media were supplemented with  $\text{Ca}^{2+}$ , SL formation was favored. These data demonstrated the necessity of  $\text{Ca}^{2+}$  ions for the *in vivo* SL monomer self-assembly process on native cells. Györvary *et al.* [87] have investigated the effect of calcium ions on the *in vitro* self-assembly process of SbpA (SL protein of *B. sphaericus* CCM 2177) on silicon surfaces. They concluded that calcium is not only required for the protein-protein interactions between the monomers, but also for the attachment of the proteins to the surfaces. Despite the importance and role of calcium in SL assembly has been mentioned, no data are currently available how calcium affects the mSbsC-eGFP fusion protein recrystallization behavior. In this study it is shown that mSbsC-eGFP tubular assembly formation did not occur in the absence of calcium due to the inefficient protein-protein interactions between the SL subunits (Fig. 39). In line with the previous observations [85, 87], we suggest that calcium ions may be binding to specific sites of the SL monomers and change the conformation of the protein in a way that suitable sites for monomer-monomer interactions are provided. In the presence of excess amounts of calcium, this process may be interfered by unspecific binding of  $\text{Ca}^{2+}$  to the monomers making them inactive binding partners.

As the theoretical isoelectric point of mSbsC-eGFP is 5.51, the protein has different net charges at the different tested pH values. As the pH of the environment rises above the pI of a

protein, it possesses a net negative charge and is expected to have a stronger affinity for  $\text{Ca}^{2+}$  binding. In line with this prediction, I observed longer tubes upon increasing the pH (Table 3). Due to the time dependency of crystal growth [88], the length of mSbsC-eGFP *in vitro* crystals also increased with the time of dialysis. These findings can be applied in nanobiotechnology to control the *in vitro* self-assembly process of SL proteins on surfaces or in solutions for the development of uniformly directed templates or novel structures.

#### 4.7. Metallization of mSbsC-eGFP Tubes with Platinum

Mertig *et al.* [49] have utilized the SL protein of *Sporocarcina ureae* as a template to chemically deposit platinum clusters. They observed the formation of highly ordered arrays of Pt clusters. It was concluded that the localization, size and the metal lattice growth of Pt particles were determined by the underlying SL protein template. Recently, Wahl *et al.* [72] have reported on the electron-beam induced formation of regular nanoparticle arrays of Pt and Pd on the SL of *B. sphaericus* NCTC 9602. In this study, I investigated the chemical deposition of Pt on *in vitro* recrystallized mSbsC-eGFP tubes. As shown in Fig. 44, I was able to produce SL tubes smoothly coated by Pt. Such metalized protein nanotubes could be used in conductive nanocircuit technologies as nanowires.

I conducted the metallization experiments at different temperatures in order to see the effect of ambient temperature on the chemical reduction of  $\text{Pt}^{2+}$ . I observed the formation of metal clusters at RT after 4 h of reaction. On the other hand I could not see any metal deposition on SL proteins at 4°C. It has been reported that most of the metal reduction reactions are endothermic [89]. In other words, the reaction needs to absorb energy from the environment. Since endothermic reaction rates decrease as the environmental temperature is reduced. When our experimental temperature dropped from RT to 4°C, the reduction reaction rate decreased dramatically so that no metal deposition occurred after 4 h of reaction time.

Interestingly, the metallization provided information about how these tube-like structures are formed. The metalized SL structure shown in Fig. 42 & Fig. 44 nicely reveals that the tube-like structures result from folded layers. Recently, Pavkov *et al.* [25] have investigated the structure and binding characteristics of SbsC. They reported that SbsC is composed of six separate domains connected by short flexible linkers. Domain I (aa31-260) is mostly composed of positively charged and aromatic side chains, which mediate the binding to

negatively charged SCWP. The remaining domains together with the C-terminal part are responsible for the monomer-monomer interactions. In the absence of SCWP inside the yeast cells or in the dialysis buffer, SL monomers may interact with each other to form monolayers that are not fixed on a surface. Bending of the SL under this condition may initiate the formation of folds. Bending of SL arrays which is also required on the bacterial cell surface for maintaining a closed lattice arrangement is most probably caused by flexible linkers. Such linkers were reported to be involved in introduction of dislocations and disclinations needed for the continuous growth of SL arrays on the cell surface [25].

mSbsC-eGFP assemblies were not detectable in brightfield, most probably due to their thinness. However, after metallization the tubes could be visualized with brightfield due to the increased contrast and thickness caused by the metal coats. In line with this, the brightfield signal was enhanced when the metal concentration increased. Interestingly, the metalized samples were no longer fluorescent. Probably the loss of fluorescence was caused by the bound metal ions or the deposited metal layers either directly to the chromophore region or the domain surrounding it affecting the proper folding of the chromophore which is constituted by three amino acid residues at positions 65-66-67 (Ser-Tyr-Gly) [73].

Metallized SL-assemblies may be used as nanowires in nanobiotechnological applications. Chemical deposition of further metals, i.e. Au, Ag or Pd on SL structures can be investigated and eventually optimized. Combining SLs with novel tags, i.e. mineralization domains may widen the technical application of SL proteins.

## V. Summary

In numerous Gram-negative and Gram-positive bacteria as well as in *Archaea* SL proteins form the outermost layer of the cell envelope. SL (glyco)monomers self-assemble with oblique (p2), tetragonal (p4), or hexagonal (p3, p6) symmetries [12]. SL subunits interact with each other and with the underlying cell surface by relatively weak non-covalent forces such as hydrogen-bonds, ionic bonds, salt-bridges or hydrophobic interactions. This makes them easy to isolate by applying chaotropic agents like urea and guanidine hydrochloride (GuHCl), chelating chemicals, or by changing the pH of the environment [10]. Upon dialysis in an ambient buffer monomers recrystallize into regular arrays that possess the forms of flat sheets, open ended cylinders, or spheres on solid substrates, at air-water interfaces and on lipid films, making them appealing for nanobiotechnological applications [3, 18]. The aim of this study was to investigate the structure, thermal stability, *in vivo* self-assembly process, recrystallization and metallization of three different recombinant SL proteins (SslA-eGFP, mSbsC-eGFP and S13240-eGFP) expressed in yeast *S. cerevisiae* BY4741 which could be further used in nanobiotechnological applications.

In order to fulfill this aim, I investigated the *in vivo* expression of SL proteins (SslA, SbsC, S13240) tagged with eGFP (SL-eGFP) in the yeast *S. cerevisiae* BY4141. First, I characterized the heterologous expression of SL fusion constructs with growth and fluorescence measurements combined with Western blot analyses. Fluorescence microscopy investigations of overnight grown cultures showed that SslA-eGFP fusion protein was expressed as fluorescent patches, mSbsC-eGFP as tubular networks, and S13240-eGFP as hollow-like fibrillar network structures, while eGFP did not show any distinct structure. Thermal stability of *in vivo* expressed SL-eGFP fusion proteins were investigated by fluorescence microscopy and immunodetection.

*In vivo* self-assembly kinetics during mitosis and meiosis was the second main issue. In parallel, association of *in vivo* mSbsC-eGFP structures with the cellular components was of interest. A network of tubular structures in the cytosol of the transformed yeast cells that did not colocalize with microtubules or the actin cytoskeleton was observed. Time-resolved analysis of the formation of these structures during vegetative growth and sporulation was investigated by live fluorescence microscopy. While in meiosis ascospores seemed to receive assembled structures from the diploid cells, during mitosis surface layer structures were

formed *de novo* in the buds. Surface layer assembly always started with the appearance of a dot-like structure in the cytoplasm, suggesting a single nucleation point.

In order to get these *in vivo* SL assemblies stably outside the cells (*in situ*), cell disruption experiments were conducted. The tubular structures formed by the protein *in vivo* were retained upon bursting the cells by osmotic shock; however their average length was decreased. During dialysis, monomers obtained by treatment with chaotropic agents recrystallized again to form tube-like structures. This process was strictly dependent on calcium ions, with an optimal concentration of 10 mM. Further increase of the  $\text{Ca}^{2+}$  concentration resulted in multiple non-productive nucleation points. It was further shown that the lengths of the S-layer assemblies increased with time and could be controlled by pH. After 48 hours the average length at pH 9.0 was 4.13  $\mu\text{m}$  compared to 2.69  $\mu\text{m}$  at pH 5.5. Successful chemical deposition of platinum indicates the potential of recrystallized mSbsC-eGFP structures for nanobiotechnological applications. For example, such metalized protein nanotubes could be used in conductive nanocircuit technologies as nanowires.



## VI. References

1. Sleytr UB, Bayley H, Sara M *et al.* (1997) VI. Applications of S-layers. FEMS Microbiol Rev 20: 151-175
2. Thomas SR, Trust TJ (1995) Tyrosine phosphorylation of the tetragonal paracrystalline array of *Aeromonas hydrophila*: Molecular cloning and high-level expression of the S-layer protein gene. J Mol Biol 245: 568-581
3. Sleytr UB, Egelseer EM, Ilk N *et al.* (2007) S-Layers as a basic building block in a molecular construction kit. FEBS J 274: 323–334
4. Ilk N, Egelseer EM, Ferner-Ortner J *et al.* (2008) Surfaces functionalized with self-assembling S-layer fusion proteins for nanobiotechnological applications. Physicochem Eng Aspects 321: 163–167
5. Pum D, Sleytr UB (1999) The application of bacterial S-layers in molecular nanotechnology. Trends Biotechnol 17: 8–12
6. Sára M, Sleytr UB (1987) Molecular-sieving through S-layers of *Bacillus stearothermophilus* strains. J Bacteriol 169: 4092–4098
7. Sára M, Sleytr UB (2000) S-layer proteins. J Bacteriol 182: 859–868
8. Stache J (2006) Untersuchungen zur Funktionalisierung von Proteinen mittels Fusion mit S-Layer Proteinen und deren rekombinante Herstellung. Diplomarbeit, Institut für Genetik, TU Dresden
9. Sleytr UB, Beveridge TJ (1994) Bacterial S-layers. Trends in Microbiol 7: 253-259.
10. Jarosch M, Egelseer EM, Huber C *et al.* (2001) Analysis of the structure-function relationship of the S-layer protein SbsC of *Bacillus stearothermophilus* ATCC 12980 by producing truncated forms. Microbiol 147: 1353–1363
11. Sleytr UB, Messner P, Pum D *et al.* (1999) Crystalline bacterial cell surface layers (S Layers): from supramolecular cell structure to biomimetics and nanotechnology. Angew Chem Int Ed 38: 1034-1054
12. Beveridge TJ (1994) Bacterial S-layers. Curr Opin Struct Biol 4: 204-212
13. Claus H, Akca E, Debaerdemaeker T *et al.* (2005) Molecular organization of selected prokaryotic S-layer proteins. Can J Microbiol 51: 731–743
14. Sleytr UB, Sara M, Pum D *et al.* (2001) Characterization and use of crystalline bacterial cell surface layers. Prog Surf Sci 68: 231-278

15. Schäffer C, Messner P (2004) REVIEW: Surface-layer glycoproteins: an example for the diversity of bacterial glycosylation with promising impacts on nanobiotechnology. *Glycobiol* 14: 31R-42R.
16. Engelhardt H (2007) Mechanism of osmoprotection by archaeal S-layers: A theoretical study. *J Struct Biol* 160: 190-199
17. Noonan B, Trust TJ (1995) Molecular analysis of an A-protein secretion mutant of *Aeromonas salmonicida* reveals a surface layer-specific protein secretion pathway. *J Mol Biol* 248: 316-327
18. Sleytr UB, Huber C, Ilk N *et al.* (2007) S-layers as a tool kit for nanobiotechnological applications. *FEMS Microbiol Lett* 267: 131–144
19. Schäffer C, Messner P (2001) Glycobiology of surface layer proteins. *Biochimie* 83: 591-599
20. Engelhardt H (2007) Are S-layers exoskeletons? The basic function of protein surface layers revisited. *J Struct Biol* 160: 5–124
21. Sára M, Pum D, (1992) Permeability and charge dependent adsorption properties of the S-layer lattice from *Bacillus coagulans* E38-66. *J Bacteriol* 174: 3487–3493
22. Merroun ML, Raff J, Rossberg A *et al.* (2005) Complexation of uranium by cells and S-layer sheets of *Bacillus sphaericus* JG-A12. *App Environ Microbiol* 71: 5532-5543
23. Golowczyc MA, Mobili P, Garrote GL *et al.* (2007) Protective action of *Lactobacillus kefir* carrying S-layer protein against *Salmonella enterica* serovar Enteritidis. *Int J Food Microbiol* 118: 264–273
24. Kern J, Schneewind O (2010) BslA, the S-layer adhesion of *B. anthracis*, is a virulence factor for anthrax pathogenesis. *Mol Microbiol* 75: 324-332
25. Pavkov T, Egelseer EM, Tesarz M *et al.* (2008) The structure and binding behavior of the bacterial cell surface layer protein SbsC. *Structure* 16: 1226-1237
26. Beveridge TJ, Pouwels PH, Sára M *et al.* (1997) Functions of S-layers. *FEMS Microbiol Rev* 20: 99–149
27. Schultze-Lam S, Harauz G, Beveridge TJ (1992) Participation of a Cyanobacterial S Layer in Fine-Grain Mineral Formation. *J Bacteriol* 174: 7971-7981
28. Smarda J, Smajs D, Komrska J *et al.* (2002) S-layers on cell walls of cyanobacteria. *Micron* 33: 257-277
29. Korkmaz N, Ostermann K, Rödel G (2010) Expression and assembly of recombinant surface layer proteins in *Saccharomyces cerevisiae*. *Current Microbiol* DOI 10.1007/s00284-010-9715-1

30. Pum D, Messner P, Sleytr UB (1991) Role of the S Layer in morphogenesis and cell division of the Archaeobacterium *Methanococcus sinense*. *J Bacteriol* 173: 6865-6873
31. Dupres V, Alsteens D, Pauwels K *et al.* (2009) In vivo imaging of S-layer nanoarrays on *Corynebacterium glutamicum*. *Langmuir* 25: 9653-9655
32. Sleytr UB, Sara M (1986) Ultrafiltration membranes with uniform pores from crystalline bacterial cell envelope layers. *Appl Microbiol Biotech* 25: 83-90
33. Weigert S, Sara M (1995) Surface modification of an ultrafiltration membrane with crystalline structure and studies on interactions with selected protein molecules. *J Membr Sci* 106: 147-159
34. Gufler PC, Pum D, Sleytr UB *et al.* (2004) Highly robust lipid membranes on crystalline S-layer supports investigated by electrochemical impedance spectroscopy. *Biochim Biophys Acta* 1661: 154-165
35. Sotiropoulou S, Mark SS, Angert ER *et al.* (2007) Nanoporous S-layer protein lattices. A biological ion gate with calcium selectivity. *J Phys Chem C* 111: 13232- 13237
36. Weiner C, Sara M, Dasgupta G *et al.* (1994) Affinity cross-flow filtration: Purification of IgG with a novel Protein a affinity matrix prepared from two-dimensional protein crystals. *Biotechnol Bioeng* 44: 55-65
37. Tschigger H, Casey JL, Parisi K *et al.* (2008) Display of a peptide mimotope on a crystalline bacterial cell surface layer (S-layer) lattice for diagnosis of Epstein–Barr virus infection. *Bioconjugate Chem* 19: 860-865
38. Smith RH, Messner P, Lamontagne LR *et al.* (1993) Induction of T-cell immunity to oligosaccharide antigens immobilized on crystalline bacterial surface layers (S-layers). *Vaccine* 11: 919-924
39. Hollmann A, Delfederico L, Glikmann G *et al.* (2007) Characterization of liposomes coated with S-layer proteins from lactobacilli. *Biochim Biophys Acta* 1768: 393–400
40. Gerstmayr M, Ilk N, Schabussova I *et al.* (2007) A novel approach to specific allergy treatment: the recombinant allergen-S-layer fusion protein rSbsC-Bet v 1 matures dendritic cells that prime Th0/Th1 and IL-10-producing regulatory T cells. *J Immunol* 179: 7270-7275
41. Schuster B, Sleytr UB (2009) Composite S-layer lipid structures. *J Str Biol* 168: 207-216
42. Schuster B, Pum D, Sleytr UB (1998) Voltage clamp studies on S-layer-supported tetraether lipid membranes. *Biochim Biophys Acta* 1369: 51-60
43. Ilk N, Küpcü S, Moncayo G *et al.* (2004) A functional chimaeric S-layer-enhanced green fluorescent protein to follow the uptake of S-layer-coated liposomes into eukaryotic cells. *Biochem J* 379: 441–448

44. Ryzhkov PM, Ostermann K, Rödel, G (2007) Isolation, gene structure and comparative analysis of the S-layer gene *sslA* of *Sporosarcina ureae* ATCC 13881. *Genetica* 131: 255-265
45. Pum D, Stangl G, Sponer C *et al.* (1996) Deep UV patterning of monolayers of crystalline S layer protein on silicon surfaces. *Colloids Surf B* 8: 157-162
46. Douglas K, Clark NA (1986) Nanometer molecular lithography. *Appl Phys Lett* 48: 676-678
47. Scheicher SR, Kainz B, Köstler S *et al.* (2009) Optical oxygen sensors based on Pt(II) porphyrin dye immobilized on S-layer protein matrices. *Biosens Bioelectron* 25: 797-802
48. Weigert S, Sara M (1996) Ultrafiltration membranes prepared from crystalline bacterial cell surface layers as model systems for studying the influence of surface properties on protein adsorption. *J Membr Sci* 121: 185–196
49. Mertig M, Kirsch R, Pompe W *et al.* (1999) Fabrication of highly oriented nanocluster arrays by biomolecular templating. *Eur Phys J D* 9: 45-48
50. Douglas K, Clark NA, Rothschild KJ *et al.* (1986) Nanometer molecular lithography. *Appl Phys Lett* 48: 676-678
51. Allred DB, Sarikaya M, Baneyx F *et al.* (2007) Bacterial surface-layer proteins for electrochemical nanofabrication. *Electrochimica Acta* 53: 193–199
52. Liu J, Mao Y, Lan E *et al.* (2008) Generation of oxide nanopatterns by combining self-assembly of S-layer proteins and area-selective atomic layer deposition. *J Am Chem Soc* 130: 16908–16913
53. Badelt-Lichtblau H, Kainz B, Völlenknecht C *et al.* (2009) Genetic engineering of the S-layer protein SbpA of *Lysinibacillus sphaericus* ccm 2177 for the generation of functionalized nanoarrays. *Bioconjugate Chem* 20: 895–903
54. Feldmann H (2000) Gene Function and Expression: Four Years of the Post-genomic Era of Yeast. *Food Technol Biotechnol* 38: 237-252
55. Romanos M, Scorer CA, Clare JJ (1992) Foreign gene expression in yeast: a review. *Yeast* 8: 423-488
56. Cereghino CP, Cregg JM (1999) Applications of yeast in biotechnology: protein production and genetic analysis. *Curr Opin Biotechnol* 10: 422-427
57. Blecha A, Zarschler K, Sjollem KA *et al.* (2005) Expression and cytosolic assembly of the S-layer fusion protein mSbsC-EGFP in eukaryotic cells. *Microb Cell Fact* 4: 28
58. Brömme D, Bonneau PR, Lachance P *et al.* (1993) Functional expression of human cathepsin S in *Saccharomyces cerevisiae*. *J Biol Chem* 268: 4832-4838

59. Lesser FC, Miller SL (2001) Expression of microbial virulence proteins in *Saccharomyces cerevisiae* models mammalian infection. *EMBO J* 20: 1840-1849
60. Sauer B (1987) Functional expression of the cre-lox site-specific recombination system in the yeast *Saccharomyces cerevisiae*. *Mol Cell Biol* 7:2087-2096
61. Cook JC, Joyce JG, George HA (1999) Purification of virus-like particles of recombinant human papillomavirus type 11 major capsid protein L1 from *Saccharomyces cerevisiae*. *Protein Expr Purif* 17: 477-484
62. Mueller A, Kadri A, Jeske H *et al.* (2010) In vitro assembly of Tobacco mosaic virus coat protein variants derived from fission yeast expression clones or plants. *J Virol Methods* 166: 77-85
63. Herskowitz, I. (1988) Life cycle of the budding yeast *Saccharomyces cerevisiae*. *Microbiol Rev* 52: 536-553
64. May KM, Hyams JS (1998) The yeast cytoskeleton: The closer we look, the more we see. *Fungal Genet Biol* 24: 110–122
65. Kilmartin JV, Adams AEM (1984) Structural rearrangements of tubulin and actin during the cell cycle of the yeast *Saccharomyces*. *J Cell Biol* 98: 922-933
66. Amberg DC (1998) Three-dimensional imaging of the yeast actin cytoskeleton through the budding cell cycle. *Mol Biol Cell* 9: 3259-3262
67. Jarosch M, Egelseer EM, Mattanovich D *et al.* (2000) S-layer gene sbsC of *Bacillus stearothermophilus* ATCC 12980: molecular characterization and heterologous expression in *Escherichia coli*. *Microbiol* 146:273-281
68. Egelseer EM, Danhorn T, Pleschberger M *et al.* (2001) Characterization of an S-layer glycoprotein produced in the course of S-layer variation of *Bacillus stearothermophilus* ATCC 12980 and sequencing and cloning of the sbsD gene encoding the protein moiety. *Arch Microbiol* 177: 70-80
69. Blecha A (2005) Gentechnisches Design bakterieller Hüllproteine für die technische Nutzung. Dissertation, TU Dresden
70. Engelhardt H, Saxton WO, Baumeister W (1986) Three-dimensional structure of the tetragonal surface layer of *Sporosarcina ureae*. *J Bacteriol* 168: 309–317
71. Ryzhkov P (2007) Bioengineering of S-layers: molecular characterization of the novel S-layer gene *sslA* of *Sporosarcina ureae* ATCC 13881 and nanotechnology application of SslA protein derivatives. PhD thesis, TU Dresden

- 
72. Wahl R, Mertig M, Raff J et al (2001) Electron-beam induced formation of highly ordered palladium and platinum nanoparticle arrays on the S layer of *Bacillus sphaericus* NCTC 9602. *Adv Mater* 13: 736-740
73. Tsien RY (1998) The green fluorescent protein. *Annu Rev Biochem* 67: 509-544
74. Imai T, Ohno T (1995) Measurement of yeast intracellular pH by image processing and the change it undergoes during growth phase. *J Biotech* 38: 165-172
75. Patterson GH, Knobel SM, Sharif WD *et al.* (1997) Use of the green fluorescent protein and its mutants in quantitative fluorescence microscopy. *Biophys J* 73: 2782-2790
76. Fujita T, Dodbiba G, Sadaki J *et al.* (2006) Removal of anionic metal ions from wastewater by hydroxide-type adsorbents. *Chin J Process Eng* 6: 357-362
77. Argos P, Rossmann MG, Grau UM *et al.* (1979) Thermal stability and protein structure. *Biochem* 18: 5698-5703
78. Ogasahara K, Imanishi A, Isemura T (1970) Studies on thermophilic  $\alpha$ -Amylase from *Bacillus stearothermophilus*. *J Biochem* 67: 77-82
79. Kumar S, Tsai CJ, Nussinov R (2000) Factors enhancing protein thermostability. *Prot Eng* 13: 179-191
80. Toca-Herrera JL, Morena-Flores S, Friedmann J *et al.* (2004) Chemical and thermal denaturation of crystalline bacterial S-layer proteins: An atomic force microscopy study. *Microsc Res Tech* 65: 226-234
81. Pum D, Neubauer A, Györvary E *et al.* (2000) S-layer proteins as building blocks in a biomolecular construction kit. *Nanotech* 11: 100-107
82. Nelson B, Parsons AB, Evangelista M *et al.* (2004) Fus1p interacts with components of the Hog1p mitogen-activated protein kinase and Cdc42p morphogenesis signaling pathways to control cell fusion during yeast mating. *Genetics* 166: 67-77
83. Thevelein JM, den Hollander JA, Shulman RC (1984) Trehalase and the control of dormancy and induction of germination in fungal spores. *Trends Biochem Sci* 9: 495-497
84. Straight AF, Marshall WF, Sedat JW *et al.* (1997) Mitosis in living budding yeast: anaphase A but no metaphase plate. *Sci* 277: 574-578
85. Doran JL, Bingle WH, Page WJ (1987) Role of calcium in assembly of the *Azotobacter vinelandii* surface array. *J Gen Microbiol* 133: 399-413
86. Mori IC, Iida H, Tsuji F *et al.* (1998) Salicylic acid induces a cytosolic  $Ca^{2+}$  elevation in yeast. *Biosci Biotechnol Biochem* 62: 986-989

- 
87. Györvary ES, Stein O, Pum D *et al.* (2003) Self-assembly and recrystallization of bacterial S-layer proteins at silicon supports imaged in real time by atomic force microscopy. *J Microsc* 212: 300-306
88. Judge RA Forsythe EL, Pusey ML (2010) Growth rate dispersion in protein crystal growth. *Cryst Growth Des* 10: 3164-3168
89. Tamaura Y (1995) Heat absorption process using endothermic reaction with metal oxide. *Prog Nucl Energy* 29: 159-163
90. Tanaka K, Mukae N, Dewar H *et al.* (2005) Molecular mechanisms of kinetochore capture by spindle microtubules. *Nature* 434: 987-994
91. Gietz RD, Schiestl RH, Willems AR *et al.* (1995) Studies on the transformation of intact yeast cells by the LiAc/SS-DNA/PEG procedure. *Yeast* 11: 355-360
92. Laemmli UK (1970) Cleavage of structural proteins during the assembly of the head of bacteriophage T4. *Nature* 227: 680-685
93. Xu EY, Zawadzki KA, Broach JR (2006) Single-cell observations reveal intermediate transcriptional silencing states. *Mol Cell* 23: 219-229
94. Howorka S, Sara M, Lubitz W *et al.* (1999) Self-assembly product formation of the *Bacillus stearothermophilus* PV72/p6 S-layer protein SbsA in the course of autolysis of *Bacillus subtilis*. *FEMS Microbiol Lett* 172: 187-196
95. Achstetter T, Wolf DH (1985) Proteinases, proteolysis and biological control in the yeast *Saccharomyces cerevisiae*. *Yeast* 1: 139-157

## Acknowledgements

I would like to express my sincere appreciation and deepest gratitude to Prof. Dr. Gerhard Rödel who is my scientific advisor and philosophical mentor for giving me the opportunity to work in his group with such an exciting subject and for his guidance, encouragement and patience through my PhD study.

I am very grateful to Kai and Kristof for their helpful discussion, support and for reviewing my thesis.

I am very thankful to my dear friends Msau and Yigit for all their support, great friendship, advice, helpful discussion and encouragement.

I would like to thank Karolina, Astrid, Jennifer, Veronika and Kristof for the friendly atmosphere in the office, and all the lab members (Mandy, Annett, Katja, Marlis, Udo, Andi, Susi, Katrin, Leo, Denise, Ivan ...) for their friendliness and support.

I would like to state my gratitude to Prof. Dr. Gerald Gerlach and all members of the research training group for their help, support and for the friendly atmosphere.

I would like to thank Axel Mensch, Ortrud Trommer and Silvia Muehle for their valuable technical assistance with SEM and Jean-Christophe Olaya, Ellen Geibelt and Hella Hartmann from Biotec for the tutorials and help for the fluorescence microscopy.

Financial Support provided by Research Training Group Nano- and Biotechnologies for Packaging of Electronic Systems (German Research Foundation, DFG 1401/1) is gratefully acknowledged.

My deepest appreciation goes to my parents, my sister and Kevin for their endless love, support, patience and understanding.



## Curriculum Vitae

**Name** Nuriye Korkmaz

**Date of Birth** July 23, 1981

**Place of Birth** Pazar-Rize / Turkey

**Marital Status** Single

**Nationality** Turkish

### Education

Sep 2007-Dec 2010 Dresden University of Technology (TU-Dresden)  
Research Training Group Nano- and Biotechnologies  
for Packaging of Electronic Systems  
Institute for Genetics (PhD)

Feb 2005-Aug 2007 Middle East Technical University (METU)  
Faculty of Engineering, Ankara  
Department of Chemical Engineering (MSc)

Sep 1999-Jan 2005 Middle East Technical University (METU)  
Faculty of Engineering, Ankara  
Department of Chemical Engineering (BSc, double major)

Sep 1999-June 2004 Middle East Technical University (METU)  
Faculty of Engineering, Ankara  
Department of Food Engineering (BSc, major)

Sep 1991-June 1999 Rize Anatolian High School, Rize

### Scientific Meetings

Workshop “DFG Report and Defense Colloquium, Bio-Nano-Tech 2010”, Dresden, Germany, 09.09.2010

Conference “6th Nanoscience and Nanotechnology”, Izmir, Turkey, 15-18.06.2010

Workshop “Taking the Next Step in Nano-and Bioelectronics Packaging”, Moritzburg, Germany, 28.10.2009

Workshop “Convergence of Life Sciences and Electronics Technologies”, North/Baltic Sea, Germany, 11-15.5.2009

Conference “Nano-Molecular Analysis for Emerging Technologies III & Surface Science of Biologically Important Interfaces 10”, NPL, Teddington, UK, 05-06.11. 2008

Workshop “Self-assembly”, Bautzen, Germany, 09-10.10.2008

Workshop “Microscopy”, Leucorea, Wittenberg, Germany, 13-15.05.2008

Workshop “Electrochemical microsensors”, Kurt-Schwabe-Institut, Meinsberg, Germany, 04-07.10.2007

4th Ankara University Biotechnology Days, 15-19.11.2005

### **Experience**

Sep 2007-Dec 2010     Dresden University of Technology (TU-Dresden)  
Research Training Group Nano- and Biotechnologies  
for Packaging of Electronic Systems  
Institute for Genetics (PhD)

**PhD Thesis:** Self-assembly and structure investigation of recombinant S-layer proteins expressed in yeast for nanobiotechnological applications

Feb 2005-Aug 2007     Middle East Technical University (METU)  
Faculty of Engineering, Ankara  
Department of Chemical Engineering (MSc)

**Master`s Thesis:** Design of a hybrid streptokinase construct and its production as an extracellular recombinant protein in *Bacillus* species

### **Summer practices**

June 2002                 Efes Pilsen Brewery, Ankara, Turkey  
June 2003                 Ersu Fruit Juice Factory, Konya, Turkey

## **Selbständigkeitserklärung**

Hiermit versichere ich, dass ich die vorliegende Arbeit ohne unzulässige Hilfe Dritter und ohne Benutzung anderer als der angegebenen Hilfsmittel angefertigt habe; die aus fremden Quellen direkt oder indirekt übernommenen Gedanken sind als solche kenntlich gemacht. Die Arbeit wurde bisher weder im Inland noch im Ausland in gleicher oder ähnlicher Form einer anderen Prüfungsbehörde vorgelegt.

Die vorliegende Arbeit wurde am Institut für Genetik der TU Dresden unter wissenschaftlicher Betreuung von Herrn Prof. Dr. rer. nat. habil. G. Rödel angefertigt.

Die Promotionsordnung wird anerkannt.

Dresden, den 12.01.2011